

PDF hosted at the Radboud Repository of the Radboud University Nijmegen

The following full text is a publisher's version.

For additional information about this publication click this link.

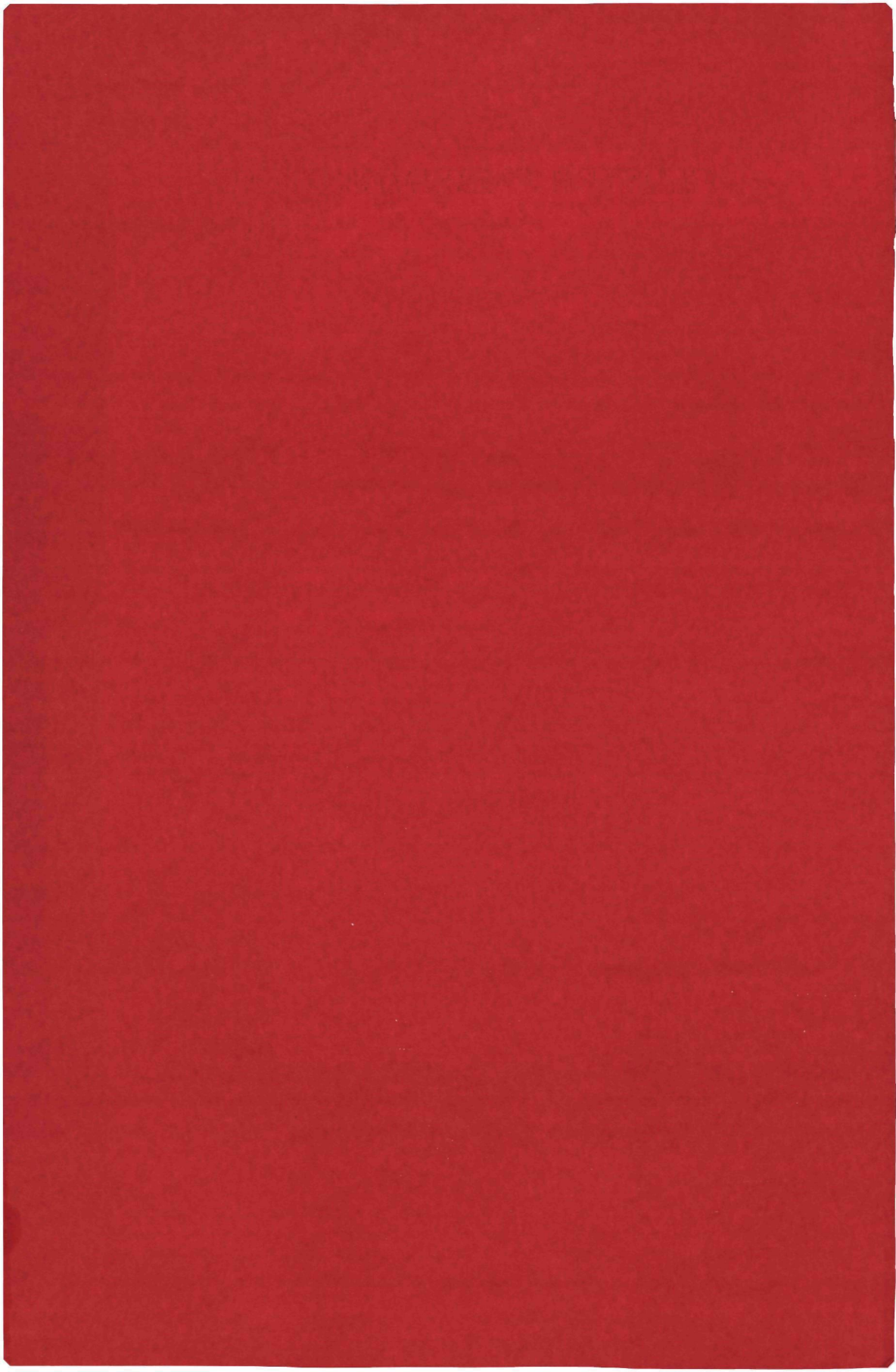
<http://hdl.handle.net/2066/113138>

Please be advised that this information was generated on 2017-12-06 and may be subject to change.

3051

**CLUSTER EMBEDDING AND
PSEUDOPOTENTIALS IN THE
HARTREE-FOCK-SLATER-LCAO
METHOD**

W. RAVENEK



**CLUSTER EMBEDDING AND
PSEUDOPOTENTIALS IN THE
HARTREE-FOCK-SLATER-LCAO
METHOD**

ISBN 90-9000784-9

Promotores: Prof.Dr.Ir. A. van der Avoird

Prof.Dr. E.J. Baerends

CLUSTER EMBEDDING AND PSEUDOPOTENTIALS IN THE HARTREE-FOCK-SLATER-LCAO METHOD

PROEFSCHRIFT

ter verkrijging van de graad van doctor in de wiskunde
en natuurwetenschappen aan de Katholieke Universiteit
te Nijmegen, op gezag van de Rector Magnificus Prof. Dr.
J.H.G.I. Giesbers, volgens besluit van het College van
Dekanen in het openbaar te verdedigen op donderdag
22 november 1984, des namiddags te 2.00 uur precies

door

Walter Ravenek

geboren te Pijnacker

1984
Offsetdrukkerij Kanters B.V.,
Alblasserdam

Hierbij wil ik eenieder bedanken die bijgedragen heeft aan het totstandkomen van dit proefschrift. Met name wil ik noemen:

- de mede-auteurs van de artikelen in hoofdstukken II - IV, in het bijzonder Ferdie Geurts, die ook een belangrijke bijdrage geleverd heeft aan het in hoofdstuk VI beschreven werk, voor de prettige samenwerking;
- de (ex-)leden van de afdeling Theoretische Chemie van de Katholieke Universiteit te Nijmegen, in het bijzonder Foppe Visser, voor plezierige kontakten;
- de (ex-)leden van de afdeling Theoretische Chemie van de Vrije Universiteit te Amsterdam voor gastvrijheid gedurende enkele maanden in 1982;
- Monique Bongers - de Bie en Maria Straatman voor het verzorgen van het manuscript;
- de North-Holland Publishing Company, in het bijzonder dhr. J. Hanraads, voor het beschikbaar stellen van een kopie van het artikel in hoofdstuk IV vóór publikatie in Chemical Physics.

Dit onderzoek werd gedeeltelijk gesteund door de Stichting Scheikundig Onderzoek in Nederland (S.O.N.) met een subsidie van de Nederlandse Organisatie voor Zuiver-Wetenschappelijk Onderzoek (Z.W.O.).

aan mijn ouders

aan Ida

C O N T E N T S

<u>CHAPTER I</u>	Introduction	1
<u>CHAPTER II</u>	Hartree-Fock-Slater-LCAO calculation of the Mössbauer parameters of some antimony compounds (W. Ravenek, J.W.M. Jacobs, A. van der Avoird, Chem. Phys. <u>78</u> (1983) 391)	5
<u>CHAPTER III</u>	The calculation of interaction energies using the pseudopotential Hartree-Fock-Slater-LCAO method (W. Ravenek, E.J. Baerends, J. Chem. Phys. <u>81</u> (1984) 865)	19
<u>CHAPTER IV</u>	The calculation of one-electron properties using the pseudopotential Hartree-Fock-Slater-LCAO method (W. Ravenek, F.M.M. Geurts, Chem. Phys. <u>90</u> (1984) 73)	31
<u>CHAPTER V</u>	On the use of perturbation theory in the pseudopotential Hartree-Fock-Slater-LCAO method	41
<u>CHAPTER VI</u>	Implementation of the moderately-large-embedded-cluster scheme in the pseudopotential Hartree-Fock-Slater-LCAO method; calculations for hydrogen on lithium (100)	47

SUMMARY

112

SAMENVATTING (Dutch summary)

114

CURRICULUM VITAE

116

INTRODUCTION

This thesis deals with a number of quantum chemical methods for computational studies of molecular systems that can be qualified as large on an atomic scale. As starting point serves the nonempirical Hartree-Fock-Slater(HFS)-LCAO method, which has been demonstrated to yield a physically realistic description of molecular systems in relatively little computational time, in comparison with the more common ab initio methods. The methods developed here may be considered as building blocks for an embedding pseudopotential HFS-LCAO scheme applicable to chemisorption calculations and capable of yielding electron densities, interaction energies and one-electron properties.

In recent years numerous chemisorption studies have been performed in which the substrate is represented by a (relatively small) cluster of atoms. The most obvious defect of these calculations is formed by the incorrect boundary conditions of the clusters, which can lead to serious artefacts in computed quantities such as the charge distribution and the chemisorption energy. Embedding methods are meant to remedy this defect by ensuring the proper connection of the cluster with the rest of the (unperturbed) substrate. Apart from being more satisfactory from a theoretical point of view, it is also expected that embedded cluster calculations show a better convergence behaviour with respect to cluster size than bare cluster calculations. The embedding method dealt with in this thesis is the so-called moderately-large-embedded-cluster scheme of Pisani, in which the effect of the substrate is represented by an embedding (Coulomb and exchange) potential and an energy dependent coupling matrix. In its application to transi-

tion metal surfaces, which we intend to study because of their technological importance, especially the pseudopotential version of the HFS-LCAO method is attractive, since it can handle systems with relatively many core electrons in an efficient manner. Although the pseudopotential HFS-LCAO method has been used previously, we found it amenable to improvement. We have generalized it for the calculation of interaction energies and studied its behaviour for one-electron properties.

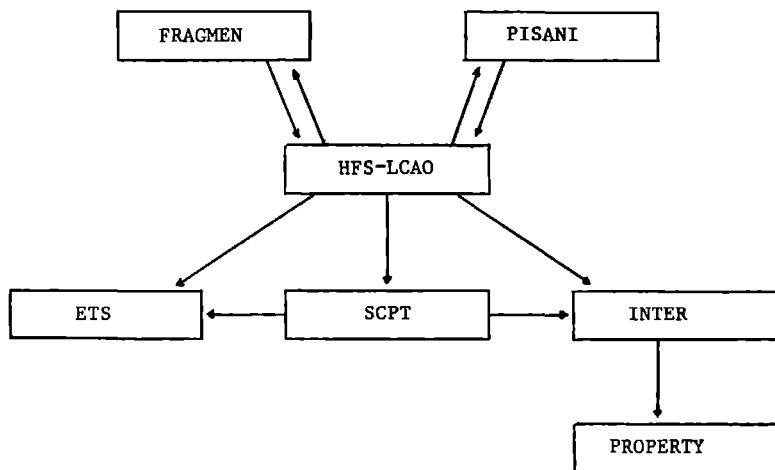
In chapter II we describe the calculation of the Mössbauer parameters for a series of thirteen antimony compounds. This study was initiated because of the unsatisfactory results for the quadrupole splittings in these compounds given by Extended Hückel calculations. The procedure to obtain electric field gradients in all-electron and frozen-core HFS-LCAO calculations is investigated for the HCl molecule. This chapter is somewhat isolated from the rest of this thesis in its physical contents; however, it involves the same method of calculating one-electron properties as used in chapter IV.

In chapters III - V we deal with the pseudopotential HFS-LCAO method as such. In chapter III we develop and test a scheme for the calculation of interaction energies. Our method involves the use of a new, self-consistent perturbational scheme for the calculation of the pseudo-orbitals. The calculation of one-electron properties is treated in chapter IV; the scheme used in chapter II is extended in order to include the use of core orthogonalized and perturbed pseudo-orbitals. We conclude our investigation of the pseudopotential method in chapter V with a discussion of the application of perturbation theory to correct for the use of averaged pseudopotentials.

In chapter VI we describe the moderately-large-embedded-cluster scheme for chemisorption calculations and its implementation in the pseudopotential HFS-LCAO method. The scheme is formulated for a finite representation of the substrate, viz. a cluster which is large compared to the original chemisorption cluster. We present some test calculations for the on-top adsorption

of hydrogen on the unreconstructed lithium (100) surface.

Quantum chemistry hinges heavily on the use of computers for its calculations. The development of computational methods consists to a large extent of writing and modifying computer programs of considerable size. The present work forms no exception to this rule. In the following scheme we have indicated the programs that play a rôle in this thesis:



The central program is, of course, the HFS-LCAO program, used for the self-consistent calculation of the molecular orbitals in the HFS model. In order to obtain the interaction energy between certain fragments upon combination to an overall molecule, the additional programs FRAGMEN and ETS are used. First, one performs HFS calculations for the separate fragments and combines the resulting data with FRAGMEN, then performs an overall molecule HFS calculation and finally calculates the interaction energy with ETS. The program ETS also performs a population analysis of the overall molecule in terms of fragment orbitals.

One-electron properties may be calculated from the molecular orbitals obtained with HFS-LCAO, by use of the standard properties program PROPERTY. An interface, INTER, is needed to expand Slater type basis functions in Gaussian type basis functions. In pseudopotential calculations the orbitals may also be orthogonalized to the cores.

Program SCPT is a self-consistent perturbational program, optionally used to correct the pseudo-orbitals calculated with averaged pseudopotentials. The perturbed pseudo-orbitals can be used to obtain perturbation corrected interaction energies and one-electron properties.

Cluster embedding calculations require three steps, two of which are performed by the HFS-LCAO program, which is extended for this purpose, viz. the self-consistent calculation on the substrate cluster and the actual embedded cluster calculation. Program PISANI is used to select a cluster from the substrate and to condense the substrate electronic structure into the form of an embedding potential and an energy dependent coupling matrix.

C H A P T E R I I

HARTREE-FOCK-SLATER LCAO CALCULATION OF THE MOSSBAUER PARAMETERS OF SOME ANTIMONY COMPOUNDS

Walter RAVNEK, Jan W M JACOBS* and Ad VAN DER AVOIRD

Institute of Theoretical Chemistry University of Nijmegen Toernooiveld, Nijmegen The Netherlands

Received 21 January 1983

This paper describes a (non empirical) Hartree Fock Slater ($X\alpha$) LCAO study of the Mössbauer parameters in a series of thirteen Sb compounds SbX_3 ($X = F Cl Br I$) $Sb(CH_3)_3$, Cl_3 , $N(N=123)$ SbX_3 ($X = F Cl$) and $Sb(CH_3)_3X_2$ ($X = F Cl Br I$) in relation with the chemical bonding in these compounds. The calculated isomer shifts agree very well with the experimental data (correlation coefficient 0.99 $\Delta R/R = -1.08 \times 10^{-3}$). The quadrupole splitting for the Sb(III) compounds is consistently (correlation coefficient 0.97) too small by a factor of 2.7 for the Sb(V) compounds the results are more scattered and even smaller. The proportionality factor could be partly due to the uncertainty in the ^{121}Sb nuclear quadrupole moment and partly to the neglect of core polarization effects in the (frozen core) HFS LCAO calculations. Test calculations on HCl which are also reported in this paper show that the HFS LCAO method can yield accurate core polarization corrections to the quadrupole splitting (Sternheimer factors) but only at the cost of an expensive numerical integration scheme. The results suggest further that the structures of some of the Sb compounds might be different from what has previously been proposed.

1 Introduction

Since 1960 a large number of Mossbauer spectra have been measured and there has been considerable theoretical effort to calculate the electronic parameters related to these spectra: the electron density and the electric-field gradient (EFG) at the nucleus of the Mossbauer-active atom. Most attempts to rationalize Mossbauer data with quantum chemical methods have made use of semi-empirical techniques such as the extended Huckel and the CNDO method. More recently the scattered-wave $X\alpha$ method has been applied, mainly to compounds containing Fe [1]. Moreover, there exist also a few (ab initio) Hartree-Fock LCAO treatments of Fe complexes [2] where the Mössbauer parameters are obtained without introducing any empirical data.

As an alternative non-empirical method which yields rather accurate molecular properties and is

cost-effective, so that it can be applied to larger molecules, we consider the Hartree-Fock-Slater LCAO method [3]. It has been used by Geurts et al. [4] to calculate the quadrupole splitting for the complexes $[Fe_4S_4(SH)_4]^{0,2-,3-}$, which model the 4-Fe active site in high-potential iron-protein and ferredoxin. Guenzburger and Ellis [5] applied the closely related HFS discrete variational method (DVM) to calculate the quadrupole splitting and the isomer shift for some linear Au(I) compounds.

The procedure applied by Guenzburger and Ellis [5] differs from the standard HFS DVM method in the numerical integration. They derived a new integration scheme that makes optimum use of the axial symmetry of their compounds and particularly emphasizes the core region. They calculate the EFG by using an analytical procedure for the one-centre terms and a numerical procedure for the two- and three-centre terms.

Geurts et al. [4] employ the standard HFS LCAO method; they calculate the EFG using a STO-GTO expansion and a standard molecular properties program, that also calculates the multi-centre contributions to the EFG analytically.

* Present address: Philips Research Laboratories Eindhoven The Netherlands

In this paper we apply the method of Geurts et al to a group of thirteen antimony compounds, viz SbX_3 ($X = \text{F, Cl, Br, I}$), $\text{Sb}(\text{CH}_3)_N\text{Cl}_{3-N}$ ($N = 0, 1, 2, 3$), SbX_5 ($X = \text{F, Cl}$) and $\text{Sb}(\text{CH}_3)_3\text{X}_2$ ($X = \text{F, Cl, Br, I}$). Moreover, the calculational procedure was subjected to a more detailed investigation and test on the HCl molecule. Our interest in the Sb compounds was aroused by Stevens and Keijzers [6], who noted a fundamental discrepancy between extended Huckel results for Sb(III) and Sb(V) compounds and the experimental Mössbauer data.

2. Calculational procedures

2.1 The HFS LCAO method

The Hartree-Fock-Slater (HFS) or $X\alpha$ method [7] is characterized by the following one-electron equation

$$\left(-\frac{1}{2} \nabla^2(1) + \sum_A (-Z_A/r_{A1}) + \frac{1}{2} \int r_{12}^{-1} \rho(2) d\tau_2 - \frac{3}{2} \alpha (3/\pi)^{1/3} [\rho(1)]^{1/3} \right) \phi_\mu(1) = \epsilon_\mu \phi_\mu(1), \quad (1)$$

with the electron density given by

$$\rho(1) = \sum_\mu n_\mu \phi_\mu^*(1) \phi_\mu(1) \quad (2)$$

(we use atomic units unless specified otherwise). In the HFS LCAO method, developed by Baerends et al [3], eq (1) is replaced by a secular problem and the matrix elements are (partly) calculated by numerical integration. In several respects, it is similar to the discrete variational method (DVM) introduced by Ellis and Painter [8]. For the further discussion we mention that the point distribution in the numerical integration is given by a superposition of Fermi distributions

$$F(r) = \{1 + \exp[\beta_A(r - r_A)]\}^{-1}, \quad (3)$$

centered at the nuclei A, where β_A and r_A are parameters to be specified, the relative weights of the distributions are given by the fractions f_A of the total number of integration points (N), that are assigned to the nuclei A

Furthermore, the HFS LCAO method makes use of fit functions for representing the electron density

$$\rho(1) \approx \sum_i a_i f_i(1), \quad (4)$$

in order to reduce the number of integrals in the calculation of the Coulomb potential

$$V_C(1) = \sum_i a_i \int r_{12}^{-1} f_i(2) d\tau_2 \quad (5)$$

The coefficients a_i are determined by a least-squares fitting procedure to the "exact" density (2) in any cycle of the iterative (SCF) scheme to solve eq (1). It is thus "exact" density which will be used, after convergence, to calculate the Mössbauer parameters.

We note here that, starting from the $X\alpha$ local exchange approximation, the HFS LCAO method is not subject to any further assumptions with respect to the form of the potential. In particular, one does not use the (rather crude) muffin-tin approximation employed in the multiple-scattering $X\alpha$ method [9]. It has been demonstrated [10] that it is a very useful tool for rather accurate calculations of various molecular properties.

2.2 Mössbauer parameters

The two parameters describing Mössbauer spectra are the isomer shift (IS) and the quadrupole splitting (QS). These quantities are directly related to the electron distribution in the molecular system, the IS to the electron density, the QS to the EFG, both at the nucleus of the Mössbauer-active atom [11,12].

The IS δ is given by the following first-order perturbation expression

$$\delta = \frac{2}{3} \pi Z R^2 (\Delta R/R) S'(S) [\rho_A(0) - \rho_S(0)], \quad (6)$$

where Z is the nuclear charge, R the nuclear radius, ΔR its increase upon excitation and $S'(Z)$ a dimensionless quantity correcting for relativistic effects (e.g., for Sb with $Z = 51$, $S' = 2.38$ [12]), the subscripts S and A refer to source and absorber, respectively. In an LCAO calculation the density (2) at the nucleus follows from

$$\rho(0) = \sum_\mu n_\mu \sum_{p,q} C_{p\mu}^* C_{q\mu} \chi_p^*(0) \chi_q(0), \quad (7)$$

where (χ_μ) denotes the set of AOs and the $C_{\rho\mu}$ are expansion coefficients. In semi-empirical calculations one calculates the contribution from the valence orbitals as

$$\rho_{\text{val}}(0) = N_{\text{val}}(1 - \beta)|\chi_{\text{val}}(0)|^2, \quad (8)$$

where N_{val} is the (Mulliken) net atomic population ($\sum_\mu n_\mu C_{\rho\mu}^2$) of the s-type valence orbital and $(1 - \beta)$ is a screening factor [13]

The electrostatic quadrupole interaction between the asymmetric nuclear charge distribution, described by the nuclear quadrupole moment Q , and an inhomogeneous electric field, described by the EFG tensor V , gives rise to a splitting of the nuclear energy levels [11].

$$E_Q = [V_{zz}Q/4I(2I - 1)][3m^2 - I(I + 1)] \times (1 + \frac{1}{3}\eta^2)^{1/2}, \quad (9)$$

where I is the nuclear spin ($> \frac{1}{2}$), m , its z component, V_{zz} the dominant element of the diagonalized EFG tensor and $\eta = (|V_{xx} - V_{yy}|/V_{zz})$ the asymmetry parameter

The elements of the EFG tensor are calculated as a sum of nuclear and electronic contributions:

$$V_{ij} = V_{ij}^{\text{nuc}} + V_{ij}^{\text{el}}, \quad i, j = \{x, y, z\},$$

$$V_{ij}^{\text{nuc}} = \sum_B Z_B (3R_{B_i}R_{B_j} - \delta_{ij}R_B^2)/R_B^5,$$

$$V_{ij}^{\text{el}} = -\langle \Phi | \sum_k (3r_{k_i}r_{k_j} - \delta_{ij}r_k^2)/r_k^5 | \Phi \rangle. \quad (10)$$

In a LCAO calculation the electronic contribution to the EFG can be separated into one-, two- and three-centre terms. Denoting the Mössbauer-active nucleus as A (all coordinates R_B and r_k are measured with respect to this nucleus), the other nuclei as B, C, one obtains:

$$V_{ij}^{\text{el}} = V_{ij}^{\text{el}1} + V_{ij}^{\text{el}2} + V_{ij}^{\text{el}3},$$

$$V_{ij}^{\text{el}1} = \sum_\mu n_\mu \sum_{a, a''}^A C_{a\mu}^* C_{a''\mu} \times \langle \chi_a | (3r_i r_j - \delta_{ij} r^2)/r^5 | \chi_a \rangle,$$

$$V_{ij}^{\text{el}2} = 2 \sum_\mu n_\mu \sum_a^A \sum_{B(\neq A)}^B \sum_b C_{a\mu}^* C_{b\mu}$$

$$\times \langle \chi_a | (3r_i r_j - \delta_{ij} r^2)/r^5 | \chi_b \rangle$$

$$+ \sum_\mu n_\mu \sum_B \sum_{b', b''} C_{b'\mu}^* C_{b''\mu}$$

$$\times \langle \chi_b | (3r_i r_j - \delta_{ij} r^2)/r^5 | \chi_b \rangle,$$

$$V_{ij}^{\text{el}3} = \sum_\mu n_\mu \sum_{B(\neq A)}^B \sum_{C(\neq A, B)}^C \sum_c C_{b\mu}^* C_{c\mu}$$

$$\times \langle \chi_b | (3r_i r_j - \delta_{ij} r^2)/r^5 | \chi_c \rangle. \quad (11)$$

In practice one often neglects the three-centre terms and assumes that the two-centre terms cancel the nuclear contribution, thus retaining the one-centre electronic terms only [14].

In semi-empirical calculations on systems with p-type valence shells one uses the Townes-Dailey equation [15], which reads

$$V_{zz} = \langle r^{-3} \rangle_p (N_p - \frac{1}{2}N_{p_x} - \frac{1}{2}N_{p_y})(1 - R). \quad (12)$$

Here $\langle r^{-3} \rangle_p$ is the expectation value over the p valence orbital in the free atom, the N_s are net atomic orbital populations and $(1 - R)$ is the Sternheimer correction discussed in section 2.3.

2.3 Frozen-core calculations. the Sternheimer effect

In molecular calculations one often uses the frozen-core approximation, assuming that the cores of the atoms in a molecular system are unaffected by the chemical bonding. Since in such a treatment the cores stay spherically symmetric, the core of the Mössbauer-active atom gives a constant contribution to the density at the nucleus $\rho(0)$ and a zero contribution to the EFG.

This approximation seems to work reasonably well for $\rho(0)$, differences in $\rho(0)$ for inner core orbitals are shown to be very small for free atoms in different oxidation states [2,16]. For outer core orbitals the situation is somewhat less clear-cut [2,16]. For the EFG, however, the approximation breaks down: the core electrons are polarized by the distorted valence-electron distribution and the field due to the nuclei and the cores of the other atoms in the system. The distortion is small, but it is amplified by the large values for $\langle r^{-3} \rangle$ in the calculation of the EFG tensor. This core polariza-

tion or Sternheimer shielding [17] is allowed for in frozen-core calculations by the use of the Sternheimer factor R

$$V_{zz}^{\text{observed}} = (1 - R)V_{zz}^{\text{valence}} \quad (13)$$

More correctly one uses a Sternheimer factor R^{ab} for every orbital pair (a, b) It is to be noted, however, that the use of Sternheimer factors corrects for approximations in the MO calculation In an all-electron calculation the core polarization is taken into account in a self-consistent manner and there is no need to use Sternheimer factors to correlate the results with experiment

One has tried to calculate Sternheimer factors from atomic models [17,18] The use of such correction factors in molecular calculations should, for various reasons, be regarded with scepticism

2.4 Computational procedure

We have used the HFS LCAO program of Baerends et al [19], adapted to IBM In all our calculations we have taken the exchange parameter α fixed at 0.7 [3] For fitting the electron density (4) we took a subset of all products of the STO basis functions on the atomic centres

The density at the nucleus of the Mossbauer-active centre may easily be obtained from the converged charge-and-bond-order matrix of the SCF calculation

The EFG was calculated using the one-electron properties package of the POLYATOM program [20], which is based on GTOs This properties package calculates all multicentre terms, so that we could check approximations made with respect to two- and three-centre terms

Further we have used an interface program that reads the converged SCF data from the HFS LCAO program, expands the STOs in GTOs and prepares the input for the properties package The STO GTO expansion is performed according to the method of maximum overlap fits of Stewart [21] Each (n, l) STO is expanded in a number of ($l+1, l$) GTOs, i.e. s-type STOs in 1s GTOs, p-type STOs in 2p GTOs, etc The number of GTOs may vary between 1 and 6

3. Test calculations on HCl

We have chosen the HCl molecule to perform some test calculations because it is sufficiently small to investigate the influence of all relevant parameters and there are extensive data available in the literature allowing us to check our results All our calculations were performed for HCl at the equilibrium geometry ($R = 2.4086$ bohr), which has an experimental EFG at the chlorine nucleus $q_{\text{exp}} = -3.641$ au (calculated from $e^2qQ = 67.0 \pm 0.6$ MHz and $Q = -0.0782$ barn [22]), hence the electronic contribution $q_{\text{exp}}^{\text{el}} = -3.498$ au

The nine occupied MOs in HCl can be subdivided into two sets on the one hand, $1\sigma, 2\sigma, 3\sigma, 1\pi_x$ and $1\pi_y$, which have mainly Cl core character and on the other hand, the occupied combinations of $3s^{\text{Cl}}, 3p_z^{\text{Cl}}$ and $1s^{\text{H}}$ 4σ and 5σ , and the non-bonding $2\pi_x$ and $2\pi_y$ (the molecule is taken along the z axis) In the calculation of the EFG we make

Table 1
STO basis sets used for HCl

Orbital	Exponent		
	Cade-Huo [23] like ^{a)}	HFS TZ [29]	
Cl	1s	18.673	13.95
	2s	16.428	5.65
	3s	5.794	
		10.116	3.30
		2.792	2.30
	2p	1.715	1.60
		14.021	6.70
		8.325	
	3p	5.267	
		2.514	2.85
1.389		2.05	
3d		1.20	
	2.40	2.40	
H	1s	1.508	
		2.568	
	2s	2.270	
	2p	1.763	

^{a)} The 3d polarization function for H has been omitted unlike Cade and Huo we take the same exponents for the σ and π basis

Table 2
EFG and $\rho(0)$ (in au) for HCl

	q^{core}	q^{val}	q^{el}	$10^3\rho(0)$
HFS LCAO, all electron ^{a)}				
$N = 800$	-3 481	-3 577	-7 038	3 1096
$N = 2500$	1 070	-3 150	-2 080	3 1654
$N = 5000$	0 148	-3 090	-2 942	3 2134
$N = 10000$	0 088	-3 055	-2 967	3 2028
$N = 15000$	-0 079	-3 058	-3 136	3 1962
$N = 20000$	-0 046	-3 072	-3 118	3 1974
$N = 25000$	-0 181	-3 092	-3 273	3 1978
$N = 30000$	-0 156	-3 082	-3 238	3 1978
HFS LCAO, frozen core ^{b)}				
$r_{\text{Cl}} = 2.0, \beta_{\text{Cl}} = 1.0$			-2 763	
$r_{\text{Cl}} = 1.44, \beta_{\text{Cl}} = 1.2$			-2 755	
$r_{\text{Cl}} = 1.0, \beta_{\text{Cl}} = 1.2$			-2 769	
$r_{\text{Cl}} = 1.44, \beta_{\text{Cl}} = 1.5$			-2 718	
Petke and Whitten [25]	-0 221	-3 687	-3 898	
Scrocco and Tomasi [26]	-0 642	-3 147	-3 789	
Moccia ^{c)}	-0 886	-2 846	-3 733	
McLean and Yoshimine [22]	-0 451	-2 952	-3 403	
Cade and Huo [23]	-0 518	-2 959	-3 478	
Grabenstetter and Whitehead [27]	-0 539	-2 955	-3 494	
experiment [2]			-3 498	

^{a)} Using the Cade-Huo like basis of table 1. Other integration parameters fixed at $f_{\text{Cl}} = 0.8$, $r_{\text{Cl}} = 1.449$, $\beta_{\text{Cl}} = 1.389$, $f_{\text{H}} = 0.2$, $r_{\text{H}} = 0.507$, $\beta_{\text{H}} = 1.508$.

^{b)} Using the HFS TZ basis of table 1. Other integration parameters fixed at $N = 1000$, $f_{\text{Cl}} = 0.8$, $f_{\text{H}} = 0.2$, $r_{\text{H}} = 0.564$, $\beta_{\text{H}} = 1.508$. See also text.

^{c)} Calculated by Grabenstetter and Whitehead [27] from the MOs given by Moccia [28].

the corresponding separation

$$q^{\text{el}} = q^{\text{core}} + q^{\text{val}} \quad (14)$$

In the HFS calculations the fractions of the integration points per centre were taken as $f_{\text{Cl}} = 4/5$, $f_{\text{H}} = 1/5$ throughout. Convergence of the SCF procedure was achieved to 3×10^{-6} for the mean change in the diagonal elements of the charge-and-bond-order matrix. For the calculation of the EFG we used an expansion of all STOs in six GTOs [4].

In the first place we performed all-electron calculations with a basis set derived from the one used by Cade and Huo [23], see table 1. We used a density fit set containing 9 s, 7 p and 5 d functions on Cl and 3 s and 1 p functions on H. Inclusion of some additional f- and g-type fit functions had no effect on the calculated EFG. Varying the integration parameters r_{A} and β_{A} (3) for the usual num-

bers of integration points ($N = 1000-2500$) we found the EFG to be extremely sensitive, much more so than the one-electron eigenvalues. This is not surprising since the HFS LCAO method has been developed for valence-electron properties, which is reflected in the use of the Fermi distribution that emphasizes the valence region. For the EFG the core region should also be very accurately described (due to the $\langle r^{-3} \rangle$ weighting).

This sensitivity with respect to the integration parameters has led us to examine the influence of increasing the number of integration points beyond the limits normally used. From table 2 one can clearly see that the instability in the EFG is mainly due to the core contribution, which is not quite stable yet at $N = 15000$. It can also be seen from table 2 that the density at the nucleus is much more well-behaved.

Comparing with the EFG calculations from the

Table 3
Comparison of some properties (in au) of HCl between the present HFS calculation and the literature

Property ^{a)}	McLean and Yoshimine (HF LCAO) [22]	HFS LCAO ^{b)}	Difference (%)
$\langle r_1^{-1} \rangle$	64 822	64 380	0.7
$\langle r_2^{-1} \rangle$	8 001	7 987	0.2
$\langle x_1 \rangle$	1 931	1 881	2.6
$\langle x_1^2 \rangle$	13 389	13 384	0.03
$\langle x_1^2 + y_1^2 \rangle$	20 871	20 861	0.05
$\langle r_1^2 \rangle$	34 260	34 245	0.04
$\langle x_1 r_1^{-3} \rangle$	0 168	0 139	21.1
$\langle z_2 r_2^{-3} \rangle$	-2 939	-2 911	1.0
$\langle (3z_1^2 - r_1^2)r_1^{-3} \rangle$	-3 419	-3 238	5.6
$\langle (3z_2^2 - r_2^2)r_2^{-3} \rangle$	2 153	2 115	1.8

^{a)} Indices 1 and 2 refer to Cl and H as origins respectively

^{b)} All-electron HFS LCAO calculation with $N = 30000$ (see table 2)

literature it is observed that the core contribution is the more variable one also in general The difference between the various results can be largely ascribed to this contribution We note that there is reasonable agreement between the HFS LCAO calculation and other (ab initio HF LCAO) calculations

In table 3 we compare some other properties of HCl with McLean and Yoshimine's HF LCAO results [22] (obtained with Cade and Huo's basis [23] extended with another 12 STOs) For the positive moments of the electron density the agreement is quite good, whereas for the negative moments it is only satisfactory Again, this reflects the valence electron directed character of the HFS LCAO method

Just as Guenzburger and Ellis [5] we tried to increase the stability of the all-electron calculation by changing the point distribution in the numerical integration, especially to improve the core description Guenzburger and Ellis performed the angular integration by imposing the axial symmetry of their molecules on the electron density In their calculations they still needed 29000 integration points to obtain core contributions stable to six decimal figures Since the antimony compounds we are interested in are non-linear, we tried a different approach First we followed a suggestion of Ellis [24] to use a superposition of two Fermi distributions centered at the Cl nucleus,

secondly we changed the Fermi distribution into an exponential distribution It turned out that for equal numbers of integration points, no substantial improvement over the usual procedure was obtained Thus indicates that the essential feature of the method employed by Guenzburger and Ellis is the full use of the $C_{\infty v}$ or $D_{\infty h}$ symmetry

Beside the all-electron calculations we also performed frozen-core calculations with the 1s, 2s and 2p orbitals as Cl core We used the HFS TZ basis [29], listed in table 1, for Cl and a Cade-Huo like basis set for H As expected from the preceding results, the calculated EFG appeared to be much more stable with respect to variations in the integration parameters than for the all-electron case (see table 2, the variation in q^{cl} over the same range of integration parameters amounts to as much as 2.7 au in the all-electron calculations) Because the core is frozen now, we neglect the core polarization, the overall Sternheimer factor is found to be $1 - R = 1.18$ for HCl

Finally, we varied the size of the Cl core It turned out that instabilities in the EFG arose as soon as the Cl 2p orbital was included in the valence set

We conclude that it is possible to obtain stable EFGs within the HFS LCAO method either by performing all-electron calculations with very large numbers of integration points or by performing frozen-core calculations with a standard choice of integration parameters Calculations of the first kind are rather expensive and, so, they are not very advantageous with respect to ab initio quantum-chemical methods For many problems of chemical interest the first option may be impractical, however If one is interested in relative changes of Mössbauer parameters among series of similar compounds (where the Sternheimer factor may be assumed constant) the HFS LCAO frozen-core method forms a more reliable alternative for the often used semi-empirical methods

4. Calculations on antimony compounds

4.1 Available Mössbauer data

Mössbauer data are known on many antimony compounds, a thorough theoretical explanation of

Table 4
Experimental Mössbauer parameters ^{a)}

Molecule	δ (mm s ⁻¹) (relative to InSb)	e^2qQ (mm s ⁻¹)	η	Ref
SbF ₃	-5.97	19.7		[38]
	-6.0	19.6		[39]
	-6.04 ^{b)}	19.6		[40]
	-6.29 ^{c)}	19.1		[41]
SbCl ₃	-5.24 ^{b)}	12.2		[40]
	-5.77 ^{d)}	12.2	0.19	[42]
	-5.87 ^{c)}	12.25	0.187	[44]
	-5.9	13.2	0.2	[43]
	-5.9	13.9		[45]
	-6.94 ^{b)}			[46]
SbBr ₃	-5.87 ^{d)}	11.6	0.1	[42]
	-5.9	11.6		[45]
	-5.9	10.7	0.3	[43]
	-5.92 ^{c)}	11.6	0.39	[44]
	-6.94 ^{b)}			[46]
	-7.24 ^{b)}			[47]
SbI ₃	-7.34 ^{b)}			[40]
	-7.67 ^{d)}	5.6		[42]
	-7.7			[43]
	-7.74 ^{b)}			[47]
	-7.94 ^{b)}			[46]
SbF ₅	10.2	8.7		[53]
	10.3	8.7		[54]
	10.79 ^{b)}			[40]
SbCl ₅	5.06 ^{b)}			[55,56]
	5.2	-5.7		[53,54]
	5.44 ^{b)}	-4.4		[40]
SbMeCl ₂	-4.2	31.0	0.35	[31]
	-4.37	30.0		[42]
SbMe ₂ Cl	-2.5	31.7	0.77	[31]
	-2.6	30.0	0.82	[31]
	-3.07 ^{d)}	-26.0	0.9	[42]
SbMe ₃	0.00 ^{d)}	15.2		[42]
	-0.22	16.3		[48]
	2.42 ^{d)}	-24.0		[49,50]
SbMe ₃ Cl ₂	2.49	-24.0		[51]
	2.86 ^{b)}	-24		[50]
	2.13 ^{d)}	-22.1		[49,50]
	2.20	-22.1		[51]
SbMe ₃ Br ₂	2.38 ^{c)}	+21.43		[52]
	2.38 ^{c)}	+20.9		[52]
	2.56 ^{b)}	-22		[51]
	2.16	-19.28		[51]

^{a)} Experimental data of SbMe₃F₂ unknown

^{b)} Measured with SnO₂ as source

^{c)} Measured with BaSnO₃ as source

^{d)} Measured with CaSnO₃ as source

the parameters in terms of electronic quantities is still lacking, however. The discussions of Sb compounds are either based on simple qualitative models [30,31] or on semi-empirical calculations [13,32–34]. Usually one treats a series of related compounds, in order to study the effect of substitution of one or more organic by inorganic ligands. One such series is $\text{Sb}(\text{CH}_3)_N \text{Cl}_{3-N}$ ($N = 0, 1, 2, 3$) for which Stevens et al. [31] gave a qualitative explanation of the IS and the QS as a function of N . Stevens et al. also performed extended Huckel calculations and they found the size of the QS to agree reasonably well with experiment. For some Sb(V) compounds, however, the method failed: the calculated QS was a factor of 10 too small compared with experiment [6].

Here we consider four series of antimony compounds: two containing Sb(III), viz SbX_3 ($X = \text{F}, \text{Cl}, \text{Br}, \text{I}$) and $\text{Sb}(\text{CH}_3)_N \text{Cl}_{3-N}$ ($N = 0, 1, 2, 3$) and two containing Sb(V), viz SbX_5 ($X = \text{F}, \text{Cl}$) and $\text{Sb}(\text{CH}_3)_3 \text{X}_2$ ($X = \text{F}, \text{Cl}, \text{Br}, \text{I}$). In table 4 we present a survey of the experimental Mossbauer data on these molecules. In order to facilitate comparison of the numbers, we have shifted all isomer-shift data relative to InSb. We used the following isomer shifts for InSb with respect to

various sources: $\delta = -8.53 \text{ mm s}^{-1}$ for CaSnO_3 [35], $\delta = -8.5 \text{ mm s}^{-1}$ for BaSnO_3 [36] and $\delta = -8.56 \text{ mm s}^{-1}$ for SnO_2 [37].

Regarding the QS, we wish to make a special comment on the sign. The fit procedure used to determine the Mossbauer parameters from experimental spectra is sensitive to the magnitude of the QS, but not very sensitive to its sign. For SbMe_3Br_2 we found contradictory data, looking at the other two compounds from the series SbMe_3X_2 we think it likely that the sign should be negative (which is confirmed by our calculations, see below). For SbMe_2Cl both the available references give a negative sign for the QS. Still we think it probable that the sign is positive since it is unlikely that in the series $\text{SbMeCl}_2\text{-SbMe}_2\text{Cl-SbMe}_3$, the QS will change sign twice upon substitution. Again, this will be confirmed by our calculations.

4.2 Calculations

Table 5 lists the geometries of the molecules used in our calculations. We have assumed C_{3v} point group symmetry for all molecules except $\text{Sb}(\text{CH}_3)_2\text{Cl}$ and $\text{Sb}(\text{CH}_3)\text{Cl}_2$, for which we adopted C_s point group symmetry. By conse-

Table 5
Geometries used for the antimony compounds^{a)}

Molecule	Ref	Distances (Å)		Angles (deg)		
		Sb-X	Sb-C	X-Sb-X	X-Sb-C	C-Sb-C
SbF_3	[31]	2.00	-	81.9	-	-
SbCl_3	[57]	2.360	-	95.2	-	-
SbBr_3	[58]	2.51	-	97	-	-
$\text{SbI}_3 \text{ A}$	[59]	2.67	-	99	-	-
$\text{SbI}_3 \text{ B}$	[31]	2.87	-	95.8	-	-
SbMeCl_2	[31]	2.355	2.132	95.2	97	-
SbMe_2Cl	[31]	2.355	2.132	-	97	105
SbMe_3	[31]	-	2.132	-	-	98
SbF_5	[13]	eq 2.00 ax 2.13	-	180 and 120	-	-
SbCl_5	[60]	eq 2.29 ax 2.34	-	180 and 120	-	-
SbMe_3F_2	[61]	2.091	1.997	180	90	120
SbMe_3Cl_2	[62, 63]	2.355	2.132	180	90	120
SbMe_3Br_2	[62]	2.471	2.143	180	90	120
SbMe_3I_2	[62]	2.609	2.164	180	90	120

^{a)} C-H = 1.091 Å and $\angle\text{H-C-H} = 95.2^\circ$ throughout

Table 6
Exponents of STO basis sets used in the calculations (in au) [29]

	H	C	F	Cl	Br	I	Sb
1s	1 383 0 783	5 40	8 33	14 55	23 90	36 40	36 65
2s		1 98 1 24	3 32 1 92	5 60	13 75	19 40	18 20
2p		2 20 0 96	3 52 1 48	6 65	14 50	24 85	24 75
3s				2 90 1 75	7 05	11 95	11 45
3p				2 45 1 30	7 35	10 50	8 95
3d					5 34	11 60	10 94
4s					3 25 1 95	6 90	6 55
4p					2 65 1 40	7 10	7 10
4d						4 69	5 45 3 05
5s						3 20 1 95	2 85 1 70
5p						2 65 1 45	2 25 1 20

quence, the asymmetry parameter η can be non-zero for the latter two molecules only. In establishing the geometries we made use of X-ray data as much as possible.

For the series SbX_3 we took the angles and distances mentioned by Bowen et al [37], for SbI_3 we also used the geometry proposed by Wells [59] (structure A). The angles in the series $\text{Sb}(\text{CH}_3)_N\text{Cl}_{3-N}$ are those suggested by Stevens et al [31], the distances were estimated. The structures of SbF_3 and SbCl_3 are rather uncertain [37], one has assumed a pure trigonal bipyramid, but also a deformed octaeder has been proposed. For SbF_3 we used Kotheekar's geometry [13], for SbCl_3 Polynova's [60] which also has been adopted by Baltranas et al [34]. We also tried to find structural data on SbBr_3 and SbI_3 , since we did not succeed, we omitted them from our calculations. The series $\text{Sb}(\text{CH}_3)_2\text{X}_2$, finally, has a trigonal bipyramidal structure with the methyl groups in the equatorial positions [62]. For $\text{X} = \text{F}$ the X-ray data are known [61]. The Sb-Cl distance was taken as in $[\text{Sb}(\text{CH}_3)_2\text{Cl}]_2$ [63]. The Sb-Br distance used is an average of some distances known from X-ray diffraction, the Sb-I distance was estimated.

We performed frozen-core HFS LCAO calculations with the exchange parameter $\alpha = 0.7$ throughout [3]. The cores taken are 1s for C and F, 1s-2p for Cl, 1s-3d for Br, 1s-4d for I and 1s-4p for Sb, so for Sb the 4d was included in the valence set. The basis sets employed [29] are listed in table 6. They are of double-zeta type for the valence orbitals, supplemented with single-zeta core functions to allow for core orthogonalization. In the density-fit procedure we gave special attention to the Sb atom, for Sb we used a fit set consisting of 12 s, 7 p, 6 d, 3 f and 2 g Slater-type functions. The number of integration points used was 2000 for Sb, 600 for halogens, 400 for C and 200 for H. Convergence in the SCF procedure was obtained to 3×10^{-5} for the mean change in the diagonal elements of the charge-and-bond-order matrix.

In the calculation of the EFG the STOs centered on Sb were expanded in five GTOs and those on other atoms in four GTOs, which gives an error of less than 0.01 au in the calculated EFG due to the STO GTO expansion.

We have checked that the Sb core was sufficiently large for the EFG to be stable with respect

to variations in the integration parameters used in the HFS calculation (cf section 3) It turned out that the core taken constitutes the "minimum choice", i.e. inclusion of the 4p orbitals in the valence set causes instabilities under normal integration conditions

4.3 Results and discussion

Tables 7 and 8 and fig 1 summarize our results Table 7 contains the Mulliken gross and net populations of the valence orbitals on Sb First we note that the gross populations of the 4d orbitals stay practically constant at the value 10 for all compounds considered, hence the 4d orbitals play no role of importance in the chemical bonding of antimony Further we see that in all three series SbX_3 , SbX_5 and $\text{Sb}(\text{CH}_3)_3\text{X}_2$ the 5s and 5p populations decrease if we go towards the more electronegative substituent Comparing our gross 5s populations with the values calculated by Kotheke [13], using the CNDO/2 method, we find somewhat larger values, the difference being in the range 0.08–0.21 for SbX_3 and SbCl_3 and 0.42 for SbF_3 The qualitative behaviour is the same, however

In the series $\text{Sb}(\text{CH}_3)_x\text{Cl}_{3-x}$ we observe a fundamentally different behaviour going towards more electronegative substituents (i.e. towards lower N) we notice a decrease in the 5p population but an increase in the 5s population This increase is compatible with the trend in the experimental IS The decreasing 5p population corroborates Steven's hypothesis [31], made to rationalize the experimental Mossbauer parameters

We can use the net orbital populations from table 7 to check the applicability of the Townes Dailey equation (12) According to this equation one would expect the QS to be proportional to the quantity $\Delta = N_{5p_x} - \frac{1}{2}N_{5p_y} - \frac{1}{2}N_{5p_z}$, which we have listed in the last column The agreement appears to be poor, there is only a slight correlation between the Δ values and the experimental QS (correlation coefficient 0.67)

Table 8 contains the calculated EFG The penultimate column contains the quantity $\chi = |(q - q^{\text{eff}})/q|$ which can be considered as a numerical measure for the validity of the assumption that the sum of the two- and three-centre electronic contributions cancels the nuclear contribution This approximation appears to work quite well

Table 7
Mulliken gross and net populations of valence orbitals on Sb

Molecule ^{a)}	Gross populations					Net populations					$Z_{\text{Sb}}^{\text{b)}}$	$\Delta^{\text{c)}}$
	4d	5s	5p _x	5p _y	5p _z	4d	5s	5p _x	5p _y	5p _z		
SbF_3	9.99	1.74	0.47	0.47	0.69	11.26	2.10	0.32	0.32	0.53	1.63	0.21
SbCl_3	9.99	1.85	0.59	0.59	0.88	11.24	2.34	0.38	0.38	0.69	1.10	0.31
SbBr_3	9.98	1.88	0.66	0.66	0.94	11.24	2.37	0.44	0.44	0.77	0.88	0.33
SbI_3 (A)	9.97	1.94	0.74	0.74	0.96	11.22	2.34	0.53	0.53	0.80	0.67	0.27
SbI_3 (B)	9.98	1.94	0.74	0.74	1.05	11.23	2.44	0.51	0.51	0.91	0.58	0.40
SbMeCl_2	9.98	1.79	0.51	0.64	0.95	11.23	2.22	0.32	0.38	0.79	1.13	0.44
SbMe_2Cl	9.98	1.69	0.46	0.60	1.00	11.23	2.09	0.29	0.32	0.87	1.27	0.56
SbMe_3	9.97	1.58	0.54	0.54	1.13	11.22	1.82	0.30	0.30	1.05	1.23	0.75
SbF_2	10.02	1.18	0.50	0.50	0.52	11.29	1.23	0.33	0.33	0.34	2.27	0.01
SbCl_2	10.03	1.41	0.78	0.78	0.80	11.28	1.47	0.51	0.51	0.52	1.21	0.00
SbMe_3F_2	10.01	1.05	0.63	0.63	0.39	11.28	0.93	0.37	0.37	0.27	2.29	-0.10
SbMe_2Cl_2	10.00	1.30	0.67	0.67	0.60	11.26	1.19	0.38	0.38	0.39	1.76	0.00
SbMe_3Br_2	10.00	1.35	0.68	0.68	0.65	11.25	1.27	0.39	0.39	0.46	1.63	0.07
SbMe_3I_2	9.98	1.41	0.67	0.67	0.75	11.24	1.33	0.38	0.38	0.59	1.51	0.21

^{a)} Molecules are placed so that the z axis is the lone pair axis

^{b)} Atomic charge of Sb from gross populations

^{c)} $\Delta = N(5p_x) - \frac{1}{2}N(5p_y) - \frac{1}{2}N(5p_z)$, where the N are net populations see also text

Table 8
Field gradients^{a)} (in au) and quadrupole splittings (in mm s⁻¹)

	q^{e1}	$q^{e1,2}$	$q^{e1,3}$	q^{e1}	χ ^{b)}	q^{nuc}	$q^{c)}$	$e^2qQ^{d)}$	Average experimental QS
SbF ₃	-3 608	-0 091	0 006	-3 693	0 0069	0 110	-3 58	7 88	19 5
SbCl ₃	-2 726	0 072	0 004	-2 649	0 0125	-0 043	-2 69	5 92	12 8
SbBr ₃	-2 252	0 066	0 004	-2 183	0 0097	-0 048	-2 23	4 91	11 4
SbI ₃ (A)	-1 320	0 030	0 003	-1 288	0 0044	-0 027	-1 31	2 89	5 6
SbI ₃ (B)	-1 921	0 056	0 004	-1 862	0 0043	-0 051	-1 91	4 21	5 6
SbMeCl ₂	-4 407	0 027	-0 011	-4 391	0 0049	-0 037	-4 43	9 74	30 5
SbMe ₂ Cl	-4 576	0 049	0 000	-4 526	0 0025	-0 038	-4 56	10 04	29 2
SbMe ₃	-3 300	0 047	0 013	-3 240	0 0015	-0 065	-3 30	7 27	15 8
SbF ₅	0 330	-0 034	0 003	-0 362	0 0280	0 040	-0 32	0 71	8 7
SbCl ₅	-0 787	-0 066	0 008	-0 845	0 0088	0 065	-0 78	1 72	-5 1
SbMe ₂ F ₂	2 529	-0 234	0 056	2 351	0 0373	0 276	2 63	-5 78	-
SbMe ₂ Cl ₂	1 518	-0 074	0 052	1 496	0 0399	0 086	1 58	-3 48	-24 0
SbMe ₃ Br ₂	1 026	-0 026	0 049	1 049	0 0518	0 033	1 08	-2 38	-21 7
SbMe ₃ I ₂	1 386	0 012	0 041	1 439	0 0034	-0 048	1 39	-3 06	-19 3

^{a)} Using the frozen core approximation no Sternheimer correction applied ^{b)} $\chi = [q - q^{e1,1}]/q$ see also text

^{c)} Calculated asymmetry parameters (in parentheses the experimental value) 0 45 (0 35) for SbMeCl₂ 0 93 (0 83) for SbMe₂Cl

^{d)} Conversion factor 1 au = 2 2 mm s⁻¹ calculated from $Q = -0 28 \pm 0 06$ barn [66]

In order to calculate the QS we used Steven's value for the nuclear quadrupole moment of ¹²¹Sb, $Q = -0 28 \pm 0 06$ barn [66] We note, however, that the value of the nuclear quadrupole moment is actually very uncertain[†] Values ranging from -0 20 to -0 54 barn are found in the literature [39,67,68]

We now compare the calculated QS (with $Q = -0 28$ barn) with experiment For the series SbX₃, the experimental values are accurately reproduced (correlation coefficient 0 99), apart from a constant factor of 2 3 Further we note that structure A for SbI₃ fits better in the trend than structure B For the series SbMe_nCl_{3-n}, the situation is similar (correlation coefficient 0 98), the factor now is 2 8 Taking the two series together one obtains a factor 2 7 (correlation coefficient 0 97) For SbMe₃X₂ the agreement is much worse (a factor of 7 6, correlation coefficient 0 37) although the discrepancy between Sb(III) and Sb(V) compounds is still not as drastic as in the extended Huckel calculations [6] The molecules SbF₅ and SbCl₅ show a very irregu-

lar behaviour, one is led to the conclusion that the geometries used are not correct, a conclusion that is supported by the IS calculations (see below), and by Kothekar's QS results [13]

Let us now briefly analyse the possible sources of the discrepancy between the calculated and the experimental QS the HFS LCAO model, AO basis set deficiency, neglect of relativistic effects, neglect of lattice contributions, neglect of core polarization and finally the uncertainty of the nuclear quadrupole moment With respect to the method and AO basis used we recall that our calculations on HCl and Guenzburger and Ellis's calculations on linear Au compounds have shown that the HFS LCAO method may yield good QSs with AO bases of similar size as used here In order to check the influence of the lattice contributions to the EFG we performed a test calculation for SbCl₃, which has an orthorhombic unit cell with lattice parameters $a = 6 37$ Å, $b = 8 12$ Å, $c = 9 47$ Å and as space group Pbnm [57] We used a point charge model with the Mulliken charges from the HFS LCAO calculation It took thirty shells of equivalent cells to obtain a result stable to two decimal places The result is a lattice contribution $q = -4 3 \times 10^{-3}$ au, which means that even with a Sternheimer factor $1 - \gamma_{\infty} \approx 10$ the lattice

[†] This uncertainty arises because the quantity amenable to measurement is the product of Q and the EFG at the nucleus accurate calculations or independent measurements of the EFG in Sb compounds are not available

contribution is negligible compared to the contribution of the central SbCl_3 molecule itself

The Sternheimer corrections for the neglect of core polarization customarily used for Sb are not much greater than unity (1.115 [64], 1.2 [13], 1.23 [6]). The uncertainty in Q may be the key factor taking $Q = -0.54$ [68] instead of $Q = -0.28$ would yield (together with a Sternheimer factor of 1.4) the factor 2.7 which would lead to very good agreement of the calculated QS with the experimental data for the Sb(III) compounds. At the same time it would reduce the error for the series SbMe_3X_2 to a factor of 3. It is also possible that Q is still larger, however, or that the core polarization effects are more important (actually the 1s-4d Sb core is considerably larger than the 1s-2p core in Cl, where we have calculated a Sternheimer factor of 1.18), while we cannot exclude that relativistic effects might be important, too.

Finally we compare the calculated asymmetry parameters in the two cases where it does not vanish on symmetry grounds SbMe_2Cl and SbMeCl_2 . As can be seen from table 8 the agreement with experiment is satisfactory.

Fig. 1 shows a plot of the calculated values for the valence-electron density at the Sb nucleus versus the (averaged) experimental isomer shifts (with respect to InSb as source). One observes a very nearly linear behaviour as expected theoretically. The only molecules falling aside are SbF_3

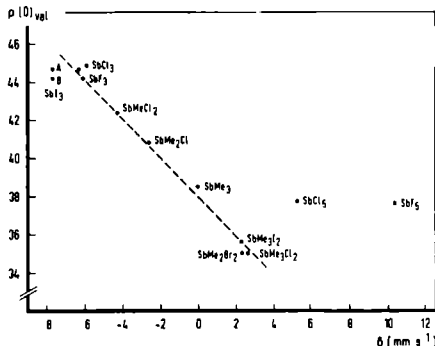


Fig. 1 Relation between the calculated valence-electron density $\rho(0)$ on the Sb nucleus (in 10^{-3} electrons/ a_0^3) and the measured Mössbauer isomer shifts of various Sb compounds

and SbCl_5 , the deviation is too large for being explicable in terms of a possible core contribution to $\Delta\rho(0)$. Hence we feel strengthened in our opinion that the trigonal bipyramidal geometry used is not correct for these molecules. Further we note that also the isomer-shift data indicate a preference of structure A over structure B for SbI_3 .

Making a least-squares fit of all points, except SbF_3 , SbCl_5 and $\text{SbI}_3(\text{B})$, and using the value $\frac{4}{3}\pi ZR^2 S'(Z) = 1.303 \times 10^{-24}$ cm s⁻¹ [13], we calculate $\Delta R/R = -1.08 \times 10^{-3}$ (correlation coefficient 0.99), which agrees very well with the values quoted in the literature, ranging from -1.44×10^{-3} to -0.85×10^{-3} [13,34,39,46,65].

Finally we also checked the linear dependency of the experimental IS on the Sb 5s net population, which has been used in semi-empirical calculations (see section 2.1). Again it is possible to obtain a reasonable linear fit of the data, the only two compounds falling aside are SbF_3 and SbCl_5 .

5. Conclusions

In this paper we have investigated the calculation of Mossbauer parameters by means of the Hartree-Fock-Slater LCAO method. Test calculations on HCl have shown that it is possible to obtain results in good agreement with *ab initio* calculations and experiments. The HFS LCAO all-electron calculations require exceedingly large numbers of numerical integration points, however, which makes the method impractical for larger systems. Frozen-core calculations, on the other hand, yield stable and accurate results (compared with *ab initio* results) at a standard choice of integration parameters. The price one has to pay is the neglect of core polarization effects, which could be corrected for by use of Sternheimer factors for the quadrupole splitting. Such factors are not accurately known, however, but the frozen-core method can still be useful for looking at relative properties in series of related compounds.

We have applied this method of calculation to a group of thirteen antimony compounds. The calculated quadrupole splittings are consistently too small by a factor of 2.7 (correlation coefficient 0.97) for Sb(III) compounds and a factor of 7.6 for

the Sb(V) compounds $\text{Sb}(\text{CH}_3)_3\text{X}_2$ (correlation coefficient 0.37) These factors may be partly due to core polarization, to the uncertainty in the nuclear quadrupole moment, and, possibly, relativistic effects The qualitative features of the experimental data are very well reproduced, however, especially for the Sb(III) compounds It is striking that also the extended Huckel and CNDO/2 results for Sb(V) compounds show the same type of discrepancy (with a factor that is even larger)

For the isomer shift the agreement between the calculated and experimental data is very good, not only qualitatively, but also quantitatively A linear relation between the valence-electron density at the Sb nucleus and the experimental isomer shift is satisfied for all compounds except SbF_5 and SbCl_5 From this relation we derive a value $\Delta R/R = -1.08 \times 10^{-3}$ for the Sb nucleus, in agreement with other values given in the literature

Our results support Stevens' hypothesis that in the series $\text{Sb}(\text{CH}_3)_N\text{Cl}_{3-N}$ the 5s character of the bonding increases, while the 5p character decreases for decreasing N In the series SbX_3 and SbX_5 , we find decreasing 5s and 5p character with the more electronegative X

Finally, we note that the comparison of our QS and IS results with the experimental data leads to some suggestions about the structures of some of the molecules We think that the trigonal bipyramidal structures for SbF_5 and SbCl_5 which have been proposed (but not yet confirmed by X-ray diffraction) need reconsideration Among the two structures proposed for SbI_3 , we prefer the structure (A) with the larger I-Sb-I angle

Acknowledgement

We thank Professor J.G Stevens and Dr. C.P. Keijzers for bringing this subject to our attention Further we thank Professor F.J Baerends, Professor D.E Ellis and Dr P.E.S Wormer for helpful discussions and Mr P Vernooys for the performance of some test calculations This investigation was supported in part by the Netherlands Foundation for Chemical Research (S O N) with financial aid from the Netherlands Organization for the Advancement of Pure Research (Z W O).

References

- [1] J.A Tossel, *J Chem Phys* 66 (1977) 5712,
A Tang Kai, H Annersten and T Encsson, *Phys Chem Miner* 5 (1980) 343,
M Braga, A.C Pavao and J.R Leite, *Phys Rev B23* (1981) 4328
M Braga and C.A Taft, *J Chem Phys* 74 (1981) 2969
- [2] W.C Nieuwpoort, D Post and P.T van Duynen, *Phys Rev B17* (1978) 91, and references therein,
P.S Bagus, U.I Walgren and J Almlöf, *J Chem Phys* 64 (1976) 2324
- [3] E.J Baerends, D.E Ellis and P Ros, *Chem Phys* 2 (1973) 41,
E.J Baerends and P Ros, *Chem Phys* 2 (1973) 52
- [4] P.J.M Geurts, J.W Gosselink, A van der Avourd, E.J Baerends and J.G Snijders, *Chem Phys* 46 (1980) 133
- [5] D Guenzburger and D.F Ellis, *Phys Rev B22* (1980) 4203
- [6] J.G Stevens and C.P Keijzers, private communication
- [7] J.C Slater *Advan Quantum Chem* 6 (1972) 1, *Quantum theory of molecules and solids*, Vol 4 (McGraw-Hill, New York 1974)
- [8] D.E Ellis, *Intern J Quantum Chem* 2S (1968) 35,
D.E Ellis and G.S Painter, *Phys Rev B2* (1970) 2887
- [9] K.H Johnson, *J Chem Phys* 45 (1966) 3085,
K.H Johnson and F.C Smith Jr, *Phys Rev B5* (1972) 831
J.C Slater and K.H Johnson, *Phys Rev B5* (1972) 844
- [10] E.J Baerends and P Ros, *Chem Phys* 8 (1975) 412,
Intern J Quantum Chem 12S (1978) 169
- [11] T.C Gibb, *Principles of Mössbauer spectroscopy* (Chapman and Hall London, 1975),
G.M Kalvius, *Hyperfine interaction in excited nuclei* (Academic Press, New York, 1972) p 523
- [12] D.A Shurley, *Rev Mod Phys* 36 (1964) 339
- [13] V Kotheekar, *Intern J Quantum Chem* 10 (1976) 993, and references therein
- [14] E.A.C Lucken, *Nuclear quadrupole coupling constants* (Academic Press, New York, 1969)
- [15] C.H Townes and B.P Dailey, *J Chem Phys* 17 (1949) 782
- [16] J.V Mallow, A.J Freeman and J.P Desclaux, *Phys Rev B13* (1976) 1884
- [17] R.M Sternheimer, *Phys Rev* 164 (1967) 10, and references therein
- [18] S.L Ruby, G.M Kalvius, G.B Beard and R.E Snijder, *Phys Rev* 159 (1967) 239,
T.P Das and R Bersohn, *Phys Rev* 131 (1963) 250,
K.D Sen and P.C Schmidt, *Phys Rev A23* (1981) 1026,
P.C Schmidt, K.D Sen, T.P Das and A Weiss, *Phys Rev A22* (1980) 4167,
K.D Sen and P.T Narasimhan, *Phys Rev B16* (1977) 107
- [19] E.J Baerends, and P Ros, HFS LCAO program, Scheikundig Laboratorium der Vrije Universiteit, Amsterdam, The Netherlands

- [20] DB Neumann, H Basch, RL Kornegay LC Snyder
JW Moscovitz, C Hornback and SP Liebman, QCPPE
11 (1971) 199
- [21] RF Stewart, J Chem Phys 52 (1970) 431
- [22] AD McLean and M Yoshimine, J Chem Phys 47
(1967) 3256
- [23] PE Cade and WM Huo, J Chem Phys 47 (1967) 649
- [24] DF Ellis, private communication
- [25] JD Peitke and JL Whitten, J Chem Phys 56 (1972) 830
- [26] F Scrocco and J Tomasi, Theoret Chim Acta 2 (1964)
386
- [27] JE Grabenstetter and MA Whitehead, Mol Phys 34
(1977) 1577
- [28] R Moccia, Theoret Chim Acta 8 (1967) 8
- [29] P Vernooys, JG Snyders and EJ Baerends, Slater type
basis functions for the whole periodic system, Internal
Report, Free University, Amsterdam, The Netherlands
(1981)
- [30] LH Bowen and GG Long, Inorg Chem 15 (1976) 1039,
and references therein
- [31] JG Stevens, JM Trooster, MA Meinema and JG
Nottes, Inorg Chem 20 (1981) 801
- [32] GD Fong, RR Kuckowski and AJ Ashe, J Mol
Spectry 70 (1978) 197, and references therein
- [33] RG Hyde and J B Peel, Mol Phys 33 (1979) 887
- [34] DI Baltranas, SP Ionov, A Yu Alexandrov and EF
Makarov, Chem Phys Letters 20 (1973) 55
- [35] JP Devort and JM Friedt, Chem Phys Letters 35
(1975) 423
- [36] JD Donaldson, JT Southern and MJ Trcker, J Chem
Soc Dalton Trans (1972) 893
- [37] LH Bowen, JG Stevens and GG Long, J Chem Phys
51 (1969) 2010
- [38] VP Gorkov RL Davidovich GV Zimna, LA
Sadokhina, F Kh Chubrova and VS Shpinel, Koord
Khim 1 (1975) 561
- [39] SL Ruby, GM Kalvius, GB Beard and RE Snyder,
Phys Rev 159 (1967) 239
- [40] JG Stevens and LH Bowen, in Mossbauer effect meth-
odology, Vol 5, ed IJ Graverman (Plenum Press, New
York, 1970) p 27
- [41] JG Ballard, T Birchall, R Fourcade and G Mascherpa,
J Chem Soc Dalton Trans (1976) 2409
- [42] JP Devort, JP Sanchez, JM Friedt and GK Shenoy, J
Phys (Paris) C-6 35 (1974) 255
- [43] JG Stevens and JM Trooster, J Chem Soc Dalton
Trans (1979) 740
- [44] F Petillon and JE Guerchais, J Inorg Nucl Chem 37
(1975) 1863
- [45] LH Bowen, KA Taylor, HK Chin and GG Long, J
Inorg Nucl Chem 36 (1974) 101
- [46] V Kothekar, BZ Iofa, SI Semonov and VS Shpinel,
Soviet Phys JETP 28 (1969) 86
- [47] A Yu Alexandrov, DI Baltranas, LM Belyaev, IS
Lyubutin and VA Lyakhovitskaya, Kristallografiya 17
(1972) 332
- [48] TB Brill, GE Parris, GG Long and LH Bowen, Inorg
Chem 12 (1973) 1888
- [49] JG Stevens and SL Ruby, Phys Letters 32A (1970) 91
- [50] GG Long, JG Stevens, RJ Tullbane and LH Bowen,
J Am Chem Soc 92 (1970) 4230
- [51] K Dehnicke, K Fleck, K Schmidt and J Pebler, Z
Anorg Allg Chem 451 (1979) 109
- [52] GK Shenoy and JM Friedt, Phys Rev Letters 31 (1973)
419
- [53] JG Ballard and T Birchall, J Chem Soc Dalton Trans
(1976) 1859
- [54] T Birchall and JG Ballard, J Phys (Paris) C-6 37 (1976)
513
- [55] Sh Sh Bashkurov and G Ya Selyatin, Soviet Phys Solid
State 9 (1968) 2284
- [56] VS Shpinel, VA Bryukhanov, V Kothekar, BZ Iofa
and S Semonov, Symp Faraday Soc 1 (1968) 69
- [57] I Lindquist and A Niggli, J Inorg Nucl Chem 2 (1956)
445
- [58] DW Cushen and R Hulme, J Chem Soc (1962) 2218
- [59] AF Wells, Structural inorganic chemistry (Clarendon
Press, Oxford, 1962) pp 663, 693
- [60] TN Polynova and MA Poraj-Koshuc Zh Strukt Khim
7 (1966) 642
- [61] W Schwartz and HJ Guder, Z Anorg Allg Chem 444
(1978) 105
- [62] AF Wells, Z Krnst 99 (1938) 367
- [63] W Schwartz and HJ Guder, Z Naturforsch 33b (1978)
485
- [64] EH Huygh and TP Das, Phys Rev 143 (1966) 452
- [65] VA Brakhanov, BZ Iofa, V Kothekar, SI Semonov and
VS Shpinel, Soviet Phys JETP 26 (1968) 912
- [66] JG Stevens and VE Stevens, Mossbauer effect data
index 1976 (IFI/Plenum, New York, 1976)
- [67] CM Lederer and VS Shirley, eds, Tables of isotopes,
7th Ed (Wiley, New York, 1978)
- [68] K Murakawa and S Suwa, Phys Rev 76 (1949) 433

The calculation of interaction energies using the pseudopotential Hartree-Fock-Slater-LCAO method

W Ravenek

Instituut voor Theoretische Chemie, Universiteit van Nijmegen, Toernooiveld, 6525 ED Nijmegen, The Netherlands

E J Baerends

Instituut voor Theoretische Chemie, Scheikundig Laboratorium der Vrije Universiteit, De Boelelaan 1083, 1081 HV Amsterdam, The Netherlands

(Received 6 December 1983, accepted 27 March 1984)

This paper describes an extension of Ziegler's transition state formalism for the calculation of interaction energies in order to include the pseudopotential Hartree-Fock-Slater-LCAO method developed by Snijders and Baerends. Perturbation corrections to the expressions based on averaged pseudopotentials are obtained within a new, self-consistent scheme. Test calculations on a variety of systems are reported. It is found that the pseudopotential method reproduces results obtained with the frozen-core HFS-LCAO method quite well. For first and second row diatomics equilibrium distances agree within 0.02 Å, dissociation energies within 0.2 eV, and vibration frequencies within 20 cm⁻¹. The spectroscopic constants are also in fair agreement with experiment. For systems containing the transition metal Cu, where the binding energy curves have rather shallow wells, dissociation energies are equally accurate, and deviations in equilibrium distances and vibration frequencies are larger.

I. INTRODUCTION

The calculation of chemical interaction energies is a longstanding problem in quantum chemistry. For small systems accurate *ab initio* methods are available. For larger systems, however, these methods become impractical and one has to resort to more approximate methods. One of these is the Hartree-Fock-Slater (HFS)-LCAO method.¹ Due to the numerical integration scheme involved in this method, it is impossible to obtain interaction energies as differences of total energies of final and initial states without using excessively large numbers of integration points. To circumvent this difficulty, Ziegler and Rauk² have developed a method to calculate interaction energies, which essentially uses a generalization of Slater's transition state concept.³ This method has been implemented for the HFS-LCAO method in its frozen-core formulation, it has been shown to yield numerically stable and physically meaningful interaction energies.

If the frozen-core HFS-LCAO method is applied to systems containing atoms with large cores, e.g., transition metals, the number of functions needed for the core orthogonalization raises the computation time significantly. To overcome this problem, Snijders and Baerends⁴ introduced a pseudopotential version of the HFS-LCAO method. The method is of the Phillips-Kleinman variety⁵ core collapse is prevented by adding a projection operator to the Fock operator. Using the pseudopotential HFS-LCAO method, core functions are completely eliminated from the SCF procedure. Also this method is capable of giving reliable and physically meaningful results,^{4,6} but, up to now, it could not be applied to the calculation of interaction energies.

In this paper we extend Ziegler's transition state formalism for the calculation of interaction energies to include the pseudopotential HFS-LCAO method. In order to do so

we found it necessary to develop a new, self-consistent perturbational scheme which corrects for the use of averaged pseudopotentials. This scheme is related to the one used for relativistic HFS-LCAO calculations.^{7,8} Section II contains the formulation of our method. First we mention the salient aspects of the frozen-core and pseudopotential HFS-LCAO methods, next we develop the perturbational scheme mentioned above, finally we obtain a numerically feasible expression for the calculation of interaction energies.

With the self-consistent perturbational scheme developed and used here we effectively apply the full Phillips-Kleinman operator, without replacement of this operator by a (local) effective potential. Thus we obviate the need for fitting or parameter adjustment. The results of the test calculations, both on some first and second row systems and on systems containing transition metal atoms are given in Sec. III.

II. FORMALISM

A. The frozen-core HFS-LCAO method

The HFS method is characterized by the one-electron equation

$$F(1)\psi_i(1) = \epsilon_i \psi_i(1), \quad (1a)$$

where

$$F(1) = T(1) + V_N(1) + V_C[\rho(1)] + V_x[\rho(1)] \quad (1b)$$

$T(1)$ is the kinetic energy operator, $V_N(1)$ the nuclear potential, $V_C[\rho(1)] = \int r_{12}^{-1} \rho(2) d\tau_2$ the electronic Coulomb potential, and $V_x[\rho(1)] = -3\alpha[(3/8\pi)\rho(1)]^{1/3}$ the electronic exchange potential (atomic units are used throughout this paper). As usual the electron density is given by

$$\rho(1) = \sum_j n_j \psi_j(1) \psi_j^*(1)$$

Equation (1) follows from the minimization of the HFS energy functional

$$E_{\text{HFS}}[\rho] = \sum_j n_j \langle \psi_j | T + V_N | \psi_j \rangle + \frac{1}{2} \iint r_{12}^{-1} \rho(1)\rho(2) d\tau_1 d\tau_2 + \frac{3}{4} \int \rho(1) V_x[\rho(1)] d\tau_1 + V_{NN}, \quad (2)$$

with V_{NN} the nucleus-nucleus interaction term

$$E_{\text{HFS}}[\rho] = E_{\text{core}} + \sum_j^{\text{val}} n_j \langle \psi_j | T + V_N + V_C[\rho_{\text{core}}] | \psi_j \rangle + \frac{1}{2} \iint r_{12}^{-1} \rho_{\text{val}}(1)\rho_{\text{val}}(2) d\tau_1 d\tau_2 + \frac{3}{4} \int \rho(1) V_x[\rho(1)] d\tau_1 + V_{NN} = E_{\text{core}} + \sum_j^{\text{val}} n_j \langle \psi_j | F | \psi_j \rangle - \frac{1}{2} \iint r_{12}^{-1} \rho_{\text{val}}(1)\rho_{\text{val}}(2) d\tau_1 d\tau_2 + \frac{3}{4} \int \rho_{\text{core}}(1) V_x[\rho(1)] d\tau_1 - \frac{1}{4} \int \rho_{\text{val}}(1) V_x[\rho(1)] d\tau_1 + V_{NN}, \quad (4)$$

with

$$E_{\text{core}} = \sum_j^{\text{core}} n_j \langle \psi_j | T + V_N | \psi_j \rangle + \frac{1}{2} \iint r_{12}^{-1} \rho_{\text{core}}(1)\rho_{\text{core}}(2) d\tau_1 d\tau_2 \quad (5)$$

depending on the core orbitals only

Using a LCAO expansion $\psi_j = \sum_\mu \chi_\mu C_{\mu j}$, for the valence orbitals Eq (4) may be rewritten in terms of matrix elements in the basis χ and the change-and-bond-order matrix P , which is defined by

$$P_{\mu\nu} = \sum_j^{\text{val}} n_j C_{\mu j} C_{\nu j}^*, \quad (6)$$

such that

$$\rho_{\text{val}}(1) = \sum_{\mu\nu} P_{\mu\nu} \chi_\mu(1) \chi_\nu^*(1) \quad (7)$$

Differentiation of the energy functional with respect to a general element of P yields

$$\frac{\partial E_{\text{HFS}}}{\partial P_{\mu\nu}} = F_{\nu\mu} \quad (8)$$

As Ziegler and Rauk² noted, Eq (8) is a generalization of Slater's³ well-known result

$$\frac{\partial E_{\text{HFS}}}{\partial n_j} = \epsilon_j \quad (9)$$

B. The pseudopotential HFS-LCAO method

In frozen-core calculations one prevents variational collapse of valence orbitals into the space spanned by the core orbitals (core collapse) by explicitly orthogonalizing the valence space to the core space. Because it is possible to achieve core-valence orthogonality with fewer basis functions in the core region than needed to accurately describe the core orbitals themselves, the basis set can be smaller than in the corresponding all-electron calculation. Still, for sys-

tems containing atoms with large cores, the total number of basis functions may become a prohibitive factor even in frozen-core calculations. One would like to completely eliminate the core basis functions from the formalism.

$$\rho(1) = \rho_{\text{core}}(1) + \rho_{\text{val}}(1) \quad (3)$$

and the energy functional (2), now to be optimized with respect to the valence density only, as

tems containing atoms with large cores, the total number of basis functions may become a prohibitive factor even in frozen-core calculations. One would like to completely eliminate the core basis functions from the formalism.

Phillips and Kleinman¹ have shown that an orthogonality constraint in an eigenvalue problem can be replaced by adding a nonlocal pseudopotential to the Hamiltonian. A large number of atomic pseudopotentials and effective core potentials have been proposed since.^{11,12} Phillips and Kleinman introduced a shift operator (or pseudopotential)

$$V_{psj} = \sum_k (\epsilon_j - \epsilon_k) |\psi_{c,k}\rangle \langle \psi_{c,k}| \quad (10)$$

In the eigenvalue problem of the pseudo-Fock operator

$$F_{psj} = F + V_{psj} \quad (11)$$

the core orbitals $\psi_{c,k}$ are shifted from their all-electron orbital energy $\epsilon_{c,k}$ to the valence energy ϵ_j , which thereby becomes degenerate. The valence orbital obtains an arbitrary admixture of core orbitals, thereby changing into a pseudo-orbital. One has a certain freedom in defining the pseudo-orbitals, e.g., by requiring them to be nodeless in the core region.

Snijders and Baerends⁴ have developed a nonparametrized pseudopotential version of the HFS-LCAO method in which the pseudopotential used is

$$\bar{V}_{psj} = \sum_k (\bar{\epsilon} - \epsilon_k) |\psi_{c,k}\rangle \langle \psi_{c,k}|, \quad (12)$$

with $\bar{\epsilon}$ an averaged valence energy. More precisely, there is one such $\bar{\epsilon}$ for each irreducible representation of the molecular point group, for simplicity of presentation we will ignore this complication. The averaging involved in Eq (12) was

corrected for by using perturbation theory, we will return to this point shortly

In this method the pseudo-orbitals are fixed by choosing all coefficients of core basis functions in the pseudo-orbitals to be zero. In general, $1 \in$, if the number of core *basis functions* in the corresponding all-electron calculation is larger than the number of *core orbitals*, this choice involves an approximation. Using the pseudo-orbitals thus defined a pseudodensity

$$\rho_{ps}(1) = \sum_j n_j \psi_{ps,j}(1) \psi_{ps,j}^*(1) \quad (13)$$

is constructed, n_j being the valence orbital occupation numbers. Furthermore, a difference density

$$\Delta\rho(1) = \rho_{val}(1) - \rho_{ps}(1) \quad (14)$$

is defined. In the actual construction of the Coulomb and exchange terms in the Fock operator the pseudodensity is always corrected with $\Delta\rho$, so that the important property of the pseudo-Fock operator [Eq. (11)] of having exactly the same valence eigenvalue spectrum as the original Fock operator is retained. It is assumed, however, that molecular $\Delta\rho$ terms may be obtained as a sum of corresponding atomic terms

$$\Delta\rho_{mol}(1) = \sum \Delta\rho_{atom}(1) \quad (15)$$

It has been shown⁴ that with this scheme reasonably accurate one-electron energies and valence orbitals (after annihilating the core part of the pseudo-orbitals) may be found.

Although the perturbational procedure implemented by Snyders and Baerends has yielded satisfactory results, its Brillouin-Wigner-like form precludes the straightforward use of the transition state scheme for the calculation of interaction energies² as developed for the frozen-core HFS-LCAO method. More specifically, it is impossible to find an expression analogous to Eq. (8) for the derivative of the pseudopotential total energy functional with respect to a general element of the pseudo charge-and-bond-order matrix. We find that a self-consistent perturbational approach,¹³ also used in the relativistic HFS-LCAO method,^{7,8} provides a useful alternative.

C. Self-consistent perturbational approach for the pseudopotential HFS-LCAO method

The perturbations we are concerned with are the differences between the exact and the averaged pseudopotentials for each pseudo-orbital $\psi_{ps,j}$

$$\begin{aligned} \Delta_j &= V_{ps,j} - \bar{V}_{ps} \\ &= \sum_k (\epsilon_j - \bar{\epsilon}) |\psi_{c,k}\rangle \langle \psi_{c,k}| \end{aligned} \quad (16a)$$

or

$$\Delta_j = (\epsilon_j - \bar{\epsilon}) P_c, \quad P_c = \sum_k |\psi_{c,k}\rangle \langle \psi_{c,k}|, \quad (16b)$$

where P_c is the projector on the space spanned by the core orbitals, these perturbations differ for each pseudo-orbital. The self-consistent problem we want to solve is

$$F_{ps,j} \psi_{ps,j} = \epsilon_j \psi_{ps,j}, \quad \langle \psi_{ps,j} | \psi_{ps,j} \rangle = 1, \quad (17)$$

where [cf. Eq. (11)]

$$F_{ps,j} = F + \bar{V}_{ps} + \lambda \Delta_j \quad (18)$$

As zeroth order problem we take the SCF problem of the averaged pseudo-Fock operator, $1 \in$,

$$F_{ps}^{(0)} \psi_{ps,j}^{(0)} = \epsilon_j^{(0)} \psi_{ps,j}^{(0)}, \quad \langle \psi_{ps,j}^{(0)} | \psi_{ps,k}^{(0)} \rangle = \delta_{jk}, \quad (19)$$

where

$$F_{ps}^{(0)} = H^{(0)} + V_c [\rho_{ps}^{(0)}] + V_x [\rho_{ps}^{(0)}], \quad (20)$$

$$H^{(0)} = T + V_N + V_c [\rho_{core} + \Delta\rho] + \bar{V}_{ps}, \quad (21)$$

$$\rho_{ps}^{(0)}(1) = \sum_j n_j \psi_{ps,j}^{(0)}(1) \psi_{ps,j}^{(0)*}(1), \quad (22)$$

$$\rho^{(0)}(1) = \rho_{core}(1) + \Delta\rho(1) + \rho_{ps}^{(0)}(1) \quad (23)$$

We now expand the pseudo-orbitals and the orbital energies in Eq. (17) as

$$\psi_{ps,j} = N_j (\lambda |\psi_{ps,j}^{(0)} + \lambda \psi_{ps,j}^{(1)} + \lambda^2 \psi_{ps,j}^{(2)} + \dots), \quad (24)$$

$$\epsilon_j = \epsilon_j^{(0)} + \lambda \epsilon_j^{(1)} + \lambda^2 \epsilon_j^{(2)} + \dots \quad (25)$$

With the intermediate normalization condition

$$\langle \psi_{ps,j}^{(0)} | \psi_{ps,k}^{(1)} \rangle = 0, \quad k = 1, 2, \quad (26)$$

the normalization constant becomes

$$N_j(\lambda) = 1 - \lambda^2 \langle \psi_{ps,j}^{(0)} | \psi_{ps,j}^{(1)} \rangle + \dots \quad (27)$$

Substituting Eq. (27) into Eq. (24) we obtain the following power series in λ for the pseudoelectron density matrix

$$\begin{aligned} \rho_{ps}(1, 1') &= \sum_j n_j \psi_{ps,j}(1) \psi_{ps,j}^*(1') \\ &= \rho_{ps}^{(0)}(1, 1') + \lambda \rho_{ps}^{(1)}(1, 1') + \lambda^2 \rho_{ps}^{(2)}(1, 1') + \dots \end{aligned} \quad (28a)$$

where

$$\rho_{ps}^{(0)}(1, 1') = \sum_j n_j \psi_{ps,j}^{(0)}(1) \psi_{ps,j}^{(0)*}(1'), \quad (28b)$$

$$\rho_{ps}^{(1)}(1, 1') = \sum_j n_j [\psi_{ps,j}^{(0)}(1) \psi_{ps,j}^{(1)*}(1') + \psi_{ps,j}^{(1)}(1) \psi_{ps,j}^{(0)*}(1')], \quad (28c)$$

$$\begin{aligned} \rho_{ps}^{(2)}(1, 1') &= \sum_j n_j [\psi_{ps,j}^{(0)}(1) \psi_{ps,j}^{(2)*}(1') + \psi_{ps,j}^{(1)}(1) \psi_{ps,j}^{(1)*}(1') \\ &\quad + \psi_{ps,j}^{(2)}(1) \psi_{ps,j}^{(0)*}(1') \\ &\quad - \langle \psi_{ps,j}^{(1)} | \psi_{ps,j}^{(1)} \rangle \psi_{ps,j}^{(0)}(1) \psi_{ps,j}^{(0)*}(1')], \dots \end{aligned} \quad (28d)$$

Using Eq. (25) we note that the (one-electron) perturbations actually are series in λ

$$\lambda \Delta_j = \lambda H_j^{(1)} + \lambda^2 H_j^{(2)} + \dots, \quad (29a)$$

$$H_j^{(1)} = (\epsilon_j^{(0)} - \bar{\epsilon}) P_c, \quad (29b)$$

$$H_j^{(2)} = \epsilon_j^{(1)} P_c, \quad (29c)$$

...

From Eqs. (1b) and (28) it follows, moreover, that the pseudo-Fock operators $F_{ps,j}$ will also contain perturbation corrections through the corrections to $\rho_{ps}^{(0)}(1)$, the so-called indirect perturbation corrections, $1 \in$, we have

$$F_{ps,j} = F_{ps}^{(0)} + \lambda F_{ps,j}^{(1)} + \lambda^2 F_{ps,j}^{(2)} + \dots, \quad (30a)$$

$$F_{ps}^{(k)} - H_j^{(k)} + V_c^{(k)} + V_x^{(k)}, \quad k = 1, 2, \quad (30b)$$

$V_c^{(k)}$ and $V_x^{(k)}$ are the k th order corrections to the electronic Coulomb and exchange operators, respectively. It may be derived that

$$V_c^{(k)}(1) = \int r_{12}^{-1} \rho_{ps}^{(k)}(2) d\tau_2, \quad k = 1, 2, \quad (31)$$

and

$$V_x^{(1)}(1) = \frac{1}{3} \left[\frac{\rho_{ps}^{(1)}(1)}{\rho_{ps}^{(0)}(1)} \right] V_x[\rho_{ps}^{(0)}(1)], \quad (32a)$$

$$V_x^{(2)}(1) = \left[\frac{1}{3} \left[\frac{\rho_{ps}^{(2)}(1)}{\rho_{ps}^{(0)}(1)} \right] - \frac{1}{9} \left[\frac{\rho_{ps}^{(1)}(1)}{\rho_{ps}^{(0)}(1)} \right]^2 \right] V_x[\rho_{ps}^{(0)}(1)], \quad (32b)$$

with $\rho_{ps}^{(0)}$ defined in Eq (23)

Substituting the series expansions obtained so far into the self-consistent problem [Eq (17)] and collecting like powers of λ we obtain the coupled-HFS equations

$$F_{ps}^{(0)} \psi_{ps}^{(0)} = \epsilon_j^{(0)} \psi_{ps}^{(0)}, \quad (33a)$$

$$F_{ps}^{(0)} \psi_{ps}^{(1)} + F_{ps}^{(1)} \psi_{ps}^{(0)} = \epsilon_j^{(0)} \psi_{ps}^{(1)} + \epsilon_j^{(1)} \psi_{ps}^{(0)}, \quad (33b)$$

$$F_{ps}^{(0)} \psi_{ps}^{(2)} + F_{ps}^{(1)} \psi_{ps}^{(1)} + F_{ps}^{(2)} \psi_{ps}^{(0)} = \epsilon_j^{(0)} \psi_{ps}^{(2)} + \epsilon_j^{(1)} \psi_{ps}^{(1)} + \epsilon_j^{(2)} \psi_{ps}^{(0)}, \quad (33c)$$

The zeroth order equation (33a) is satisfied by assumption

The first order equation (33b) yields

$$\epsilon_j^{(1)} = \langle \psi_{ps}^{(0)} | F_{ps}^{(1)} | \psi_{ps}^{(0)} \rangle, \quad (34a)$$

$$\psi_{ps}^{(1)} = \sum_k \psi_{ps}^{(0)} a_{kj}^{(1)}, \quad (34b)$$

$$a_{kj}^{(1)} = \frac{\langle \psi_{ps}^{(0)} | F_{ps}^{(1)} | \psi_{ps}^{(0)} \rangle}{\epsilon_j^{(0)} - \epsilon_k^{(0)}} \quad (34c)$$

As usual in self-consistent perturbation theory, the first order corrections to the orbitals are given implicitly, they can be solved using a self-consistent procedure. The second order equation (33c) yields

$$\epsilon_j^{(2)} = \langle \psi_{ps}^{(0)} | F_{ps}^{(2)} | \psi_{ps}^{(0)} \rangle + \langle \psi_{ps}^{(0)} | F_{ps}^{(1)} | \psi_{ps}^{(1)} \rangle, \quad (35a)$$

$$\psi_{ps}^{(2)} = \sum_k \psi_{ps}^{(0)} a_{kj}^{(2)}, \quad (35b)$$

$$a_{kj}^{(2)} = \frac{\langle \psi_{ps}^{(0)} | F_{ps}^{(2)} | \psi_{ps}^{(0)} \rangle - \epsilon_j^{(1)} \langle \psi_{ps}^{(0)} | \psi_{ps}^{(1)} \rangle + \langle \psi_{ps}^{(0)} | F_{ps}^{(1)} | \psi_{ps}^{(1)} \rangle}{\epsilon_j^{(0)} - \epsilon_k^{(0)}} \quad (35c)$$

Again, this set of equations can be solved self-consistently. Unlike in conventional Rayleigh-Schrodinger perturbation theory it is not possible to obtain the second order corrections to the orbital energies from the first corrections to the orbitals alone.

Having formally solved the self-consistent problem [Eq (17)] we now turn towards the total energy functional in the pseudopotential framework. As basic relation we use the identity of valence orbital energies in all-electron and (exact) pseudopotential schemes

$$\langle \psi_j | F | \psi_j \rangle = \langle \psi_{ps,j} | F + V_{ps,j} | \psi_{ps,j} \rangle \quad (36)$$

Combining Eq (36) with Eqs (4) and (14), we obtain after some manipulations

$$\begin{aligned} E_{\text{PSSHFS}}[\rho] &= \left\{ E_{\text{core}} + \sum_j n_j \langle \psi_{ps,j} | H^{(0)} + \lambda \Delta_j | \psi_{ps,j} \rangle \right. \\ &\quad + \frac{1}{2} \int \int r_{12}^{-1} \rho_{ps}(1) \rho_{ps}(2) d\tau_1 d\tau_2 + \frac{3}{4} \int \rho(1) V_x[\rho(1)] d\tau_1 + V_{NN} \left. \right\} \\ &\quad - \frac{1}{2} \int \int r_{12}^{-1} \Delta \rho(1) \Delta \rho(2) d\tau_1 d\tau_2 - \int \Delta \rho(1) \{ V_c[\rho_{ps}(1)] + V_x[\rho(1)] \} d\tau_1 \end{aligned} \quad (37)$$

It may be noted that we do not have to make the usual approximation of neglecting the noncommutativity of the two-electron operator with the core projector (i.e., of using ρ_{ps} instead of ρ_{ps} in the two-electron part of the energy), since we explicitly retain $\Delta \rho$ in our expressions

Using the perturbation expression derived previously, we now write

$$E_{\text{PSSHFS}}[\rho] = E^{(0)} + \lambda E^{(1)} + \lambda^2 E^{(2)} + \quad (38)$$

The zeroth order term reads

$$\begin{aligned} E^{(0)} &= E_{\text{core}} + \int_{j=1}^N H^{(0)}(1) \rho_{ps}^{(0)}(1, 1') d\tau_1 + \frac{1}{2} \iint r_{12}^{-1} \rho_{ps}^{(0)}(1) \rho_{ps}^{(0)}(2) d\tau_1 d\tau_2 + \frac{3}{4} \int \rho_{ps}^{(0)}(1) V_x[\rho_{ps}^{(0)}(1)] d\tau_1 \\ &\quad + V_{NN} + \frac{1}{2} \iint r_{12}^{-1} \Delta \rho(1) \Delta \rho(2) d\tau_1 d\tau_2 - \int \Delta \rho(1) \{ V_c[\rho_{ps}^{(0)}(1)] + V_x[\rho_{ps}^{(0)}(1)] \} d\tau_1 \end{aligned} \quad (39)$$

Using the identity

$$\begin{aligned} \int_{j=1}^N H^{(0)}(1) \rho_{ps}^{(0)}(1, 1') d\tau_1 + \iint r_{12}^{-1} \rho_{ps}^{(0)}(1) \rho_{ps}^{(0)}(2) d\tau_1 d\tau_2 \\ + \int \rho_{ps}^{(0)}(1) V_x[\rho_{ps}^{(0)}(1)] d\tau_1 = 0, \end{aligned} \quad (40)$$

which follows from the intermediate normalization condition [Eq (26)], we obtain for the first order term

$$\begin{aligned} E^{(1)} &= \sum_j n_j \langle \psi_{ps,j}^{(0)} | H_j^{(1)} | \psi_{ps,j}^{(0)} \rangle \\ &\quad - \int \Delta \rho(1) \{ V_c^{(1)}(1) + V_x^{(1)}(1) \} d\tau_1 \end{aligned} \quad (41)$$

Further, using an identity analogous to Eq (40) and the first order perturbation equation (33b), we obtain

$$E^{(2)} = \sum_j n_j \langle \psi_{ps}^{(0)}, H_j^{(2)} | \psi_{ps}^{(0)} \rangle + \frac{1}{2} \sum_j n_j \langle [\psi_{ps}^{(0)}, H_j^{(1)} | \psi_{ps}^{(1)} \rangle + \langle \psi_{ps}^{(1)}, H_j^{(1)} | \psi_{ps}^{(0)} \rangle] - \int \Delta\rho(1) [V_c^{(2)}(1) + V_s^{(2)}(1)] d\tau_1 \quad (42)$$

We note the occurrence of $\Delta\rho$ -dependent terms in all energy expressions [Eqs (39), (41), and (42)] These originate from the use of $\rho_{\nu,ai}$ instead of $\rho_{\nu,i}$ in the two-electron part of the total energy There is another important difference between our scheme and current pseudopotential methods⁹⁻¹² since we use the full Phillips-Kleinman operator As Christiansen *et al*¹² have shown, the mixing of core orbitals into pseudo-orbitals transfers electron density from the valence region to the core Therefore these pseudo-orbitals alone cannot be used to construct an effective potential U^{EP} in the Goddard-Kahn manner,⁹ yielding long negative tails in U^{EP} To solve this problem Christiansen *et al* require their atomic pseudo-orbitals to match the all-electron valence orbitals beyond a certain radius (cf the Durand-Barthelet pseudo-orbitals¹¹) In the pseudopotential HFS-LCAO method this problem does not arise, due to the use of the full Phillips-Kleinman operator in conjunction with the $\Delta\rho$ term [Eq (14)]

D. The calculation of interaction energies

In this section we derive an expression for the calculation of interaction energies within the pseudopotential framework First we obtain the zeroth order contribution, following the methodology of Ziegler and Rauk², next we consider the perturbation corrections

Consider a molecular system and assume it to be a buildup of certain subsystems (A, B, ...) which we call *fragments* We label the overall system *after convergence* by ΣA The interaction energy is given by the quantity

$$\Delta E = E_{\text{PSHFS}}[\Sigma A] - \sum_{\Lambda} E_{\text{PSHFS}}[A] \quad (43)$$

Using the perturbation series [Eq (38)], we rewrite Eq (43) as

$$\Delta E = \Delta E^{(0)} + \lambda \Delta E^{(1)} + \lambda^2 \Delta E^{(2)} + \dots \quad (44a)$$

$$\Delta E^{(k)} = E^{(k)}[\Sigma A] - \sum_{\Lambda} E^{(k)}[A], \quad k = 0, 1, 2, \quad (44b)$$

Due to numerical difficulties the zeroth order contribution cannot be obtained simply as a difference of total energies Following Ziegler and Rauk² we calculate $\Delta E^{(0)}$ in two steps, using an intermediate "state" ΣA

$$\Delta E^{(0)} = (E^{(0)}[\Sigma A] - E^{(0)}[\Sigma A]) + (E^{(0)}[\Sigma A] - \sum_{\Lambda} E^{(0)}[A]) \quad (45)$$

$E^{(0)}[\Sigma A]$ does not correspond to a state of the total system (i.e., to a wave function), but it simply is $E^{(0)}$ evaluated with the density matrix $\rho_{ps}^{(0)}(1, 1') = \sum_{\Lambda} \rho_{ps}^{(0)\Lambda}(1, 1')$ The (diag-

onal) electron density then is the sum of the densities of the fragments in their positions in the overall system

$$\rho^{(0)\Sigma A}(1) = \sum_{\Lambda} [\rho_{ps}^{\Lambda}(1) + \Delta\rho^{\Lambda}(1) + \rho_{ps}^{(0)\Lambda}(1)] \quad (46)$$

We note that we define $\bar{V}_{ps}^{\Sigma A}$ as containing the average orbital energies $\bar{\epsilon}$ of the converged overall system for reasons to become clear, explicitly

$$\bar{V}_{ps}^{\Sigma A} = \bar{V}_{ps}^{\Lambda A} \quad (47)$$

First we calculate the term $E^{(0)}[\Sigma A] - \sum_{\Lambda} E^{(0)}[A]$ Using the zeroth order energy expression [Eq (39)], we obtain

$$E^{(0)}[\Sigma A] - \sum_{\Lambda} E^{(0)}[A] = \Delta E_{ei} + \Delta E_{exch} + \Delta E_{\text{ppopot}}^{(0)} + E_{\Delta\rho}^{(0)}, \quad (48)$$

where

$$\Delta E_{ei} = \sum_{\Lambda} \int \rho_{ps}^{(0)\Lambda}(1) [V_N^{\Lambda}(1) + V_C [\rho_{\text{core}}^{\Lambda}(1)]] d\tau_1 + \frac{1}{2} \sum_{\Lambda} \sum_{\beta} \int \int r_{12}^{-1} \rho_{ps}^{(0)\Lambda}(1) \rho_{ps}^{(0)\beta}(2) d\tau_1 d\tau_2 + \frac{1}{2} \sum_{\Lambda} \sum_{\beta} \sum_{\alpha} R_{\alpha\beta}^{-1} Z_{\alpha} Z_{\beta}, \quad (49)$$

$$\Delta E_{exch} = \frac{3}{4} \sum_{\Lambda} \rho^{(0)\Lambda}(1) \left\{ V_x \left[\sum_{\beta} \rho^{(0)\beta}(1) \right] - V_x [\rho^{(0)\Lambda}(1)] \right\} d\tau_1, \quad (50)$$

$$\Delta E_{\text{ppopot}}^{(0)} = \sum_{\Lambda} \int_{-1}^1 [\bar{V}_{ps}^{\Sigma A}(1) - \bar{V}_{ps}^{\Lambda}(1)] \rho_{ps}^{(0)\Lambda}(1, 1') d\tau_1, \quad (51)$$

and

$$\Delta E_{\Delta\rho}^{(0)} = -\frac{1}{2} \sum_{\Lambda} \int \int r_{12}^{-1} \Delta\rho^{\Lambda}(1) \Delta\rho^{\beta}(2) d\tau_1 d\tau_2 - \sum_{\Lambda} \int \Delta\rho^{\Lambda}(1) \left\{ V_x \left[\sum_{\beta} \rho^{(0)\beta}(1) \right] - V_x [\rho^{(0)\Lambda}(1)] \right\} d\tau_1 \quad (52)$$

We note that $\sum_{\Lambda} \int \Delta\rho^{\Lambda}(1) V_C [\rho_{ps}^{(0)\Lambda}(1)] d\tau_1$ in $\Delta E_{\Delta\rho}^{(0)}$ and ΔE_{ei} have cancelled The terms ΔE_{ei} and ΔE_{exch} have exactly the same functional form as in the frozen-core formalism, except that in ΔE_{ei} the pseudodensity replaces the valence density $\Delta E_{\text{ppopot}}^{(0)}$ has no analog, it is due to the inequality of the pseudopotential in initial and final states $\Delta E_{\Delta\rho}^{(0)}$ contains correction terms involving $\Delta\rho$ to ΔE_{ei} and ΔE_{exch} We expect it to be small, since $\Delta\rho$ integrates to zero and the magnitude of $\Delta\rho$ is quite small in the valence region, where pseudo- and valence density do not differ much

Secondly we calculate the energy difference $E^{(0)}[\Sigma A] - E^{(0)}[\Sigma A]$ Let $\rho_{ps}^{\Sigma A}$ be given in the basis of the fragment pseudo-orbitals, i.e.,

$$\rho_{ps}^{\Sigma A} = \sum_j P_{ps}^{(0)} \phi_j \phi_j^*, \quad (53)$$

then we can express $\rho_{ps}^{\Sigma A}$ as

$$\rho_{ps}^{\Sigma A} = \rho_{ps}^{\Lambda A} + \sum_j \Delta P_{ps}^{(0)} \phi_j \phi_j^* \quad (54)$$

Following Ziegler we define a transition state, labeled TS,

$$\rho_{\mu\nu}^{\text{TS}} = \frac{1}{2} (\rho_{\mu\nu}^{\Sigma\Lambda} + \rho_{\mu\nu}^{\Sigma\bar{\Lambda}})$$

$$\begin{aligned} &= \rho_{\mu\nu}^{\Sigma\Lambda} + \frac{1}{2} \sum_{i,j} \Delta P_{\mu\nu ij}^{(0)} \phi_i \phi_j^* \\ &= \sum_{i,j} Q_{ij} \phi_i \phi_j^* \end{aligned} \quad (55)$$

Using a Taylor expansion of the zeroth order energy functional one may derive²

$$\begin{aligned} \Delta E_{\mu\nu} &= E^{(0)}[\bar{\Sigma}\bar{\Lambda}] - E^{(0)}[\Sigma\Lambda] \\ &= \sum_{i,j} \left\{ \frac{1}{6} \frac{\partial E^{(0)}}{\partial Q_{ij}} \Big|_{\Sigma\Lambda} + \frac{2}{3} \frac{\partial E^{(0)}}{\partial Q_{ij}} \Big|_{\text{TS}} + \frac{1}{6} \frac{\partial E^{(0)}}{\partial Q_{ij}} \Big|_{\Sigma\Lambda} \right\} \Delta P_{\mu\nu ij}^{(0)} \end{aligned} \quad (56)$$

which is correct to fourth order in the $\Delta P_{\mu\nu ij}^{(0)}$. Equation (56) is independent of the actual form of the energy functional. For the zeroth order energy functional [Eq. (39)], the derivative with respect to a general element of the (pseudo) charge-and-bond-order matrix is given by

$$\begin{aligned} \frac{\partial E^{(0)}}{\partial P_{\mu\nu ij}^{(0)}} &= G_{ij} \\ &= F_{\mu\nu ij}^{(0)} + \left\langle \phi_j \left| \left(-V_C[\Delta\rho] - \frac{1}{3} \frac{\Delta\rho}{\rho^{(0)}} V_x[\rho^{(0)}] \right) \right| \phi_i \right\rangle, \end{aligned} \quad (57)$$

which differs from the analogous result in the frozen-core formalism [Eq. (8)] in some $\Delta\rho$ -dependent terms

Combining Eqs. (56) and (57) we arrive at

$$\Delta E_{\mu\nu} = \text{tr}(\bar{G}\Delta P_{\mu\nu}^{(0)}), \quad (58)$$

$$+ \frac{1}{6} \left(1 - \frac{1}{3} \frac{\Delta\rho}{\rho^{\Sigma\Lambda}} \right) V_x[\rho^{\Sigma\Lambda}] \quad (59)$$

where \bar{G} is the matrix representation of the operator

$$\begin{aligned} G &= T + V_N + V_C[\rho^{\text{TS}} - \Delta\rho] + \bar{V}_{\mu\nu}^{\Sigma\Lambda} \\ &+ \frac{1}{6} \left(1 - \frac{1}{3} \frac{\Delta\rho}{\rho^{\Sigma\Lambda}} \right) V_x[\rho^{\Sigma\Lambda}] \\ &+ \frac{2}{3} \left(1 - \frac{1}{3} \frac{\Delta\rho}{\rho^{\text{TS}}} \right) V_x[\rho^{\text{TS}}] \end{aligned}$$

It is our specific choice of the intermediate state $\Sigma\Lambda$, viz. Eq. (47), that allows us to treat the (average) pseudopotential in the transition state term in a simple manner, that corresponds closely to existing programs for the frozen-core HFS-LCAO method.

As we will illustrate in the next section, the perturbation corrections to the zeroth order interaction energy do not

TABLE I Exponents of STO basis sets used^{a,b}

	H-dz	H-1z	C-1z	O-1z	F-1z	Cl-1z	Cu-dz	Cu-1z
1z	1.28 0.76	1.58 0.92 0.69	(5.40)	(7.36)	(8.33)	(13.95)	(24.45)	(14.30)
2z			4.60 2.10 1.28	7.58 2.88 1.72	3.24 1.94 0.74	(5.65)	(8.35)	(12.80)
3z						3.30 2.30 1.60	(6.60)	(5.30)
4z							1.90 1.00	2.45 1.40 0.85
2p	1.00	1.00	2.94 1.48 0.82	4.08 2.08 1.12	4.54 2.30 1.24	(6.70)	(11.71)	(11.71)
3p						2.85 2.05 1.20	(4.53)	(4.53)
4p							1.45	2.00 1.00
3d			2.00	2.00	1.54	1.08	5.10 1.65	6.90 3.10 1.28

^aNumbers in brackets denote STO's used for core orthogonalization in frozen-core calculations

^bReference 14

present instability problems, they can simply be obtained as differences of the corresponding overall system and fragment perturbation corrections. From Eqs (41) and (42) it can be seen that they may be considered as corrections to $\Delta E_{\text{pprot}}^{(0)}$ and $\Delta E_{\text{dp}}^{(0)}$.

In summary, using the pseudopotential HFS-LCAO formalism, we have obtained the interaction energy of an overall system, thought to be composed of fragments, as a perturbation series. The zeroth order term reads

$$\Delta E^{(0)} = \Delta E_{\text{cl}} + \Delta E_{\text{exch}} + \Delta E_{\text{pprot}}^{(0)} + \Delta E_{\text{dp}}^{(0)} + \Delta E_{\text{tr}} \quad (60)$$

The first and second order corrections are defined through Eqs (41), (42), and (44)

III. CALCULATIONS AND DISCUSSION

In all our calculations we have taken the exchange parameter α fixed at 0.7^{-1} . The basis sets used are listed in Table I, they were obtained by a least squares fit to numerical HFS orbitals.¹⁴

We have implemented the computational scheme developed in Sec II. In particular we have implemented the self-consistent perturbational scheme up to second order in a computer program that can be used in conjunction with the HFS-LCAO program. The Fock matrices are constructed using the numerical scheme of the pseudopotential HFS-LCAO method, however, with the option of using fewer integration points. We find convergence of the calculations to be quite rapid, using a standard damping procedure in the self-consistent calculation of the first and second order pseudoelectron densities.

In Tables II and III we list the converged orbital energies for Cu and F_2 at different levels of approximation. We note that even for the pathological case of the copper atom with the $3s$ and $3p$ orbitals included in the valence set, the convergence of the perturbation series is quite rapid. The average deviation of the orbital energies from the frozen-core calculations for the "real" valence orbitals $3d$ and $4s$ is 0.0297 , 0.0037 , and 0.0035 a.u. for zeroth, first, and second order, respectively. The spread in the orbital energies within one irreducible representation for F_2 , approximately 18 eV, is more typical for the molecules we intend to use the pseudopotential method for. From these and other calculations it appears that for most practical purposes first order perturbation theory suffices. Further we conclude that the valence orbital energies are accurate to about 0.007 a.u. or 0.2 eV,

TABLE II Orbital energies (in a.u.) for Cu with $3s^2 3p^6 3d^{10} 4s^1$ valence in restricted description using a double zeta basis.

	Pseudopotential			
	Zeroth order	First order	Second order	Frozen core
$3s$	-3.8894	-4.1433	-4.1972	-4.2546
$4s$	-0.2066	-0.1550	-0.1727	-0.1772
$3p$	-2.7766	-2.8058	-2.8022	-2.8050
$3d$	-0.1977	-0.2293	-0.2240	-0.2274
dev ^a	0.0646	0.0141	0.0090	

^a Average deviation $\text{dev} = \frac{1}{N} \sum n_i |e_i^{\text{ps}} - e_i^{\text{fc}}|$

TABLE III Orbital energies (in a.u.) for F_2 at $R = 2.70$ a.u.

	Pseudopotential			
	Zeroth order	First order	Second order	Frozen core
$2\sigma_g$	-1.1755	-1.1958	-1.1973	1.2051
$3\sigma_g$	-0.5443	0.5420	-0.5419	-0.5494
$2\sigma_u$	-0.9662	-0.9652	-0.9651	0.9776
$1\pi_g$	-0.3238	-0.3231	-0.3231	0.3283
$1\pi_u$	-0.4440	-0.4440	-0.4440	-0.4484
dev ^a	0.0091	0.0069	0.0067	

^a Average deviation $\text{dev} = \frac{1}{N} \sum n_i |e_i^{\text{ps}} - e_i^{\text{fc}}|$

which is slightly better than the value 0.01 a.u. given previously by Snijders and Baerends.⁴

In Table IV we illustrate the convergence of the perturbation corrections with the number of integration points for another typical molecule (CO) at its equilibrium geometry. It can be seen that already for small numbers of integration points the results are close to their converged value. This pleasing property enables us to obtain self-consistent perturbation corrections in relatively little computing time (typically a few iterations of the zeroth order calculation). The rapid convergence can be explained by two observations. In the first place, the higher order pseudoelectron densities, Eqs (28c) and (28d), exactly integrate to zero and are relatively smooth in space, which makes it easy to integrate them with a small number of integration points. In the second place, the dominant contributions to the corrections come from the direct perturbations $H_j^{(k)}$ [Eq (29)], which depend on lower order terms only.

The numerical stability of the perturbation corrections to the total energy provides the justification for the calculation of the corrections to the zeroth order interaction energy as differences of these terms [Eq (44)].

Having investigated the characteristics of the self-consistent perturbational approach as such, we now turn to the calculation of interaction energies. We reiterate that the pseudopotential method is meant to reproduce the results obtained with the frozen-core method. Therefore our main objective is the comparison of both methods, where possible,

TABLE IV Convergence of correction terms (in a.u.) with number of integration points N for CO at $R = 2.132$ a.u.

N	250	500	1000	2500
$e_{3\sigma}^{(1)}$	-0.026 98	-0.027 36	-0.027 25	-0.027 24
$e_{4\sigma}^{(1)}$	-0.001 60	-0.001 69	-0.001 65	-0.001 61
$e_{5\sigma}^{(1)}$	+0.004 12	+0.004 05	+0.004 14	+0.004 15
$e_{1\pi}^{(1)}$	-0.005 29	-0.005 05	-0.005 16	-0.005 14
$e_{3\sigma}^{(2)}$	-0.002 05	-0.002 05	-0.002 05	-0.002 06
$e_{4\sigma}^{(2)}$	+0.000 52	+0.000 50	+0.000 49	+0.000 49
$e_{5\sigma}^{(2)}$	-0.000 07	-0.000 07	-0.000 07	0.000 07
$e_{1\pi}^{(2)}$	+0.000 32	+0.000 32	+0.000 32	+0.000 32
$E^{(1)}$	-0.020 15	-0.020 17	-0.020 14	-0.020 14
$E^{(2)}$	-0.005 33	-0.005 36	-0.005 35	-0.005 35

TABLE V Energy differences ΔE (restricted -unrestricted) (in a.u.) for some atoms

Atom	Valence	Basis*	Pseudopotential	Frozen-core	Difference
H	1s ¹	dz		-0.0607	
		tz		-0.0610	
C	2s ² 2p ²	tz	0.0586	-0.0620	+0.0033
O	2s ² 2p ⁴	tz	-0.0678	0.0704	+0.0026
F	2s ² 2p ⁵	tz	-0.0179	0.0185	+0.0006
Cl	3s ² 3p ⁵	tz	-0.0105	-0.0100	-0.0005
Cu	3d ¹⁰ 4s ¹	dz	-0.0129	-0.0118	-0.0011
		tz	0.0142	-0.0137	-0.0006

* See Table I

however, we will compare our results with experiment

In Table V we list the energy differences connected with the change from a spin-restricted to an unrestricted description for some atoms. It can be seen that the numbers obtained with the pseudopotential and frozen-core methods agree well, differences ranging from a few hundredths to a tenth of an eV. Both restricted and unrestricted calculations are performed using fractional occupation numbers, hence they describe (different) averages over pure spin states. The pseudopotentials used are the ones generated for the restricted atoms.⁴ Therefore the differences in ΔE reflect the ability of a single atomic pseudopotential to describe different pure spin states.

In Tables VI and VII we give the interaction energy for CO and Cu₂ as a function of internuclear separation. We note that the interaction energy is calculated with respect to unrestricted atoms at infinite separation using the identity

$$\begin{aligned} \Delta E(\text{AB}) &= E_R(\text{AB}) - E_U(\text{A}) - E_U(\text{B}) \\ &= [E_R(\text{AB}) - E_R(\text{A}) - E_R(\text{B})] \\ &\quad - [E_U(\text{A}) - E_R(\text{A})] - [E_U(\text{B}) - E_R(\text{B})], \quad (61) \end{aligned}$$

where the subscripts R and U denote restricted and unrestricted calculations, respectively. For both molecules there is just one irreducible representation of the molecular point group with more than one occupied valence orbital. The spread in the valence orbital energies within this irreducible representation is quite different, however: for CO at $R = 2.132$ a.u. it is 15 eV, for Cu₂ at $R = 4.00$ a.u. it is only 2 eV. This obviously influences the effect of averaging and the magnitude of the perturbation corrections, the second order corrections for CO are found to be larger than the first order corrections for Cu₂.

From the two cases shown a general feature of our calculations emerges. The pseudopotential method reproduces the interaction energies obtained with the frozen-core method accurately for large values of R . For small values of R , however, it gives increasingly too negative interaction energies. Of course for small R both methods eventually break down. It may very well be that the pseudopotential method breaks down more quickly, because its assumptions are more severe. Both frozen-core and pseudopotential methods require the core orbitals to have their atomic form, in addition to this the pseudopotential method also requires them to have their atomic orbital energy. The phenomenon of core-level binding-energy shifts, in which initial state effects are known to be important, contradicts the validity of the last assumption. The consequences of this shift for pseudopotential calculations are unknown, however. Apart from these assumptions our pseudopotential method also approximates $\Delta\rho$ by a sum of atomic terms [cf. Eq. (15)]. For molecules with covalent bonding we expect the effect of this approximation to be small.

From the data in Tables VI and VII and similar data for some other diatomics we have calculated the spectroscopic constants listed in Table VIII. Comparing the results obtained with pseudopotential and frozen-core methods for CO, F₂, and Cl₂ we find a good agreement, differences amount to 0.01–0.02 Å in R_e , 0.1–0.2 eV in D_e , and 10–20 cm⁻¹ in ω_e . For Cu₂ and CuH the results are somewhat less satisfactory. Agreement in D_e is the same as for the first and second row systems, but due to the very shallow wells in the potential curves (the binding energy only slowly varying with R), R_e and ω_e are very sensitive to small inaccuracies in the binding energy. This is illustrated by the effect of a

TABLE VI Interaction energy (in a.u.) for CO with respect to atoms in unrestricted description

R	Pseudopotential			Frozen core
	Zeroth order	First order	Second order	
1.832	-0.3296	-0.3607	-0.3689	-0.3455
1.932	-0.3793	-0.4057	-0.4128	-0.3970
2.032	-0.4047	-0.4276	-0.4337	-0.4229
2.132	-0.4128	-0.4330	-0.4383	-0.4307
2.232	-0.4087	-0.4268	-0.4315	-0.4261
2.332	-0.3962	-0.4129	0.4171	-0.4130
2.432	-0.3781	-0.3939	-0.3977	-0.3943
2.532	-0.3566	-0.3718	-0.3752	-0.3722
2.632	-0.3329	-0.3479	-0.3510	-0.3491

TABLE VII Interaction energies (in a.u.) for Cu_2 with respect to atoms in unrestricted description using a double zeta basis set

R	Pseudopotential			
	Zeroth order	First order	Second order	Frozen core
3.50	-0.0875	-0.0869	-0.0875	-0.0594
3.75	-0.1068	-0.1059	-0.1064	-0.0932
4.00	-0.1112	-0.1102	-0.1105	-0.1055
4.25	-0.1063	-0.1053	-0.1055	-0.1048
4.50	-0.0969	-0.0959	-0.0961	-0.0974
4.75	0.0861	-0.0850	-0.0851	-0.0870
5.00	-0.0751	-0.0740	-0.0740	-0.0756

change of basis set in the Cu_2 calculations. In the triple zeta basis the curve is more shallow than in the double zeta basis, deviations are consistently larger as well.

The perturbation corrections can be seen to influence D_e most (cf F_2), R_e and ω_e being rather insensitive. This can be attributed to the fact that the perturbation correction to the interaction energy varies relatively slowly with distance. Generally the corrected spectroscopic constants are in better agreement with the ones calculated with the frozen-core method. The only exception is Cl_2 , although differences are still quite small.

It is interesting to compare the results for F_2 and Cl_2 with results obtained with other pseudopotential methods. Kahn *et al.*⁹ find the following deviations from all-electron results $\Delta R_e(F_2) = 4.9\%$, $\Delta D_e(F_2) = 43\%$, $\Delta R_e(\text{Cl}_2) = 6.9\%$, and $\Delta D_e(\text{Cl}_2) = 69\%$. The corresponding results obtained by Hay *et al.*⁹ are 0.7%, 8.8%, 2.5%, and 8.9%

The best results are obtained by Christiansen *et al.*¹² 0.7%, 1.4%, <0.2%, and 4.8%. Our series of deviations reads 0.7%, 2.7%, 0.5%, and 6.5%. Hence our results for the spectroscopic constants are only slightly less accurate than Christiansen's, however, for small R deviations in the energies are larger.

Although we did not optimize our basis sets, our primary goal being the comparison of pseudopotential and frozen-core methods, it appears that our results are fairly close to the Hartree-Fock-Slater limits obtained with Becke's numerical method¹⁶ (cf also Refs. 17-19 for accurate HFS calculations on diatomics). Becke found for CO $R_e = 1.12 \text{ \AA}$, $D_e = 12.0 \text{ eV}$, $\omega_e = 2170 \text{ cm}^{-1}$, and for F_2 $R_e = 1.38 \text{ \AA}$, $D_e = 3.2 \text{ eV}$, $\omega_e = 1060 \text{ cm}^{-1}$.

We note that the agreement of the HFS results with experiment is quite good, the only exception being D_e and ω_e for F_2 . However, F_2 is a notoriously difficult molecule, Har-

TABLE VIII Spectroscopic constants for some diatomics

		$R_e(\text{Å})$	$D_e(\text{eV})$	$\omega_e(\text{cm}^{-1})$
CO	PS ₀ ^a	1.14	11.2	2110
	PS ₁	1.12	11.8	2120
	PS ₂	1.12	11.9	2130
	FC	1.14	11.7	2140
	Exp	1.13	11.1	2170
F_2	PS ₀	1.42	2.12	1060
	PS ₁	1.42	3.03	1050
	FC	1.41	2.95	1050
	Exp	1.41	1.60	917
Cl_2	PS ₀	2.08	2.40	537
	PS ₁	2.09	2.62	516
	FC	2.08	2.46	532
	Exp	1.99	2.48	560
Cu_2-dz^2	PS ₀	2.10	3.01	358
	PS ₁	2.10	2.98	358
	FC	2.17	2.90	364
α	PS ₀	2.07	2.31	315
	PS ₁	2.08	2.30	316
	FC	2.20	2.10	275
	Exp	2.22	2.03	265
CuH dz	PS ₀	1.47	2.6	1930
	PS ₁	1.47	2.5	1950
	FC	1.50	2.5	2520
	Exp	1.46	2.7	1940

^a PS₀, PS₁, and PS₂ denote zeroth, first, and second order pseudopotential calculations, respectively. FC denotes a frozen-core calculation.

^b See Table I.

TABLE IX Binding energies (in eV) for some polyatomic molecules in their (experimental) equilibrium geometry^a

	Pseudopotential			Frozen-core	Exp ^b
	Zeroth order	First order	Second order		
CO ₂	18.3	18.9	19.1	18.6	16.5
C ₂ H ₂	16.3	16.6	16.7	16.7	16.8
C ₂ H ₄	21.7	22.0	22.1	22.2	23.1
CuCO ^c	0.13	0.64	0.87	0.64	
Cu ₂ ^d	7.32	7.28		7.16	

^a Basis sets used: double zeta for Cu, triple zeta for H, C, and O, see Table I

^b Reference 22

^c R (Cu-C) = 3.75 a.u., R (C-O) = 2.20 a.u., energy relative to Cu and free CO

^d Cu₂(5, 0) cluster with bulk Cu-Cu distances (4.82 a.u.)

tree-Fock does not even predict bonding. We also note that the HFS Cu₂ results are comparable to recent effective potential²⁰ and all-electron²¹ *ab initio* calculations only after inclusion of CI in the latter.

In Table IX we list the binding energies for some polyatomic molecules. The results indicate that the pseudopotential method reproduces frozen-core results equally well for larger systems. The differences found are in the order of a few tenths of an eV, except for CO₂, where it is 0.5 eV (which amounts to 2.7%).

IV. CONCLUSIONS

In this paper we have developed a computationally feasible scheme for the calculation of interaction energies using the pseudopotential Hartree-Fock-Slater-LCAO method. The scheme is based on a pseudopotential energy functional which we derived using the formal identity of orbital energies in all-electron and pseudopotential methods, and on a self-consistent perturbational scheme to correct for the use of averaged pseudopotentials. We wish to emphasize that the generation of pseudopotentials, and the subsequent SCF and total energy calculation, are completely straightforward, without any need for parameterization or fitting of effective potentials.

It is found that the perturbation series converges rapidly, for most practical purposes the first order result being sufficient. The results of the perturbation calculations are found to be numerically stable, enabling the use of a relatively cheap numerical integration scheme. The orbital energies on the average differ by less than 0.2 eV from the corresponding frozen-core values.

Test calculations on a number of molecules show good agreement between the pseudopotential and the frozen-core HFS-LCAO results. General tendency is that the pseudopotential binding energies are slightly too large, which becomes more prominent for short internuclear separations. For systems of first and second row atoms the spectroscopic constants calculated with the two methods differ by 0.01–0.02 Å in R_e , 0.1–0.2 eV in D_e , and up to 20 cm⁻¹ in the more sensitive ω_e . These results are comparable to the ones obtained with best pseudopotential and effective core potential methods currently available.

For systems containing the transition metal Cu the re-

sults are comparable except that due to the shallow well in the binding energy curve R_e and ω_e are less accurate. Calculations on polyatomic systems show that the performance of the pseudopotential method does not depend on the size of the system.

In conclusion, we find that the general agreement between pseudopotential and frozen-core HFS-LCAO methods is good. Moreover, agreement with experiment is satisfactory as well. Therefore the pseudopotential method seems accurate enough to investigate physical effects, such as the influence of cluster size in chemisorption calculations.

ACKNOWLEDGMENTS

We are happy to acknowledge the contribution of Mr E. Bastiaan in early stages of this work. Further we thank Professor Dr A. van der Avoird and Dr J. G. Snijders for helpful discussions and Mrs F. Geurts and P. Vernooijs for the performance of some of the calculations.

This investigation was supported in part by the Netherlands Foundation for Chemical Research (S.O.N.) with financial aid from the Netherlands Organization for the Advancement of Pure Research (Z.W.O.).

¹E. J. Baerends, D. E. Ellis, and P. Ros, *Chem Phys* **2**, 41 (1973); E. J. Baerends and P. Ros, *ibid.* **2**, 52 (1973).

²T. Ziegler and A. Rauk, *Theor. Chim. Acta* **46**, 1 (1977).

³J. C. Slater, *Quantum Theory of Molecules and Solids* (McGraw-Hill, New York, 1974), Vol. 4.

⁴J. G. Snijders and E. J. Baerends, *Mol. Phys.* **33**, 1651 (1977).

⁵J. C. Phillips and L. Kleinman, *Phys. Rev.* **116**, 287 (1959).

⁶P. J. M. Geurts, J. W. Gosselink, A. van der Avoird, E. J. Baerends, and J. G. Snijders, *Chem. Phys.* **46**, 133 (1980); P. Geurts and A. van der Avoird, *Surf. Sci.* **102**, 185 (1981); **103**, 416 (1981); P. Geurts, H. Burgers, and A. van der Avoird, *Chem. Phys.* **54**, 397 (1981); P. Geurts, W. Ravenek, and A. van der Avoird, *Surf. Sci.* **103**, 431 (1981).

⁷J. G. Snijders and E. J. Baerends, *Mol. Phys.* **36**, 1789 (1978); **38**, 1909 (1979).

⁸T. Ziegler, J. G. Snijders, and E. J. Baerends, *J. Chem. Phys.* **74**, 1271 (1981).

⁹L. R. Kahn and W. A. Goddard III, *J. Chem. Phys.* **56**, 2685 (1972); C. F. Melius, W. A. Goddard III, and L. R. Kahn, *ibid.* **56**, 3342 (1972); L. R. Kahn, P. Baybutt, and D. G. Truhlar, *ibid.* **65**, 3826 (1976); P. J. Hay, W. R. Wadt, and L. R. Kahn, *ibid.* **68**, 3059 (1978).

¹⁰V. Bonifacic and S. Huznaga, *J. Chem. Phys.* **60**, 2779 (1974); Y. Sakai and S. Huznaga, *ibid.* **76**, 2537 (1982).

- ¹¹P Durand and J C Barthelat, *Theor Chim Acta* **38**, 283 (1975), J C Barthelat, Ph Durand, and A Serafini, *Mol Phys* **33**, 159 (1977)
- ¹²P A Christiansen, Y S Lee, and K S Pitzer, *J Chem Phys* **71**, 4445 (1979)
- ¹³A Dalgarno, *Adv Phys.* **11**, 281 (1962), and references therein
- ¹⁴P Vermooy, J G Snyders, and E J Baerends, *Slater Type Basis Functions for the Whole Periodic System, Internal Report* (Free University Amsterdam, The Netherlands, 1981)
- ¹⁵K P Huber and G Herzberg, *Molecular Spectra and Molecular Structure IV* (Van Nostrand Reinhold, New York, 1979)
- ¹⁶A. D Becke, *J Chem Phys* **76**, 6037 (1982), **78**, 4787 (1983)
- ¹⁷B I Dunlap, J W D Connolly, and J R Sabin, *J Chem Phys* **71**, 4993 (1979)
- ¹⁸G S Painter and F W Averil, *Phys. Rev B* **26**, 1781 (1982)
- ¹⁹L Laaksonen, D Sundholm, and P Pyykko (private communication)
- ²⁰M Pelissier, *J Chem Phys* **75**, 775 (1981)
- ²¹C W Bauschlicher, Jr., S P Walch, and P E. M Siegbahn, *J Chem Phys.* **76**, 6015 (1982), **78**, 3347 (1983)
- ²²A G Gaydon, *Dissociation Energies and Spectra of Diatomic Molecules* (Chapman and Hall, London, 1953)

C H A P T E R I V

**THE CALCULATION OF ONE-ELECTRON PROPERTIES
USING THE PSEUDOPOTENTIAL HARTREE-FOCK-SLATER LCAO METHOD**

W RAVENEK and F M M GEURTS

Institute of Theoretical Chemistry University of Nijmegen, Toernooiveld, Nijmegen, The Netherlands

Received 14 May 1984

Using the pseudopotential and frozen core Hartree-Fock-Slater LCAO methods we have calculated electric multipole moments the diamagnetic susceptibility potential electric field electric field gradient and diamagnetic shielding for the molecules HF HCl LiH LiF LiCl CO CO₂ C₂H₂ and C₂H₄. The pseudopotential method is found to reproduce frozen core results very well if the pseudo-orbitals are core orthogonalized. The calculated dipole and quadrupole moments agree well with the available Hartree-Fock and experimental values.

1. Introduction

In the past decade numerous pseudopotential and effective core potential methods [1-23] (hereafter collectively referred to as pseudopotential methods) have been developed that accurately reproduce all-electron (or frozen-core [22,23]) results in electronic structure calculations. For instance, Christiansen et al [18] have calculated potential curves for F₂ and Cl₂ that differ by only 0.02 bohr in the equilibrium separation and by less than 0.1 eV in the binding energy. In the evaluation of these methods most attention has been directed towards the calculation of energetic quantities such as ionization potentials and spectroscopic constants that can be obtained from potential curves.

In a number of cases also one-electron properties have been calculated [1-3,10,14,19-21], mostly the electric dipole moment. These properties are commonly evaluated from the pseudo-orbitals as such without core orthogonalization, although it is realized that this involves an approximation. The agreement between pseudopotential and all-electron values for the dipole moment is generally good, differences being 0.1 debye or less. Exceptions to this rule form the differences found by Dixon and Hugo [10] for NaCl (0.35 debye) and by Preuss et al [20] for HCl (0.3 debye). We note

that in the majority of cases hydrides were studied, which constitute a relatively mild test for pseudopotentials.

Other properties have only been considered sporadically. Kahn and Goddard [1] calculated the quadrupole moment, the potential and the electric field gradient at the nucleus for LiH and Li₂. Melius et al [2] did the same for some excited states of LiH. The potential at the nucleus has also been calculated for HF and HBr by Kahn et al [3]. We will return to these calculations in the discussion of our results (section 4).

Pseudopotential methods aim at a similarity in the valence region between pseudo-orbitals and valence orbitals obtained from all-electron calculations. Proper valence orbitals may be obtained by orthogonalizing the pseudo-orbitals to the core (cf section 2). Dixon and Hugo [10] explicitly assume that, due to the spherical character of the cores, this will only have a small influence on the dipole moment. Qualitatively it is clear that this will hold for all properties that mainly sample the valence region, such as electric multipole moments and the diamagnetic susceptibility. In this paper we will pursue this matter quantitatively by actually evaluating one-electron properties before and after core orthogonalization of the pseudo-orbitals for a variety of molecules. We will also consider properties that mainly sample the core region, viz the

potential, the electric field, the electric field gradient and the diamagnetic shielding at the nuclei

In our calculations we use the Hartree-Fock-Slater (HFS) LCAO method of Baerends et al [24,25] in the pseudopotential version of Snijders and Baerends [22]. In section 2 we will outline its essential features. Since the computational scheme of the HFS LCAO method concentrates on the valence electrons, we will compare our pseudopotential calculations with the corresponding frozen-core calculations.

The HFS LCAO method is known to yield good agreement with experiment for a variety of properties [26]: equilibrium geometries, binding energies, stretching frequencies, electronic transition energies, dipole moments and dipole moment derivatives. Recently Snijders et al [27] have calculated electric field gradients for H_2 and CH_4 using the fitted one-electron density

$$\rho(r) = \sum_{\mu} P_{\mu} \chi_{\mu}(r) \chi_{\mu}^*(r) = \sum_i a_i f_i(r),$$

with very satisfactory results. In the present paper we have used the "exact" density, calculated from the MOs, rather than the fitted density. After a STO-GTO expansion [30] of the STO basis functions χ_{μ} we can use a standard one-electron properties program [31] for gaussian-type orbitals (GTOs).

2 The pseudopotential HFS LCAO method

In the pseudopotential HFS LCAO method [22,23] core collapse is prevented by adding to the Fock operator a pseudopotential

$$V_{ps} = \sum_k (\epsilon_j - \epsilon_k^c) |\psi_k^c\rangle \langle \psi_k^c|, \quad (2.1)$$

which shifts the core orbitals ψ_k^c from their all-electron orbital energies ϵ_k^c to the valence energy ϵ_j . This valence level thereby becomes degenerate. The solution of the SCF problem then gives a pseudo-orbital of the form

$$\psi_j^{ps} = \psi_j^v + \sum_k \psi_k^c a_{kj}, \quad (2.2)$$

with arbitrary coefficients a_{kj} .

In order to determine the coefficients a_{kj} in eq

(2.2) one usually requires the pseudo-orbitals to be nodeless and to have maximum similarity with the corresponding valence orbitals ψ_j^v in some sense. For instance, one may require ψ_j^{ps} and ψ_j^v to have maximum overlap [3], to be identical beyond a certain radius [7-9,19] or to have the same first moment $\langle r \rangle$ after core orthogonalization [10]. A notable exception is formed by the method of Huzinaga [5,6] in which the valence orbitals keep their full nodal structure, the price to be paid for the latter is that the basis sets needed are larger than in other methods.

In the pseudopotential HFS LCAO method one uses another common device, viz. one truncates the basis by deleting all core basis functions. Since one has a number of a_{kj} (for given j) equal to the number of core orbitals only, this involves an approximation.

Due to the local exchange approximation and the computational scheme used, the HFS LCAO method allows a straightforward inclusion of the core contributions to the electronic Coulomb and exchange potentials, no parameterized effective core potential is required. Further, one does not use the pseudo-orbitals as such to calculate the valence potential, instead one uses the less severe assumption

$$\Delta\rho_{molecule}(1) = \sum \Delta\rho_{atom}(1), \quad (2.3)$$

where

$$\Delta\rho(1) = \sum_j n_j [\psi_j^v(1)\psi_j^{v*}(1) - \psi_j^{ps}(1)\psi_j^{ps*}(1)], \quad (2.4)$$

with the n_j occupation numbers. We note that this assumption is equivalent to the one employed by Dixon et al [11], viz

$$(G^v - G^{ps})_{molecule} = \sum (G^v - G^{ps})_{atom}, \quad (2.5)$$

where G^x is the sum of Coulomb and exchange potentials summed over the set x .

$$G^x = \sum_i^x (2J_i - K_i) \quad (2.6)$$

The problem which valence level ϵ_j to shift the core orbitals to, is solved by using an average

pseudopotential

$$\bar{V}_{ps} \Gamma = \sum_k (\bar{\epsilon}_\Gamma - \epsilon_k^c) |\psi_k^c\rangle \langle \psi_k^c| \quad (2.7)$$

for each irreducible representation Γ (with average valence energy $\bar{\epsilon}_\Gamma$) of the molecular point group. For each particular valence level the averaging is corrected for by the use of perturbation theory. Recently [23] we have developed a self-consistent perturbation scheme that allows incorporation of the pseudopotential version of the HFS LCAO method in Ziegler's [32] transition-state scheme for calculating chemical interaction energies.

Given the pseudo-orbitals (2.2) calculated with the pseudopotential HFS LCAO method, or with any other pseudopotential scheme, one may recover the valence orbitals by orthogonalizing to the cores

$$\psi_j^v = (1 - \hat{P}_c) \psi_j^{ps}, \quad (2.8)$$

with

$$\hat{P}_c = \sum_k |\psi_k^c\rangle \langle \psi_k^c| \quad (2.9)$$

the projector on the space spanned by the core orbitals.

3. Computational procedure

The scheme used for calculating one-electron properties is similar to the one used previously for the calculation of electric field gradients of some antimony compounds [29]. The Hartree-Fock-Slater calculations were performed with the HFS LCAO program of Baerends et al. [24,25] in its pseudopotential version [22], adapted to IBM. This program is based on STOs. Self-consistent perturbation calculations for the pseudo-orbitals were performed using a recently developed program [23]. The actual calculation of the properties was performed using the one-electron properties program of the POLYATOM package, which is based on GTOs.

Further we used an interface program which reads the converged SCF data from the HFS LCAO program or the perturbational program, expands the STOs in GTOs and prepares the input

Table 1
Exponents of STO basis sets used^{a)} [33]

	H	Li	C	O	F	Cl
1s	1.58 0.92 0.69	(2.46)	(5.40)	(7.36)	(8.33)	(13.95)
2s		2.36 0.68 0.46	4.60 2.10 1.28	7.58 2.88 1.72	3.24 1.94 0.74	(5.65)
3s						3.30 2.30 1.60
2p	1.00	2.36 0.68 0.46	2.94 1.48 0.82	4.08 2.08 1.12	4.54 2.30 1.24	(6.70)
3p						2.85 2.05 1.20
3d			2.00	2.00	1.54	1.08

^{a)} Numbers in parentheses denote STOs used for core orthogonalization in frozen-core calculations.

for the properties program. The STO/GTO expansion performed according to the method of maximum overlap fits of Stewart [30], each (n, l) STO is expanded in 1 to 6 $(l+1, l)$ GTOs. Compared with its previous version we have added the option of orthogonalizing the pseudo-orbitals to the cores (cf. eq. (2.8)). The orbitals are renormalized after the orthogonalization.

In all our calculations we have taken the exchange parameter α fixed at 0.7 [25]. The STO basis sets used [33] are listed in table 1. They are of triple-zeta quality, supplemented with polarization functions. For the calculation of chemical interaction energies these basis sets are known to be close to the HFS limit.

4. Results and discussion

One-electron properties have been calculated for a number of molecules at their experimental equilibrium geometries: HF ($R = 1.733$), HCl ($R = 2.409$), LiH ($R = 3.015$), LiF ($R = 2.995$), LiCl ($R = 3.819$), CO ($R = 2.132$), CO₂ ($R_{CO} = 2.194$), C₂H₂ ($R_{CC} = 2.274$, $R_{CH} = 2.004$) and C₂H₄ ($R_{CC} = 2.530$, $R_{CH} = 2.050$, $\angle HCH = 117.8^\circ$). All distances are in atomic units. The linear molecules

were placed along the z axis, C_2H_4 in the xz plane with the carbon nuclei on the z axis. We divide the properties considered in two groups

(I) Properties that mainly sample the valence region (characterized by a positive power of r in the corresponding quantum-mechanical operators), viz the electric multipole moments up to $l = 3$ and the diamagnetic susceptibility

(II) Properties that mainly sample the core region (characterized by a negative power of r in the corresponding operators) viz the potential, the electric field, the electric field gradient and the diamagnetic shielding

The core contributions to the properties have been calculated in the frozen-core approximation. The effect of cores other than that of the center at which a property is evaluated is taken into account by the use of effective nuclear charges. The contribution of the core of the nucleus at which a property is evaluated is zero due to the spherical symmetry, except for the potential and the diamagnetic shielding, where it is a non-zero constant. Keeping the cores frozen we obviously neglect core polarization effects and a priori no agreement with experiment may be expected for the group II properties. For these properties we consider our calculations as a methodological test of the pseudopotential method.

The results are presented in tables 2-9. We give core-orthogonalized pseudopotential results up to first order in the perturbation treatment. For the zeroth-order results we have included non-core-orthogonalized results in parentheses. We compare these results with frozen-core values and, in a number of cases, also with Hartree-Fock (HF) and experimental values.

4.1 Valence region directed properties

We give the dipole, quadrupole and octupole moments in their tesseral harmonic form [34,35] for a molecule with nuclei at positions $r_i = (r_i, \theta_i, \varphi_i)$ and with charges Z_i and one-electron density $\rho(r)$ we have in atomic units

$$Q_{lm} = \left(\frac{4\pi}{2l+1} \right)^{1/2} \left(\sum_i Z_i r_i^l S_{lm}(\theta_i, \varphi_i) - \int \rho(r) r^l S_{lm}(\theta, \varphi) dr \right) \quad (4.1)$$

The S_{lm} are the normalized tesseral harmonics. As the origin of the coordinate system we have taken the molecule's center of mass. In particular

$$Q_{10} = \sum_i Z_i z_i - \int \rho(r) z dr, \quad (4.1a)$$

$$Q_{20} = \frac{1}{2} \sum_i Z_i (3z_i^2 - r_i^2) - \frac{1}{2} \int \rho(r) (3z^2 - r^2) dr \quad (4.1b)$$

and

$$Q_{30} = \frac{1}{2} \sum_i Z_i (5z_i^3 - 3z_i^2 r_i^2) - \frac{1}{2} \int \rho(r) (5z^3 - 3zr^2) dr \quad (4.1c)$$

We note that for a linear closed-shell molecule along the z axis only the Q_{lm} with $m = 0$ are non-zero.

The elements of the diamagnetic susceptibility tensor are given by

$$\chi_{\mu\nu}^d = \frac{1}{4} \int \rho(r) (r_\mu r_\nu - \delta_{\mu\nu} r^2) dr, \quad (4.2)$$

where μ and ν take the values x , y and z . We only list the average diamagnetic susceptibility

$$\chi_{av}^d = \frac{1}{3} (\chi_{xx}^d + \chi_{yy}^d + \chi_{zz}^d) = -\frac{1}{6} \int \rho(r) r^2 dr \quad (4.3)$$

For the linear molecules the diamagnetic susceptibility anisotropy, $\Delta\chi^d = \chi_{||}^d - \chi_{\perp}^d$ is directly related to the electronic contribution to the quadrupole moment.

In discussing our results we first consider the dipole moment (cf table 2). In their review paper Baerends and Ros [26] list the values $Q_{10}(\text{HF}) = 1.71$ D, $Q_{10}(\text{LiH}) = 5.46$ D, $Q_{10}(\text{LiF}) = 5.87$ D and $Q_{10}(\text{CO}) = -0.25$ D, the average discrepancy between our frozen-core results and theirs is 0.27 D. Our calculations differ from theirs in the internuclear separations and in the basis sets used. We evaluated the dipole moment at the experimental equilibrium geometry, whereas Baerends and Ros used the calculated equilibrium geometry. Using their values for the dipole-moment derivatives [26] it can be seen that the difference in geometry has only a minor effect on the (average) discrepancy.

Table 2
Dipole moment $Q_{10}^{(a)}$ (in debye $1D = 3.336 \times 10^{-30} \text{ C m}$)

Molecule	Pseudopotential		Frozen core	HF ^(c)	Exp ^(d)
	zeroth order ^(b)	first order			
HF	1.76 (1.74)	1.71	1.76	1.92	1.80
HCl	1.19 (1.26)	0.95	1.06	1.22	1.09
LiH ^(e)	5.51 (5.38)	5.51	5.49	6.00	5.88
LiF	6.01 (5.78)	6.05	6.05	6.30	6.28
LiCl	6.80 (6.66)	6.79	6.71	7.22	7.09
CO	-0.12(-0.11)	-0.11	-0.20	0.26	-0.12

^{a)} A positive value denotes a + - polarity for the molecule as written

^{b)} Numbers in parentheses are obtained without core orthogonalizing the pseudo-orbitals

^{c)} Hartree-Fock values HF [36], HCl [37], LiH [38-39], LiF [40], LiCl [41], CO [36]

^{d)} Experimental values HF [42], HCl [43], LiH [44], LiF [45], LiCl [45], CO [46]

^{e)} Since no averaging is involved in the pseudopotential in this case, perturbation corrections are identically zero

Therefore the differences must be attributed to the basis sets used. Baerends and Ros used Clementi's basis sets, obtained by total energy optimization, which is to a large extent a core property. Here we use basis sets obtained by a least-squares fit to numerical HFS valence orbitals [33]. These basis sets give dipole moments that are uniformly closer to the experimental values.

Agreement of the HFS LCAO dipole moments with experiment is good, it is equally good as for the near-HF-limit dipole moments. Note however, that HFS predicts the correct sign for CO, whereas HF does not.

All the quadrupole moments (cf. table 3) agree well with experiment, although differences are decidedly larger than for the dipole moments. Two reasons may be suggested to explain this phenomenon. First, the experimental quadrupoles are not as accurately known as the experimental dipoles, the errors given for the values quoted [50-53] range from 0.03 au for CO to 0.11 au for CO₂. Secondly, it has been established by McCullough [47] that quadrupole moments are quite sensitive to basis-set errors. Comparing HF LCAO calculations with his numerical HF calculations McCullough found that even with moderately large

Table 3
Quadrupole moment Q_{20} with respect to center of mass (in atomic units, $1 \text{ au} = 4.487 \times 10^{-40} \text{ C m}^2$)

Molecule	Pseudopotential		Frozen-core	HF ^(a)	Exp ^(b)
	zeroth order	first order			
HF	1.87 (1.88)	1.88	1.89	1.73	1.64
HCl	3.11 (3.19)	3.00	2.94	2.78	2.62
LiH	-2.37(-2.18)	-2.37	-2.35		
LiF	4.55 (4.57)	4.50	4.47		
LiCl	10.3 (10.2)	10.2	10.2		
CO	-1.34(-1.26)	-1.38	-1.38	-1.53	-1.44
CO ₂	-2.85(-2.59)	-2.84	-2.85	-3.84	-3.34
C ₂ H ₂	4.83 (4.99)	4.83	4.87	5.46	6.2
C ₂ H ₄ ^(c)	1.33 (1.39)	1.31	1.32	1.50	1.47

^{a)} Hartree-Fock values HF [47], HCl [37], CO [47], CO₂ [48], C₂H₂ [49], C₂H₄ [49]

^{b)} Experimental values HF [50], HCl [50], CO [51], CO₂ [52], C₂H₂ [49], C₂H₄ [53]

^{c)} See also text

basis sets and some exponent optimization, quadrupole moment basis-set errors in the range 0.05-0.1 au can be expected. Since we used standard basis sets which only one set of polarization functions per atom (except for Li) and no exponent optimization, we consider the agreement with HF and with experiment as satisfactory.

The C₂H₄ molecule merits a separate discussion. The recent experimental quadrupole moment of Gray et al. [53], obtained from collision-induced adsorption measurements, differs rather drastically from earlier values, but agrees well with our results (and with ab initio results [49]). Our frozen-core values are $Q_{xx} = 1.40 \text{ au}$ and $Q_{yy} = -2.72 \text{ au}$, the experimental values $Q_{xx} = 1.50 \text{ au}$ and $Q_{yy} = -2.97 \text{ au}$, the pseudopotential results are again very similar. In tesseral harmonic form (eq. (4.1)) the two non-zero moments are Q_{20} and $Q_{22} = 3^{-1/2}(Q_{xx} - Q_{yy})$.

We now compare pseudopotential and frozen-core methods for the group I properties. As we have stated in section 1 typical differences between pseudopotential and all-electron dipole moments are 0.1 D (without core orthogonalization), but much larger values are also reported. Our calculations yield a maximum difference of 0.11 D and an average difference of 0.02 D. For

Table 4
Octupole moment Q_{30} with respect to center of mass^{a)} (in atomic units $1 \text{ au} = 2.374 \times 10^{-50} \text{ C m}^3$)

Molecule	Pseudopotential		Frozen-core
	zeroth order	first order	
HF	2.85 (2.85)	2.87	2.88
HCl	5.40 (5.20)	5.20	5.00
LiH	3.58 (3.19)	3.58	3.48
LiF	10.4 (10.4)	10.6	10.5
LiCl	32.3 (32.0)	32.6	32.6
CO	-3.31(-3.25)	-3.37	-3.38

^{a)} Sign corresponds to that of the dipole moment (cf. table 2)

the quadrupole moment few comparisons between pseudopotential and all-electron methods exist. Using the G1 method Kahn and Goddard [1] found differences of 0.03 and 0.55 au for the ground states of LiH and Li₂, respectively. Using the same method Melius et al. [2] found differences up to 1.3 au for some excited states of LiH. These rather disappointing results were obtained without core orthogonalization.

As can be seen from tables 2-5 the pseudopotential and frozen-core HFS LCAO results agree very well. In table 10 we list the average absolute deviations, they are very small indeed. The relative error of 9.6% for the dipole moment is mainly caused by the small absolute value for CO (excluding CO lowers the difference to 2.9%). It can be seen that differences in the behaviour of the four properties are small for the molecules considered. It is also clear that the effect of the perturbation

Table 5
Average diamagnetic susceptibility with respect to center of mass (in atomic units $1 \text{ au} = 7.891 \times 10^{-29} \text{ J T}^{-2} \text{ mole}^{-1}$)

Molecule	Pseudopotential		Frozen-core
	zeroth order	first order	
HF	-2.43 (-2.41)	-2.43	-2.41
HCl	-5.41 (-5.20)	-5.44	-5.50
LiH	-3.75 (-3.70)	-3.75	-3.75
LiF	-5.18 (-5.16)	-5.23	-5.22
LiCl	-10.3 (-10.1)	-10.3	-10.4
CO	-6.60 (-6.54)	-6.61	-6.63
CO ₂	-18.8 (-18.7)	-18.8	-18.8
C ₂ H ₂	-10.1 (-10.1)	-10.1	-10.2
C ₂ H ₄	-13.8 (-13.7)	-13.8	-13.8

corrections to the pseudo-orbitals on the properties is small, although overall agreement with frozen-core results definitely improves.

The influence of core orthogonalization is also small. To obtain quantitative agreement with the frozen-core results, however, it is necessary to use core-orthogonalized pseudo-orbitals. In the cases investigated core orthogonalization has a larger effect than the perturbation corrections.

4.2 Core region directed properties

The properties considered that mainly sample the core region are the potential

$$\phi = \sum_i Z_i r_i^{-1} - \int \rho(r) r^{-1} dr, \quad (4.4)$$

the electric field

$$E_\mu = \sum_i Z_i r_{i\mu} r_i^{-3} - \int \rho(r) r_\mu r^{-3} dr, \quad (4.5)$$

the electric field gradient

$$V_{\mu\nu} = \sum_i Z_i (3r_{i\mu} r_{i\nu} - \delta_{\mu\nu} r_i^2) r_i^{-5} - \int \rho(r) (3r_\mu r_\nu - \delta_{\mu\nu} r^2) r^{-5} dr \quad (4.6)$$

and the diamagnetic shielding

$$\sigma_{\mu\nu}^d = \frac{1}{2} \int \rho(r) (r_\mu r_\nu - \delta_{\mu\nu} r^2) r^{-3} dr \quad (4.7)$$

Since the average diamagnetic shielding is proportional to the electronic contribution to the potential, we only list the diamagnetic shielding anisotropy for the linear molecules,

$$\Delta\sigma^d = \sigma_{\parallel}^d - \sigma_{\perp}^d \quad (4.8)$$

As described earlier in this section the core contributions are obtained using the frozen-core assumption. In valence-electron-only calculations of the electric field gradient core polarization is usually corrected for by the use of Sternheimer factors. Since we are principally interested in comparing pseudopotential and frozen-core methods, we will not consider such corrections.

The results of our calculations are presented in

tables 6-9 In table 10 we have again summarized these results by listing average differences, we have considered hydrogen and other atoms separately.

The potential at the nucleus has been investigated by Kahn and Goddard [1] for LiH and Li₂, by Melus et al [2] for some excited states of LiH and by Kahn et al [3] for HF and HBr, in all cases non-core-orthogonalized pseudo-orbitals were used It was found that the potential at the hydrogen nucleus was almost identical in pseudo-potential and all-electron calculations, whereas larger differences were found for the potential at other nuclei In the hydrides of Li, F and Br the differences were 0.015, ≈ 0.3 and ≈ 0.3 au respectively Due to the large core contribution the relative errors were still quite small (1.3% for F, 0.2% for Br)

The orthogonalization of the pseudo-orbitals to the core transfers electron density from the core to the valence region The effect is to lower the potential at the nucleus, as can be clearly seen in table 6 Thus, the agreement between pseudo-

Table 6
Potential at the nucleus^{a)} (in atomic units, 1 au = 27.21 V)

Molecule	Nucleus	Pseudopotential		Frozen-core
		zeroth order	first order	
HF	H	-0.881(-0.882)	-0.884	-0.880
	F	-9.32(-9.02)	-9.33	-9.38
HCl	H	-0.894(-0.885)	-0.914	-0.905
	Cl	-5.64(-5.12)	-5.64	-5.56
LiH	Li	-0.380(-0.353)	-0.380	-0.392
	H	-1.18(-1.17)	-1.18	-1.18
LiF	Li	-0.422(-0.401)	-0.397	-0.403
	F	-9.50(-9.17)	-9.49	-9.56
LiCl	Li	-0.352(-0.334)	-0.334	-0.351
	Cl	-5.71(-5.18)	-5.71	-5.66
CO	C	-3.40(-3.21)	-3.38	-3.41
	O	-6.97(-6.69)	-7.00	-7.01
CO ₂	C	-3.32(-3.18)	-3.33	-3.33
	O	-7.00(-6.72)	-7.00	-7.04
C ₂ H ₂	C	-3.46(-3.32)	-3.47	-3.49
	H	-1.01(-1.01)	-1.01	-1.01
C ₂ H ₄	C	-3.49(-3.35)	-3.49	-3.52
	H	-1.09(-1.09)	-1.09	-1.09

^{a)} Apart from a constant core contribution, which is -5.290 au for Li, -11.224 au for C, -15.181 au for O, -17.162 au for F and -58.784 au for Cl

Table 7
z component of electric field at the nucleus^{a)} (in atomic units 1 au = 5.142×10^{11} V m⁻¹)

Molecule	Nucleus	Pseudopotential		Frozen-core
		zeroth order	first order	
HF	H	0.090(0.086)	0.087	0.083
	F	-0.125(-0.405)	-0.116	-0.131
HCl	H	0.046(0.033)	0.044	0.059
	Cl	-0.087(-0.124)	-0.065	-0.081
LiH	Li	-0.037(-0.096)	-0.037	-0.035
	H	-0.006(-0.000)	-0.006	-0.004
LiF	Li	-0.043(-0.136)	-0.043	-0.042
	F	-0.042(-0.127)	-0.044	-0.049
LiCl	Li	-0.026(-0.091)	-0.027	-0.025
	Cl	-0.019(-0.039)	-0.014	-0.022
CO	C	0.066(0.169)	0.060	0.065
	O	-0.077(-0.265)	-0.076	-0.070
CO ₂	O	0.087(0.394)	0.085	0.084
C ₂ H ₂	C	-0.003(-0.066)	-0.004	-0.003
	H	0.045(0.041)	0.044	0.047
C ₂ H ₄	C	-0.011(-0.018)	-0.010	-0.005
	H	0.006(0.004)	0.007	0.009
average ^{b)}		0.048(0.123)	0.045	0.048

^{a)} Molecules AB are placed with A towards the positive z axis, for CO₂, C₂H₂ and C₂H₄ the atoms referred to are the ones with the larger z coordinate

^{b)} Defined in terms of absolute values

Table 8
Electric field gradient at the nucleus (in atomic units, 1 au = 9.717×10^{21} V m⁻²)

Molecule	Nucleus	Pseudopotential		Frozen-core
		zeroth order	first order	
HF	H	-0.645(-0.635)	-0.643	-0.636
	F	-2.53(-2.51)	-2.53	-2.50
HCl	H	-0.340(-0.314)	-0.343	-0.366
	Cl	-2.32(-0.241)	-2.92	-2.74
LiH	Li	0.038(0.044)	0.038	0.040
	H	-0.065(-0.059)	-0.065	-0.062
LiF	Li	0.043(0.066)	0.048	0.050
	F	0.118(-0.176)	0.302	0.254
LiCl	Li	0.023(0.034)	0.026	0.026
	Cl	0.489(0.003)	-0.216	-0.156
CO	C	0.947(0.962)	0.955	0.964
	O	0.724(0.707)	0.702	0.746
CO ₂	C	0.367(0.484)	0.343	0.348
	O	-0.782(-0.848)	-0.710	-0.664
C ₂ H ₂	C	0.290(0.368)	0.287	0.278
	H	-0.370(-0.361)	-0.370	-0.375
C ₂ H ₄	C	0.185(0.202)	0.186	0.173
	H	-0.314(-0.306)	-0.315	-0.319

Table 9
Diamagnetic shielding anisotropy at the nucleus (in atomic units 1 au = 26.61 ppm)

Molecule	Nucleus	Pseudopotential		Frozen core
		zeroth order	first order	
HF	H	-1.80 (-1.81)	-1.80	-1.80
	F	-0.006(-0.005)	-0.006	-0.006
HCl	F	-2.78 (-2.82)	-2.78	-2.77
	Cl	-0.044(-0.048)	-0.039	-0.041
LiH	Li	-0.168(-0.166)	-0.168	-0.167
	H	-0.333(-0.337)	-0.333	-0.334
LiF	Li	-1.40 (-1.40)	-1.40	-1.40
	F	-0.355(-0.351)	-0.361	-0.360
LiCl	Li	-2.06 (-2.07)	-2.06	-2.05
	Cl	-0.280(-0.278)	-0.274	-0.277
CO	C	-1.52 (-1.52)	-1.52	-1.52
	O	-0.976(-0.981)	-0.975	-0.979
CO ₂	C	-2.88 (-2.88)	-2.88	-2.88
	O	-1.74 (-1.75)	-1.75	-1.75
C ₂ H ₂	C	-1.20 (-1.21)	-1.20	-1.20
	H	-1.66 (-1.67)	-1.66	-1.66

potential and all-electron results could also be improved in the calculations on LiH, Li₂, HF and HBr, quoted above

We note that the electric field at the nucleus (cf table 7) is almost zero due to the near cancellation

of electronic and nuclear contributions as required by the Hellmann-Feynman theorem (which also holds in the HFS method [54]) for the equilibrium geometry. We have included average absolute differences from zero in table 7. It can be seen that frozen-core and pseudopotential calculations behave equally well. Core orthogonalization is essential, however.

Regarding the electric field gradients (cf table 8) we note that the present value for the electric field gradient at Cl in HCl, -2.74 au, agrees well with our previous work [29]. In these calculations we obtained a number of values in the range -2.72 to -2.77 au by variation of the integration parameters. Comparing the frozen-core calculations with an extensive all-electron HFS LCAO calculation for HCl, we arrived at an overall Sternheimer factor $1 - R = 1.18$.

For the group II properties we again compare the performance of pseudopotential and frozen-core methods. Bearing in mind the occurrence of negative powers of r in the quantum-mechanical operators, the overall agreement is surprisingly good. For the potential and the diamagnetic shielding (anisotropy) the agreement is in fact just as good as for the electric multipole moments and the (average) diamagnetic susceptibility (cf table

Table 10
Average effect of core orthogonalization and average differences between pseudopotential and frozen-core results^{a)} (in au and %)

Property	Core orthogonalization	Pseudopotential versus frozen-core	
		zeroth order	first order
Q_{10}	0.039 (3.8%)	0.023 (9.1%)	0.023(9.6%)
Q_{20}	0.102 (3.8%)	0.054 (1.7%)	0.026(0.7%)
Q_{20}^d	0.154 (3.0%)	0.181 (2.7%)	0.073(1.4%)
χ_{aa}^d	0.089 (1.2%)	0.040 (0.6%)	0.031(0.5%)
ϕ	all atoms	0.026 (1.0%)	0.023(0.9%)
	only H	0.006 (0.6%)	0.004 (0.4%)
	except H	0.224 (5.2%)	0.034 (1.2%)
E_x	all atoms	0.079	0.004
	only H	0.006	0.005
	except H	0.109	0.004
V_{zz}	all atoms	0.182(36%)	0.083(32%)
	only H	0.010 (4.8%)	0.009 (3.4%)
	except H	0.248(49%)	0.111(42%)
$\Delta\sigma^d$	all atoms	0.006 (1.8%)	0.004 (1.4%)
	only H	0.014 (0.9%)	0.006 (0.4%)
	except H	0.003 (2.0%)	0.003 (1.8%)

^{a)} Defined in terms of absolute values of differences

9) For the electric field gradient the agreement is still quite reasonable, the pseudopotential values could be combined with Sternheimer factors to yield results that are equally reliable as those that use frozen-core values. We did not include relative errors for the electric field in table 10, since they are meaningless in this case.

Also for the properties that mainly sample the core region the role of the pseudopotential perturbation corrections is a small but positive one. The influence of core orthogonalization is more important now than for the electric multipole moments and the diamagnetic susceptibility.

5. Conclusions

The main conclusions of this paper may be summarized as follows:

(i) The agreement between properties calculated with the pseudopotential and frozen-core Hartree-Fock-Slater methods is very good, also for nearly ionic compounds. Electric multipole moments, the diamagnetic susceptibility, the potential and the diamagnetic shielding all yield differences in the order of 1-2%. The electric field gradient is still sufficiently accurate to be used in combination with Sternheimer factors. According to the Hellmann-Feynman theorem the electric field at the nuclei must be zero for the equilibrium geometry. Pseudopotential and frozen-core calculations satisfy this criterion equally well.

(ii) Although generally good qualitative agreement can be obtained by using pseudo-orbitals, quantitative agreement can only be obtained by using core-orthogonalized pseudo-orbitals.

(iii) In comparing the calculated dipole and quadrupole moments with experiment we find good agreement, in particular, the HFS LCAO method predicts the correct sign for the dipole moment of CO and a recent measurement of the quadrupole moment of C_2H_4 is confirmed.

Acknowledgement

We thank Professors A. van der Avoird and E.J. Baerends for their critical reading of the

manuscript and their general interest in the work. Further we thank F. Visser for helpful discussions. This investigation was supported in part by the Netherlands Foundation for Chemical Research (SON) with financial aid from the Netherlands Organization for the Advancement of Pure Research (ZWO).

References

- [1] L.R. Kahn and W.A. Goddard III, *J. Chem. Phys.* 56 (1972) 2685.
- [2] C.F. Melius, W.A. Goddard III and L.R. Kahn, *J. Chem. Phys.* 56 (1972) 3342.
- [3] L.R. Kahn, P. Baybutt and D.G. Truhlar, *J. Chem. Phys.* 65 (1976) 3826.
- [4] P.J. Hay, W.R. Wadt and L.R. Kahn, *J. Chem. Phys.* 68 (1978) 3059.
- [5] V. Bonafaci and S. Huzinaga, *J. Chem. Phys.* 60 (1974) 2779.
- [6] Y. Sakai and S. Huzinaga, *J. Chem. Phys.* 76 (1982) 2537.
- [7] Ph. Durand and J.C. Barthelat, *Theoret. Chim. Acta* 38 (1975) 283.
- [8] J.C. Barthelat, Ph. Durand and A. Serafini, *Mol. Phys.* 33 (1977) 159.
- [9] M. Pelissier and Ph. Durand, *Theoret. Chim. Acta* 55 (1980) 43.
- [10] R.N. Dixon and J.M.V. Hugo, *Mol. Phys.* 29 (1975) 953.
- [11] R.N. Dixon, P.W. Tasker and G.G. Balint-Kurti, *Mol. Phys.* 34 (1977) 1455.
- [12] R.N. Dixon and J.L. Robertson, *Mol. Phys.* 37 (1979) 1223.
- [13] C.S. Ewig and J.R. van Wazer, *J. Chem. Phys.* 63 (1975) 4035.
- [14] C.S. Ewig, P. Coffey and J.R. van Wazer, *Inorg. Chem.* 14 (1975) 1848.
- [15] C.S. Ewig, R. Osman and J.R. van Wazer, *J. Chem. Phys.* 66 (1977) 3557.
- [16] A. Zunger and M.A. Ratner, *Chem. Phys.* 30 (1978) 423.
- [17] A. Zunger and M.L. Cohen, *Phys. Rev. B* 18 (1978) 5449.
- [18] P.A. Christiansen, Y.S. Lee and K.S. Pitzer, *J. Chem. Phys.* 71 (1979) 4445.
- [19] S.R. Langhoff, R.L. Jaffe and D.P. Chong, *Intern. J. Quantum Chem.* 23 (1983) 875.
- [20] H. Preuss, H. Stoll, U. Wedig and Th. Krüger, *Intern. J. Quantum Chem.* 19 (1981) 113.
- [21] H. Stoll, P. Fuentealba, M. Dolg, L. von Szentpaly and H. Preuss, *J. Chem. Phys.* 79 (1983) 5532.
- [22] J.G. Snijders and E.J. Baerends, *Mol. Phys.* 33 (1977) 1651.
- [23] W. Ravenek and E.J. Baerends, *J. Chem. Phys.* 81 (1984) 865.
- [24] E.J. Baerends, D.E. Ellis and P. Ros, *Chem. Phys.* 2 (1973) 41.

- [25] E.J. Baerends and P. Ros, *Chem Phys* 2 (1973) 52
- [26] E.J. Baerends and P. Ros, *Intern J Quantum Chem S12* (1978) 169
- [27] J.G. Snijders, W. van der Meer, E.J. Baerends and C.A. de Lange *J Chem Phys* 79 (1983) 2970
- [28] P.J.M. Geurts, J.W. Gosselink, A. van der Avoird, E.J. Baerends and J.G. Snijders, *Chem Phys* 46 (1980) 133
- [29] W. Ravenek, J.W.M. Jacobs and A. van der Avoird, *Chem Phys* 78 (1983) 391
- [30] R.F. Stewart, *J Chem Phys* 52 (1970) 431
- [31] D.B. Neumann, H. Basch, R.L. Kornegay, L.C. Snijders, J.W. Moscovitz, C. Hornback and S.P. Liebman, *QCPE* 11 (1971) 199
- [32] T. Ziegler and A. Rauk *Theoret Chim Acta* 46 (1977) 1
- [33] P. Vernooijs, J. Snijders and E.J. Baerends, Slater-type Basis Functions for the Whole Periodic System Internal report, Free University, Amsterdam, The Netherlands (1981)
- [34] E.O. Steinborn and K. Ruedenberg, *Advan Quantum Chem* 7 (1973) 1
- [35] J.L. Prather, Atomic energy levels in crystals, NBS Monograph 19 (1961)
- [36] P.A. Christiansen and E.A. McCullough Jr., *J Chem Phys* 67 (1977) 483
- [37] A.D. McLean and M. Yoshimine, *J Chem Phys.* 47 (1967) 3256
- [38] P.E. Cade and W.M. Huo, *J Chem Phys* 45 (1966) 1063
- [39] E.A. McCullough Jr., *J Chem Phys* 62 (1975) 3991
- [40] M. Yoshimine and A.D. McLean, *Intern J Quantum Chem S1* (1967) 313
- [41] R.L. Matchka, *J Chem Phys* 47 (1965) 4595
- [42] J.S. Muenier and W. Klemperer, *J Chem Phys* 52 (1970) 6033
- [43] E.W. Kaiser, *J Chem Phys* 53 (1979) 1686
- [44] L. Wharton, L.P. Gold and W. Klemperer, *J Chem Phys* 37 (1962) 2149
- [45] A.J. Hebert, F.J. Lovas, C.A. Melendres, C.D. Hollowell, T.L. Story Jr and K. Street Jr., *J Chem Phys* 48 (1968) 2824
- [46] J.S. Muenier, *J Mol Spectry* 55 (1970) 490
- [47] E.A. McCullough Jr., *Mol Phys* 42 (1981) 943
- [48] F. Visser and P.E.S. Wormer, to be published
- [49] R.D. Amos and J.H. Williams, *Chem Phys Letters* 66 (1979) 471
- [50] F.H. de Leeuw and A. Dymanus, *J Mol Spectry* 48 (1973) 427
- [51] W.L. Meerts, F.H. de Leeuw and A. Dymanus, *Chem Phys* 22 (1977) 319
- [52] M.R. Battaglia, A.D. Buckingham, D. Neumark, R.K. Perens and J.H. Williams, *Mol Phys* 43 (1981) 1015
- [53] C.G. Gray, K.E. Gubbins, I.R. Dagg and L.A.A. Read, *Chem Phys Letters* 73 (1980) 278
- [54] J.C. Slater, Quantum theory of molecules and solids, Vol 4 (McGraw-Hill, New York, 1974) app 2

C H A P T E R V

ON THE USE OF PERTURBATION THEORY IN THE
PSEUDOPOTENTIAL HARTREE-FOCK-SLATER-LCAO METHOD

In order to deal with core electrons in large molecular systems by means of the Hartree-Fock-Slater(HFS)-LCAO method [1] two pseudopotential schemes have been proposed [2,3]. Both schemes start with an averaged pseudopotential for all valence electrons and employ perturbation theory to correct for the deviations of the valence level energies from the averaged value used in the pseudopotential. In the original formulation [2] a Brillouin-Wigner type perturbation theory is used; recently [3] a self-consistent perturbational approach has been formulated that allows for the calculation of chemical interaction energies. In this chapter we will show how the pseudopotential HFS-LCAO method may be simplified to yield a computational scheme that avoids the use of perturbation theory in the calculation of the pseudo-orbitals. The present formulation does not allow for the calculation of interaction energies with Ziegler's transition state method [4], however.

The pseudo-orbitals $\psi_{ps,j}$ satisfy the set of equations

$$F_{ps,j} \psi_{ps,j} = \psi_{ps,j} \epsilon_j, \quad (1)$$

$$\langle \psi_{ps,j} | \psi_{ps,j} \rangle = 1. \quad (2)$$

The pseudo-Fock operator $F_{ps,j}$ is given by

$$F_{ps,j} = F + V_{ps,j}, \quad (3)$$

with F the Fock operator and

$$V_{ps,j} = \sum_k (\epsilon_j - \epsilon_{c,k}) |\psi_{c,k}\rangle\langle\psi_{c,k}| \quad (4)$$

the Phillips-Kleinman [5] pseudopotential. $V_{ps,j}$ shifts the core orbitals $\psi_{c,k}$ from their all-electron orbital energies $\epsilon_{c,k}$ to the valence energy ϵ_j . In the previous formulations of the pseudopotential HFS-LCAO method [2,3] the problem which valence level to shift the core orbitals to, was solved by use of an averaged pseudopotential

$$\bar{V}_{ps} = \sum_k (\bar{\epsilon} - \epsilon_{c,k}) |\psi_{c,k}\rangle\langle\psi_{c,k}| \quad (5)$$

for each irreducible representation of the molecular point group and by application of perturbation theory afterwards. Although this approach gives perfectly satisfactory results, it is computationally somewhat involved.

We rewrite the pseudopotential (4) as

$$V_{ps,j} = \epsilon_j P^C + P^E, \quad (6)$$

where

$$P^C = \sum_k |\psi_{c,k}\rangle\langle\psi_{c,k}|, \quad (7)$$

$$P^E = \sum_k (-\epsilon_{c,k}) |\psi_{c,k}\rangle\langle\psi_{c,k}|. \quad (8)$$

P^C is the projector onto the space spanned by the core orbitals. Eq. (1) can now be written as

$$(F + P^E)\psi_{ps,j} = (1 - P^C)\psi_{ps,j}\epsilon_j. \quad (9)$$

Expanding the pseudo-orbitals in a basis χ with overlap matrix S ,

$$\psi_{ps,j} = \sum_{\mu} \chi_{\mu} C_{ps,\mu j}, \quad (10)$$

we obtain

$$\tilde{F} C_{ps} = \tilde{S} C_{ps} \epsilon, \quad (11)$$

where \tilde{F} is the matrix representation of $(F + P^E)$ and \tilde{S} the matrix representation of $(1 - P^C)$. Thus, the pseudo-orbitals may be solved from the generalized eigenvalue problem (11). Since standard procedures yield solutions \tilde{C}_{ps} in the normalization

$$\tilde{C}_{ps}^{\dagger} \tilde{S} \tilde{C}_{ps} = 1, \quad (12)$$

the pseudo-orbitals must be renormalized as

$$C_{ps} = \tilde{C}_{ps} N, \quad (13)$$

where

$$N_{ij} = \delta_{ij} [\tilde{C}_{ps}^{\dagger} S \tilde{C}_{ps}]_{jj}^{-\frac{1}{2}}. \quad (14)$$

The pseudo-density matrix may be obtained from

$$P_{ps,\mu\nu} = \sum_j n_j C_{ps,\mu j} C_{ps,\nu j}^* \quad (15)$$

the n_j being the valence orbital occupation numbers.

Although the present formulation obviates the need for perturbation theory in the calculation of the pseudo-orbitals, it does not seem to be suitable for the calculation of interaction energies in the manner of Ref. 3.

Use of the basic relation

$$\langle \psi_j | F | \psi_j \rangle = \langle \psi_{ps,j} | F + V_{ps,j} | \psi_{ps,j} \rangle \quad (16)$$

[Eq. (36) of Ref. 3] leads to a term

$$\sum_{\mu\nu} \tilde{P}_{\mu\nu} \tilde{F}_{\nu\mu} \quad (17)$$

in the total energy functional, with \tilde{P} defined in terms of \tilde{C}_{ps} :

$$\tilde{P}_{ps,\mu\nu} = \sum_j n_j \tilde{C}_{ps,\mu j} \tilde{C}_{ps,\nu j}^* \quad (18)$$

In Ziegler's transition state method [4] one needs the derivative of the total energy functional with respect to a general element $P_{\mu\nu}$ of the pseudo density matrix. However, P and \tilde{P} are related in a nontrivial manner, and the present approach seems to end in a deadlock.

References

1. E.J. Baerends, D.E. Ellis, P. Ros, Chem. Phys. 2 (1973) 41;
E.J. Baerends, P. Ros, Chem. Phys. 2 (1973) 52.
2. J.G. Snijders, E.J. Baerends, Mol. Phys. 33 (1977) 1651.
3. W. Ravenek, E.J. Baerends, J. Chem. Phys. 81 (1984) 865;
chapter III of this thesis.
4. T. Ziegler, A. Rauk, Theoret. Chim. Acta 46 (1977) 1.
5. J.C. Phillips, L. Kleinman, Phys. Rev. 116 (1959) 287.

C H A P T E R V IIMPLEMENTATION OF THE MODERATELY-LARGE-EMBEDDED-CLUSTER SCHEME
IN THE PSEUDOPOTENTIAL HARTREE-FOCK-SLATER-LCAO METHOD;
CALCULATIONS FOR HYDROGEN ON LITHIUM (100)1. Introduction

In recent years numerous cluster calculations for chemisorption on metal surfaces have been performed [e.g. Refs. 1-4]. The cluster approach is usually justified by assuming that chemisorption is a local phenomenon, i.e., that the perturbation of the substrate electronic structure, caused by the adsorbate, is localized in a small region. It is certainly true that some aspects of the adsorbate-substrate bonding may be considered local. For instance, the height of carbon monoxide above a metal surface is largely determined by the exchange repulsion with the core and low-lying valence levels of the nearest atoms [3].

The cluster model of chemisorption suffers from a serious defect, however: the cluster's finiteness introduces unwanted boundary effects into the calculation. These effects can have a strong influence on the charge distribution in the cluster and on the adsorption energy. The poor convergence of the adsorption energy with cluster size has been related [3] to the polarizability of the cluster, which changes significantly with the addition of each new substrate atom.

Embedding methods [5-14] aim to remove the artefacts of the cluster model by supplying the proper connection of the cluster with the underlying (unperturbed) substrate. Many of these methods [5,9-12] are based in essence on the Koster-Slater method [15,16] for treating impurities in solids by considering the effect of a local perturbation in a Green's function formalism.

In this work we aim to develop an embedding scheme which is convenient for self-consistent calculations by means of the Hartree-Fock-Slater(HFS)-LCAO method [17,18]. We have chosen the moderately-large-embedded-cluster (MLEC) method of Pisani [7,8] because it resolves some of the computational problems of other methods and because of its compatibility with standard quantum chemical methods.

We use the pseudopotential [19-21] version of the HFS-LCAO method. Comparison of interaction energies [20] and one-electron properties [21] has shown that the pseudopotential method reproduces results of the (less approximate) frozen-core method fairly accurately. The first reason for using the pseudopotential method is that we want to be able, eventually, to treat transition metal clusters of considerable size without excessive computational effort. The second reason is that it is advantageous in the Green's matrix method [13] to use the same (symmetry adapted) basis functions in the description of the substrate and in the description of the embedded cluster. In the pseudopotential method with a nonorthogonal basis this is straightforward. In the frozen-core method complications arise due to the valence-core orthogonality requirement. Although still valid, this second reason is somewhat obscured by the technical necessity to use a semi-orthogonal basis [cf. Sec. 2H].

In order to test the effect of embedding as such it is preferable to use the same quantum chemical method both for the cluster and the substrate into which the cluster is to be embedded. In our present approach this condition is met by use of a finite representation for the substrate, treated with the same pseudopotential HFS-LCAO method. In principle, the use of a two-dimensional band structure program would be preferable, but such a program was not available at the HFS-LCAO level. In this respect, our approach is similar to that of Whitten and Pakkanen [14], who also use a cluster for the characterization of the substrate.

Although the finiteness of the substrate gives rise, in principle, to the same boundary effects we want to avoid, their influence can be reduced by use of a sufficiently large cluster for the substrate. Thus, in practical calculations the profit will be found in computation time; investigation of different adsorbates and different geometries requires the treatment of the substrate cluster only once, while the quality of the embedded cluster calculations is expected to be close to the "full" adsorbate-substrate calculations. Incidentally, our approach also gives access to another application of embedding, viz., the embedding of different functional groups as substituents in a large molecule.

2. Formalism

In this section we give a detailed derivation of the moderately-large-embedded-cluster (MLEC) method of Pisani [7,8]. The presentation is directed towards the implementation of the formalism in the Hartree-Fock-Slater-LCAO method (introduction of a semi-orthogonal basis, symmetry adaptation).

Our treatment is specific on a number of points. First of all, we treat the embedding of a cluster in a finite representation of the solid surface. Secondly, we only consider the chemisorption case, thus disregarding the vacancy and substitutional impurity problems (which could be treated along similar lines, however). Thirdly, we incorporate the correct matrix representations of the quantities involved from the start; Pisani [8] has indicated the steps to be taken in an orthogonal basis, we consider the nonorthogonal case throughout. Finally, for simplicity of notation we use a spin-restricted formalism; the generalization to an unrestricted formalism is straightforward.

A. Description of the chemisorption system

The chemisorption system is indicated schematically in figure 1; it represents the adsorption of a molecule on a solid surface (the substrate). The adsorbate is denoted by A, the solid by $S = B \cup D$. Note that we use a finite representation of the solid. Hence boundary effects are present, but D will be made sufficiently large for their effect on the adsorbate to be small. The chemisorption cluster is denoted by $C = A \cup B$. D, finally, is called the defective or indented solid.

Quantum mechanical operators will be represented in a finite basis of localized functions $\chi = \{\chi_{\mu}\}$. Overcompleteness problems [6] are absent in this basis. However, if the number of basis functions per atom increases, near-linear-dependency problems may arise. The basis set χ is partitioned into subsets of

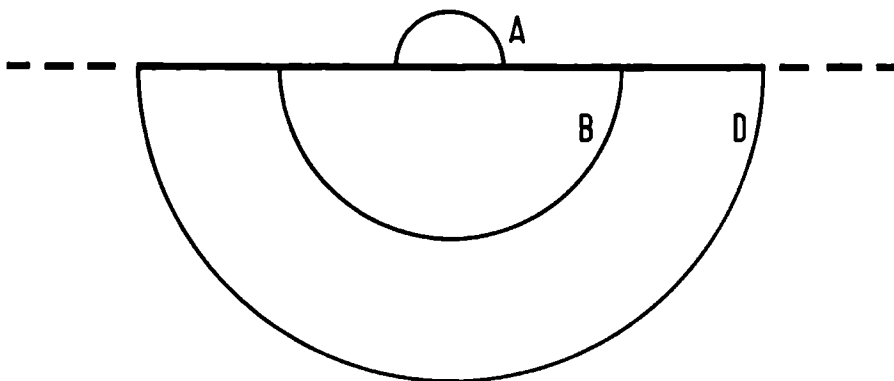


Figure 1. Schematic representation of the chemisorption system

functions localized in different parts of the chemisorption system:

$$\chi = \chi_A \cup \chi_B \cup \chi_D. \quad (2.1)$$

All matrices are partitioned accordingly, e.g., for the overlap matrix we write

$$S = \begin{bmatrix} S_{AA} & S_{AB} & S_{AD} \\ S_{BA} & S_{BB} & S_{BD} \\ S_{DA} & S_{DB} & S_{DD} \end{bmatrix}. \quad (2.2)$$

At present we consider the description of the chemisorption system by a general one-electron Hamiltonian \hat{F} , with matrix representation F ; in our applications we will use the Hartree-Fock-Slater model. Our task is the solution of the self-consistent problem

$$F = F(P), \quad (2.3)$$

$$FC = SCE, \quad E_{kl} = \delta_{kl} e_k, \quad (2.4)$$

$$C^\dagger SC = 1, \quad (2.5)$$

$$P = CNC^\dagger, \quad N_{kl} = \delta_{kl} n_k. \quad (2.6)$$

Given a density matrix P , the Fock matrix F is constructed [Eq. (2.3)], the generalized eigenvalue problem [Eqs. (2.4) and (2.5)] is solved and the density matrix is recalculated according to Eq. (2.6). This process is repeated until self-consistency is reached. We assume that the self-consistent solution of Eqs. (2.3)-(2.6) is obtained by applying the Aufbau principle. Thus, the occupation numbers n_k in Eq. (2.6) can assume fractional values at the Fermi energy ϵ_F only.

The self-consistent problem may be equivalently formulated in terms of the Green's matrix [cf. Appendix A]:

$$F = F(P), \quad (2.7)$$

$$(\zeta S - F)G(\zeta) = 1, \quad \zeta = \epsilon + i\eta, \quad (2.8)$$

$$P = -\frac{1}{\pi} \lim_{\eta \rightarrow 0^+} \text{Im} \int_{-\infty}^{\epsilon_F} d\epsilon G(\epsilon + i\eta). \quad (2.9)$$

Given a density matrix P , the Fock matrix F is calculated, the matrix $(\zeta S - F)$ is inverted to yield the Green's matrix $G(\zeta)$ and the density matrix is recalculated according to Eq. (2.9). Again the process is repeated until self-consistency is reached. In the following we will use the notation

$$Q(\zeta) = \zeta S - F. \quad (2.10)$$

B. The general embedding equations

Chemisorption is considered to be a local phenomenon, i.e., it is assumed that the perturbation induced by an adsorbate is local. We will investigate the consequences of the local perturbation assumption in the Green's matrix formalism. As a first step we will extend the description of the unperturbed solid to the full basis χ , next we will derive the general embedding equations.

Consider the unperturbed or "free" solid, i.e., the solid in the absence of an adsorbate. We suppose that the self-consistent problem [Eqs. (2.7)-(2.9)] has been solved in its natural basis $\chi_B \cup \chi_D$. Suppressing the variable ζ we have

$$Q_{SS}^f G_{SS}^f = 1_{SS}, \quad (2.11a)$$

or, equivalently,

$$\begin{bmatrix} Q_{BB}^f & Q_{BD}^f \\ Q_{DB}^f & Q_{DD}^f \end{bmatrix} \begin{bmatrix} G_{BB}^f & G_{BD}^f \\ G_{DB}^f & G_{DD}^f \end{bmatrix} = \begin{bmatrix} 1_{BB} & 0_{BD} \\ 0_{DB} & 1_{DD} \end{bmatrix}. \quad (2.11b)$$

We use the index f to refer to the free solid.

Our first problem is to extend the solution for the free solid to the full basis $\chi = \chi_A \cup \chi_S$ without modifying the unperturbed density. This extension is a prerequisite for matrix operations in the following to be meaningful. We define a Green's matrix $\tilde{G}(\zeta)$ in the full basis χ as the inverse of the matrix

$$\tilde{Q}(\zeta) \equiv \begin{bmatrix} (\zeta - e)S_{AA} & 0_{AS} \\ 0_{SA} & Q_{SS}^f(\zeta) \end{bmatrix}, \quad e > \epsilon_F. \quad (2.12)$$

Note that the AA-block of the Fock matrix \tilde{F} has been defined as $\tilde{F}_{AA} = e S_{AA}$, where e is an energy above the Fermi energy. The Green's matrix $\tilde{G}(\zeta)$ is easily seen to be

$$\tilde{G}(\zeta) = \begin{bmatrix} \frac{1}{\zeta - e} (S_{AA})^{-1} & 0_{AS} \\ 0_{SA} & G_{SS}^f(\zeta) \end{bmatrix}. \quad (2.13)$$

Since $e > \epsilon_F$ the AA-block of $\tilde{G}(\zeta)$ gives a zero contribution to the density matrix:

$$\begin{aligned} \tilde{P}_{AA} &= -\frac{1}{\pi} \lim_{\eta \rightarrow 0^+} \text{Im} \int_{-\infty}^{\epsilon_F} d\epsilon \tilde{G}_{AA}(\epsilon + i\eta) \\ &= \int_{-\infty}^{\epsilon_F} d\epsilon \delta(\epsilon - e) (S_{AA})^{-1} \\ &= 0_{AA}. \end{aligned} \quad (2.14)$$

Hence

$$\tilde{P} = \begin{bmatrix} 0_{AA} & 0_{AS} \\ 0_{SA} & P_{SS}^f \end{bmatrix}, \quad (2.15)$$

i.e., the density associated with \tilde{P} is the one of the free solid.

The procedure followed above is referred to by Williams, Feibelman and Lang [13] as the adspace idea. As long as \tilde{F}_{AA} is such that the unperturbed density remains unchanged, its explicit form is immaterial. It will cancel when considering the embedding equations, as will become clear in the sequel. We note that the ease with which it is possible to include extra basis functions in the formalism constitutes one of the advantages of the Green's matrix method over the

Green's function method. E.g., compare the complications that arise in the cluster-extended Green's function method of Baraff, Schlüter and Allan [12].

We now consider the self-consistent problem for the full interacting system A U B U D. The perturbation V to the modified free solid problem is

$$\begin{aligned}
 V &\equiv F - \tilde{F} \\
 &= \tilde{Q} - Q \\
 &= \begin{bmatrix} \tilde{Q}_{AA} - Q_{AA} & -Q_{AB} & -Q_{AD} \\ -Q_{BA} & \tilde{Q}_{BB} - Q_{BB} & \tilde{Q}_{BD} - Q_{BD} \\ -Q_{DA} & \tilde{Q}_{DB} - Q_{DB} & \tilde{Q}_{DD} - Q_{DD} \end{bmatrix} .
 \end{aligned} \tag{2.16}$$

The local perturbation assumption, characteristic for chemisorption theory, reads explicitly

$$Q_{AD} = 0_{AD}, \tag{2.17a}$$

$$Q_{BD} = \tilde{Q}_{BD}, \quad \text{i.e.,} \quad F_{BD} = F_{BD}^f, \tag{2.17b}$$

$$Q_{DD} = \tilde{Q}_{DD}, \quad \text{i.e.,} \quad F_{DD} = F_{DD}^f. \tag{2.17c}$$

We note that it is not only necessary to assume $F_{AD} = 0_{AD}$, but also $S_{AD} = 0_{AD}$. However, since F and S are intimately related, this is perfectly reasonable. The interaction between the adsorbate and the indented solid can show up in F, in S, or in both. Using Eq. (2.17) we may write

$$v = \begin{bmatrix} v_{CC} & 0_{CD} \\ 0_{DC} & 0_{DD} \end{bmatrix} . \tag{2.18}$$

The implications of the local perturbation assumption can be found as follows. Write Eq. (2.8) for the full problem as

$$\begin{bmatrix} Q_{CC} & Q_{CD} \\ Q_{DC} & Q_{DD} \end{bmatrix} \begin{bmatrix} G_{CC} & G_{CD} \\ G_{DC} & G_{DD} \end{bmatrix} = \begin{bmatrix} 1_{CC} & 0_{CD} \\ 0_{DC} & 1_{DD} \end{bmatrix}, \quad (2.19)$$

and solve G_{CC} by performing the inversion [cf. Appendix B]:

$$G_{CC} = [Q_{CC} - Q_{CD}(Q_{DD})^{-1} Q_{DC}]^{-1}. \quad (2.20)$$

The corresponding relation for the free solid in the full basis χ is

$$\tilde{G}_{CC} = [\tilde{Q}_{CC} - \tilde{Q}_{CD}(\tilde{Q}_{DD})^{-1} \tilde{Q}_{DC}]^{-1}. \quad (2.21)$$

Combining Eqs. (2.16), (2.18), (2.20), and (2.21) we obtain

$$(G_{CC})^{-1} = (\tilde{G}_{CC})^{-1} - v_{CC}. \quad (2.22)$$

From Eq. (2.13) it follows that

$$(\tilde{G}_{CC})^{-1} = \begin{bmatrix} \tilde{Q}_{AA} & 0_{AB} \\ 0_{BA} & (G_{BB}^f)^{-1} \end{bmatrix}, \quad (2.23)$$

hence

$$\begin{bmatrix} G_{AA} & G_{AB} \\ G_{BA} & G_{BB} \end{bmatrix} = \begin{bmatrix} \tilde{Q}_{AA} - (\tilde{Q}_{AA} - Q_{AA}) & -(-Q_{AB}) \\ -(-Q_{BA}) & (G_{BB}^f)^{-1} - (Q_{BB}^f - Q_{BB}) \end{bmatrix}^{-1}$$

$$= \begin{bmatrix} Q_{AA} & Q_{AB} \\ Q_{BA} & (G_{BB}^f)^{-1} - (Q_{BB}^f - Q_{BB}) \end{bmatrix}^{-1}. \quad (2.24)$$

Again we use the inverse of a partitioned matrix [Appendix B]:

$$G_{BB}^f = \left[Q_{BB}^f - Q_{BD}^f (Q_{DD}^f)^{-1} Q_{DB}^f \right]^{-1}, \quad (2.25)$$

and obtain

$$\begin{bmatrix} G_{AA} & G_{AB} \\ G_{BA} & G_{BB} \end{bmatrix} = \begin{bmatrix} Q_{AA} & Q_{AB} \\ Q_{BA} & Q_{BB} - Q_{BD}^f (Q_{DD}^f)^{-1} Q_{DB}^f \end{bmatrix}^{-1} \quad (2.26)$$

Due to the cancellation of \tilde{Q}_{AA} in Eq. (2.24), the final result [Eq. (2.26)] is independent of our particular choice for \tilde{F}_{AA} in Eq. (2.12).

The consequence of the local perturbation assumption [Eq. (2.17)] is that the self-consistent problem to be solved is confined to the chemisorption cluster C, once the solution of the free solid is known. In realistic chemisorption calculations, however, Eq. (2.26) is rather cumbersome to apply [8]. In each iteration of the self-consistent procedure the Green's matrix [Eq. (2.26)] must be integrated to yield the density matrix:

$$P_{CC} = -\frac{1}{\pi} \lim_{\eta \rightarrow 0^+} \text{Im} \int_{-\infty}^{\epsilon_F} d\epsilon G_{CC}(\epsilon + i\eta), \quad (2.27)$$

where ϵ_F is the Fermi energy for the free solid. The (numerical) integration implied by Eq. (2.27) necessitates the inversion of relatively large matrices at a large number of energy points.

C. The MLEC method

Pisani [7, 8] has proposed an embedding scheme that overcomes the difficulties in applying Eq. (2.26), however, at the cost of another approximation. We will introduce this approximation and derive its consequences.

The additional assumption can be formally stated as

$$J_{CC}(\epsilon)V_{CC} = V_{CC} \ , \quad (2.28)$$

where the auxiliary matrix J_{CC} is defined by

$$J_{CC}(\epsilon) \equiv \tilde{Q}_{CC}(\epsilon) \tilde{G}_{CC}(\epsilon) \\ = \begin{bmatrix} 1_{AA} & 0_{AB} \\ 0_{BA} & Q_{BB}^f(\epsilon) G_{BB}^f(\epsilon) \end{bmatrix} \ . \quad (2.29)$$

Eq. (2.28) corresponds to the requirement that the cluster B comprises a border region, where the connection of the cluster with the defective solid is established, but where the perturbing potential is already very small. Thus, the size of the cluster for which the self-consistent calculation is performed needs to be larger than required by the local perturbation assumption alone. Therefore the embedding scheme may be characterized as a moderately-large-embedded-cluster (MLEC) method. We refer to assumption (2.28) as the MLEC assumption; we will return to its nature after we have derived an explicit expression for the matrix J_{CC} .

In order to proceed we assume the validity of Eq. (2.28) and use it to simplify the general embedding equations. Combining Eqs. (2.22) and (2.28) we obtain

$$\begin{aligned}
G_{CC} &= [(\tilde{G}_{CC})^{-1} - v_{CC}]^{-1} \\
&= [J_{CC}(\tilde{G}_{CC})^{-1} - J_{CC} v_{CC}]^{-1} J_{CC} \\
&= [\tilde{Q}_{CC} - v_{CC}]^{-1} J_{CC} \\
&= (Q_{CC})^{-1} J_{CC}.
\end{aligned} \tag{2.30}$$

The matrix $(Q_{CC})^{-1}$ corresponds to the Green's matrix obtained from the generalized eigenvalue problem of the full Fock operator (i.e., including the potential of the frozen indented solid), confined to the chemisorption cluster C. We introduce the notation

$$(Q_{CC})^{-1} \equiv \bar{G}_{CC} \tag{2.31}$$

and use Eq. (2.29) to rewrite Eq. (2.30) as

$$\begin{bmatrix} G_{AA} & G_{AB} \\ G_{BA} & G_{BB} \end{bmatrix} = \begin{bmatrix} \bar{G}_{AA} & \bar{G}_{AB} J_{BB} \\ \bar{G}_{BA} & \bar{G}_{BB} J_{BB} \end{bmatrix}. \tag{2.32}$$

Again, the density matrix P_{CC} may be evaluated from G_{CC} [Eq. (2.27)]. The advantage of Eq. (2.32) over Eq. (2.26) lies in the relative ease with which the density matrix can be obtained. We will return to the evaluation of P_{CC} after we have derived an explicit expression for J_{CC} .

D. The matrix J_{CC} and the nature of the MLEC assumption

We now derive an explicit expression for the auxiliary matrix J_{CC} , defined in Eq. (2.29). Using the Green's matrix $G^f(\zeta)$ in terms of the solution of the generalized eigenvalue problem for the free solid [cf. Appendix A],

$$G_{\beta\nu}^f(\epsilon+i\eta) = \sum_{\beta} \frac{C_{\beta\lambda}^f C_{\nu\lambda}^{f*}}{\epsilon - e_{\lambda}^f + i\eta}, \quad (2.33)$$

we obtain after some manipulations

$$\begin{aligned} J_{\alpha\nu}(\epsilon) &= \lim_{\eta \rightarrow 0^+} \sum_{\beta} Q_{\alpha\beta}^f(\epsilon+i\eta) G_{\beta\nu}^f(\epsilon+i\eta) \\ &= \sum_{\beta} \sum_{\lambda} S_{\alpha\beta} C_{\beta\lambda}^f C_{\nu\lambda}^{f*} \\ &\quad + P \sum_{\beta} \sum_{\lambda} \left[\frac{e_{\lambda}^f S_{\alpha\beta} - F_{\alpha\beta}^f}{\epsilon - e_{\lambda}^f} \right] C_{\beta\lambda}^f C_{\nu\lambda}^{f*} \\ &\quad - i\pi \sum_{\beta} \sum_{\lambda} (\epsilon S_{\alpha\beta} - F_{\alpha\beta}^f) C_{\beta\lambda}^f C_{\nu\lambda}^{f*} \delta(\epsilon - e_{\lambda}^f). \end{aligned} \quad (2.34)$$

In the derivation of Eq. (2.34) we have used

$$\lim_{\eta \rightarrow 0} \frac{x}{x^2 + \eta^2} = P \frac{1}{x}, \quad (2.35)$$

where P stands for principal part, and

$$\lim_{\eta \rightarrow 0^+} \frac{\eta}{x^2 + \eta^2} = \pi \delta(x), \quad (2.36)$$

with δ the Dirac delta function.

In order to write Eq. (2.34) in a more compact form, we introduce the matrices

$$D \equiv S_{BB} (S_{SS}^{-1})_{BB}, \quad (2.37)$$

and

$$X \equiv S_{BB} C_B^f E^f - F_{BB}^f C_B^f, \quad (2.38)$$

where C_B^f contains the coefficients of χ_B in the eigenvectors C^f of the free solid problem. After some algebra we arrive at

$$J_{\alpha\nu}(\epsilon) = D_{\alpha\nu} + P \sum_{\ell} \frac{X_{\alpha\ell} C_{\nu\ell}^{f*}}{\epsilon - e_{\ell}^f} - i\pi \sum_{\ell} X_{\alpha\ell} C_{\nu\ell}^{f*} \delta(\epsilon - e_{\ell}^f). \quad (2.39)$$

At this point we again consider the MLEC assumption [Eq. (2.28)]. Suppose that the basis χ_B can be partitioned into a subset of central functions and a subset of border functions, such that if either α or ν in $J_{\alpha\nu}$ belongs to the central region, the sums over β in Eq. (2.34) can be extended to the set $B \cup D$ without appreciable consequences. This would result in $D_{\alpha\nu} = \delta_{\alpha\nu}$ and $X_{\alpha\nu} = 0$ for either α or ν in the central region, hence the structure of J_{CC} would be [cf. Eq. (2.29)]

$$J_{CC}(\epsilon) = \begin{bmatrix} 1 & 0 \\ 0 & Z \end{bmatrix}, \quad (2.40)$$

with Z pertaining to the border region only. To obtain Eq. (2.28) it is now sufficient to assume that V is different from zero in the central region only. Hence the MLEC assumption corresponds to the requirement that the cluster B comprises a border region, where the connection of the cluster with the defective solid is established, but where the perturbing potential is already very small.

E. The density matrix in the MLEC method

We complete the derivation of the embedding equations in the MLEC method by the calculation of the density matrix P_{CC} from the Green's matrix Eq. (2.32) according to Eq. (2.27).

As noted in the discussion following Eq. (2.30) the auxiliary Green's matrix \bar{G}_{CC} is obtained from the generalized eigenvalue problem of the Fock matrix for the full problem, confined to the chemisorption cluster. Explicitly:

$$F_{CC} \bar{C} = S_{CC} \bar{C} \bar{E} , \quad (2.41)$$

$$\bar{C}^\dagger S_{CC} \bar{C} = 1 , \quad (2.42)$$

and

$$\bar{G}_{\mu\alpha} = \sum_k \frac{\bar{C}_{\mu k} \bar{C}_{\alpha k}^*}{(\epsilon - \bar{e}_k) + i\eta} . \quad (2.43)$$

Using Eqs. (2.27) and (2.32) we obtain for $\mu \in C$, $\nu \in A$:

$$\begin{aligned} P_{\mu\nu} &= -\frac{1}{\pi} \lim_{\eta \rightarrow 0^+} \text{Im} \int_{-\infty}^{\epsilon_F} d\epsilon \bar{G}_{\mu\nu}(\epsilon + i\eta) \\ &= \sum_k \bar{C}_{\mu k} \bar{C}_{\nu k}^* \theta(\epsilon_F - \bar{e}_k) , \end{aligned} \quad (2.44)$$

where $\theta(x)$ denotes the unit step function:

$$\begin{aligned} \theta(x) &= 0 \quad \text{for } x < 0 \\ &= 1 \quad \text{for } x > 0 , \end{aligned} \quad (2.45)$$

and ϵ_F is the Fermi energy of the free solid. For $\mu \in C$, $\nu \in B$ we obtain

$$\begin{aligned}
P_{\mu\nu} &= -\frac{1}{\pi} \lim_{\eta \rightarrow 0^+} \text{Im} \int_{-\infty}^{\epsilon_F} d\epsilon \sum_{\alpha} \bar{G}_{\mu\alpha}(\epsilon+i\eta) J_{\alpha\nu}(\epsilon+i\eta) \\
&= \sum_{\alpha} \sum_k \bar{C}_{\mu k} \bar{C}_{\alpha k}^* \Theta(\epsilon_F - \bar{e}_k) \left[D_{\alpha\nu} + \sum_{\ell} \frac{X_{\alpha\ell} C_{\nu\ell}^{f*}}{\bar{e}_k - e_{\ell}^f} \right] \\
&\quad + \sum_{\alpha} \sum_k \frac{\bar{C}_{\mu k} \bar{C}_{\alpha k}^*}{e_{\ell}^f - e_k} \sum_{\ell} X_{\alpha\ell} C_{\nu\ell}^{f*} \Theta(\epsilon_F - e_{\ell}^f). \tag{2.46}
\end{aligned}$$

We write Eq. (2.46) as

$$P_{\mu\nu} = \sum_k \sum_{\alpha} \bar{C}_{\mu k} \bar{C}_{\alpha k}^* M_{\alpha\nu}(\bar{e}_k), \tag{2.47}$$

with the energy dependent coupling matrix $M(e)$ defined by

$$M_{\alpha\nu}(e) \equiv D_{\alpha\nu} - \sum_{\ell} \frac{X_{\alpha\ell} C_{\nu\ell}^{f*}}{e_{\ell}^f - e} \Theta(e_{\ell}^f - \epsilon_F), \quad e < \epsilon_F, \tag{2.48a}$$

$$M_{\alpha\nu}(e) \equiv \sum_{\ell} \frac{X_{\alpha\ell} C_{\nu\ell}^{f*}}{e_{\ell}^f - e} \Theta(\epsilon_F - e_{\ell}^f), \quad e > \epsilon_F. \tag{2.48b}$$

The coupling matrix $M(e)$ plays a central rôle in the MLEC method. Since it depends only on the electronic structure of the free solid and on the choice of the cluster $B \subset S$, and not on the adsorbate, it can be said to summarize the adsorptive properties of the substrate. In Sec. 4 we will give some examples of the energy dependence of the coupling matrix.

F. Limiting conditions

An important characteristic of the MLEC method is that it yields correct results in the limiting cases where either of the sets A or D is empty. Since the algebra involved is straightforward, we merely give the results.

If the cluster B coincides with the representation of the substrate, i.e., if $D = \emptyset$, the embedded cluster calculation should be identical with the corre-

sponding nonembedded cluster calculation. Indeed, we find

$$M_{\alpha\nu}(e) = \delta_{\alpha\nu} \Theta(\epsilon_F - e), \quad (2.49)$$

and hence

$$P_{\mu\nu} = \sum_k \bar{C}_{\mu k} \bar{C}_{\nu k}^* \Theta(\epsilon_F - \bar{e}_k), \quad \mu, \nu \in C \quad (2.50)$$

In the absence of an adsorbate, i.e., if $A = \emptyset$, the embedded cluster calculation should reproduce the results obtained for the free solid. Calculating the density matrix with the matrix \bar{C} that satisfies

$$F_{BB}^f \bar{C} = S_{BB} \bar{C} \bar{E}, \quad (2.51)$$

$$\bar{C}^\dagger S_{BB} \bar{C} = 1, \quad (2.52)$$

we find the correct result

$$P_{BB} = P_{BB}^f. \quad (2.53)$$

G. The iterative procedure; summary of main formulas

The procedure to be followed when actually performing embedded cluster calculations with the MLEC method is as follows:

- i) Obtain an initial guess for P_{CC} . (A good choice seems the direct sum of the adsorbate density matrix and P_{BB}^f from the free solid calculation.)
- ii) Calculate the Fock matrix originating from the full one-electron Hamiltonian (including the frozen indented solid), restricted to the embedded cluster.

iii) Solve the generalized eigenvalue problem for the embedded cluster C:

$$F_{CC} \bar{C} = S_{CC} \bar{C} \bar{E}, \quad (2.54)$$

$$\bar{C}^\dagger S_{CC} \bar{C} = 1. \quad (2.55)$$

iv) Construct the new density matrix P_{CC} as follows:

$$P_{\mu\nu} = \sum_k \bar{C}_{\mu k} \bar{C}_{\nu k}^* \Theta(\epsilon_F - \bar{e}_k), \quad \mu \in C, \nu \in A, \quad (2.56a)$$

$$P_{\mu\nu} = \sum_k \sum_\alpha \bar{C}_{\mu k} \bar{C}_{\alpha k}^* M_{\alpha\nu}(\bar{e}_k), \quad \mu \in C, \nu \in B, \quad (2.56b)$$

where

$$M_{\alpha\nu}(e) = D_{\alpha\nu} - \sum_l \frac{X_{\alpha l} C_{\nu l}^{f*}}{e_l^f - e} \Theta(e_l^f - \epsilon_F), \quad e < \epsilon_F, \quad (2.57a)$$

$$M_{\alpha\nu}(e) = \sum_l \frac{X_{\alpha l} C_{\nu l}^{f*}}{e_l^f - e} \Theta(\epsilon_F - e_l^f), \quad e > \epsilon_F. \quad (2.57b)$$

The matrices D and X, occurring in the coupling matrix M(e), are given by

$$D = S_{BB} (S_{SS}^{-1})_{BB}, \quad (2.58)$$

$$X = S_{BB} C_B^f E^f - F_{BB}^f C_B^f; \quad (2.59)$$

they are obtained from the free solid calculation.

Steps ii), iii), and iv) constitute the iterative steps of the procedure.

They must be repeated until self-consistency is reached.

H. Reformulation of the MLEC method in a semi-orthogonal basis

Our calculations have shown that in a nonorthogonal basis the elements of the coupling matrix M may become quite large (elements of order 10^2 or 10^3 are not exceptional). In the calculation of the density matrix [Eq. (2.56)] this leads to numerical problems in the Hartree-Fock-Slater-LCAO method, as will be shown in Sec. 4. Therefore we propose to perform a basis transformation which reduces these problems.

We transform the basis χ as follows:

$$\chi' = \chi W, \quad W = \begin{bmatrix} 1_{AA} & 0_{AB} & 0_{AD} \\ 0_{BA} & 1_{BB} & -Y \\ 0_{DA} & 0_{DB} & 1_{DD} \end{bmatrix}, \quad (2.60a)$$

where

$$Y = S_{BB}^{-1} S_{BD}. \quad (2.60b)$$

This amounts to an orthogonalization of D to B . We refer to χ' as the semi-orthogonal basis. The inverse transformation is easily found to be [cf. Appendix B]

$$\chi = \chi' W^{-1}, \quad W^{-1} = \begin{bmatrix} 1_{AA} & 0_{AB} & 0_{AD} \\ 0_{BA} & 1_{BB} & Y \\ 0_{DA} & 0_{DB} & 1_{DD} \end{bmatrix}. \quad (2.61)$$

The matrix Q , defined in Eq. (2.10), transforms to

$$Q' = W^\dagger Q W = \begin{bmatrix} Q_{AA} & Q_{AB} & Q_{AD} - Q_{AB} Y \\ Q_{BA} & Q_{BB} & Q_{BD} - Q_{BB} Y \\ Q_{DA} - Y^\dagger Q_{BA} & Q_{DB} - Y^\dagger Q_{BB} & Q_{DD} - Q_{DB} Y - Y^\dagger Q_{BD} + Y^\dagger Q_{BB} Y \end{bmatrix}.$$

(2.62)

Note that, although we transform the basis χ , the density remains unchanged, and hence S , F , and Q transform in the same way. For the overlap matrix S we obtain from Eqs. (2.60) and (2.62)

$$S' = \begin{bmatrix} S_{AA} & S_{AB} & S_{AD} - S_{AB} S_{BB}^{-1} S_{BD} \\ S_{BA} & S_{BB} & 0_{BD} \\ S_{DA} - S_{DB} S_{BB}^{-1} S_{BA} & 0_{DB} & S_{DD} - S_{DB} S_{BB}^{-1} S_{BD} \end{bmatrix}. \quad (2.63)$$

Therefore in the new basis χ' the matrix D [Eq. (2.58)], which occurs in the coupling matrix M , becomes

$$D' = 1_{BB}. \quad (2.64)$$

Of course, Eq. (2.64) is the rationale of the transformation Eq. (2.60).

The derivations in sections 2B - 2E may now be repeated in the new basis. In particular, we obtain for the perturbation to the modified free solid problem

$$v' = \tilde{Q}' - Q' \\ = \begin{bmatrix} \tilde{Q}'_{AA} - Q'_{AA} & -Q'_{AB} & -Q'_{AD} \\ -Q'_{BA} & \tilde{Q}'_{BB} - Q'_{BB} & \tilde{Q}'_{BD} - Q'_{BD} \\ -Q'_{DA} & \tilde{Q}'_{DB} - Q'_{DB} & \tilde{Q}'_{DD} - Q'_{DD} \end{bmatrix}. \quad (2.65)$$

The local perturbation assumption, which leads to the general embedding equations in the semi-orthogonal basis, reads

$$Q'_{AD} = 0_{AD}. \quad (2.66a)$$

$$F'_{BD} = F_{BD}^{f'} \quad (2.66b)$$

$$F'_{DD} = F_{DD}^{f'} \quad (2.66c)$$

As stated above F transforms exactly as Q [Eq. (2.62)], hence Eqs. (2.66b) and (2.66c) are equivalent to the corresponding relations Eqs. (2.17b) and (2.17c) in the nonorthogonal basis. However, Eqs. (2.66a) and (2.17a) are not equivalent. To obtain Eq. (2.66a) from Eq. (2.17a) we have to make the additional assumption

$$O_{AB} S_{BB}^{-1} S_{BD} = O_{AD} \quad (2.67)$$

It may be noted that this assumption is similar to assumption (b) in Pisani's first paper on the MLEC method [7], viz., the neglect of compound quantities with both indices A and D occurring. Therefore we feel that in the MLEC method assumptions (2.66a) and (2.17a) will yield comparable results.

Assuming the validity of Eq. (2.66) we may again go through the algebra as before and arrive at

$$(G'_{CC})^{-1} = (\tilde{G}'_{CC})^{-1} - V'_{CC} \quad (2.67)$$

[cf. Eq. (2.22)]. Invoking the MLEC assumption

$$J'_{CC} V'_{CC} = V'_{CC} \quad (2.68)$$

where

$$J'_{CC} = \begin{bmatrix} 1_{AA} & 0_{AB} \\ 0_{BA} & Q_{BB}^{f'} G_{BB}^{f'} \end{bmatrix}, \quad (2.69)$$

we obtain the analogue of Eq. (2.32) in the semi-orthogonal basis:

$$G'_{CC} = \bar{G}'_{CC} J'_{CC}. \quad (2.70)$$

This leads to equations for the calculation of P'_{CC} analogous to Eqs. (2.56) - (2.59).

Finally, we may obtain the density matrix in the nonorthogonal basis χ by transforming P' :

$$P = W P' W^\dagger$$

$$= \begin{bmatrix} P'_{AA} & P'_{AB} & 0_{AD} \\ P'_{BA} & P'_{BB} & P'_{BD} - Y P'_{DD} \\ 0_{DA} & P'_{DB} - P'_{DD} Y^\dagger & P'_{DD} \end{bmatrix}, \quad (2.71a)$$

where we have used $P'_{AD} = 0_{AD}$ and $P'_{DA} = 0_{DA}$; further,

$$P_{BB} = P'_{BB} - Y P'_{DB} - P'_{BD} Y^\dagger + Y P'_{DD} Y^\dagger. \quad (2.71b)$$

A similar relation holds for $P^{f'}$. Therefore

$$P_{BB} = P'_{BB} + (P_{BB}^f - P_{BB}^{f'})$$

$$\equiv P'_{BB} + R, \quad (2.72)$$

which is the transformation formula employed in our calculations with the semi-orthogonal basis.

I. Transformation properties and symmetry adaptation

In this subsection we will show that the MLEC method may be adapted to the geometrical symmetry of the chemisorption system without serious complications.

We note from the outset that the only symmetry available to us will be that of the point group C_{nv} . Still, exploiting this symmetry can yield a substantial reduction of the computational effort.

We start by considering a basis transformation T of the form

$$\tilde{\chi} = \chi T, \quad T = \begin{bmatrix} T_{AA} & 0_{AB} & 0_{AD} \\ 0_{BA} & T_{BB} & 0_{BD} \\ 0_{DA} & 0_{DB} & T_{DD} \end{bmatrix}, \quad (2.73)$$

i.e., we restrict ourselves to transformations of the subsets χ_R ($R = A, B, D$) among themselves. The necessity of this restriction is, of course, that without it the localization in parts A, B, and D of the chemisorption system would be lost. Such a transformation corresponds to the natural symmetry of the chemisorption system, however.

We now obtain the transformation properties of various quantities occurring in our embedding formalism. In the new basis the (unchanged!) eigenvectors of the free solid problem can be expressed as

$$\begin{aligned} \psi^f &= \tilde{\chi}_B \tilde{C}_B^f + \tilde{\chi}_D \tilde{C}_D^f \\ &= \chi_B C_B^f + \chi_D C_D^f; \end{aligned} \quad (2.74)$$

hence

$$\tilde{C}_R^f = T_{RR}^{-1} C_R^f \quad (R = B, D). \quad (2.75)$$

For the eigenvectors of the embedded cluster problem we have

$$\tilde{C}_R = T_{RR}^{-1} \bar{C}_R \quad (R = A, B). \quad (2.76)$$

Due to the block diagonal character of the transformation matrix T it follows for the overlap matrix that

$$\tilde{S}_{RQ} = T_{RR}^\dagger S_{RQ} T_{QQ} \quad (R, Q = A, B, D). \quad (2.77)$$

A similar result holds for the Fock matrix.

The transformation properties of the coupling matrix M may most easily be studied by considering the matrix D. From Eq. (2.77) it follows that

$$(\tilde{S}_{SS}^{-1})_{BB} = T_{BB}^{-1} (S_{SS}^{-1})_{BB} (T_{BB}^{-1})^\dagger, \quad (2.78)$$

hence

$$\begin{aligned} \tilde{D} &= \tilde{S}_{BB} (\tilde{S}_{SS}^{-1})_{BB} \\ &= T_{BB}^\dagger D (T_{BB}^\dagger)^{-1}. \end{aligned} \quad (2.79)$$

Therefore also

$$\tilde{M} = T_{BB}^\dagger M (T_{BB}^\dagger)^{-1}. \quad (2.80)$$

For completeness we mention that the matrix X transforms as

$$\tilde{X} = T_{BB}^\dagger X, \quad (2.81)$$

which follows easily by use of Eqs. (2.75) and (2.77).

To check our results we calculate the density matrix \tilde{P}_{CC} using the quantities in the transformed basis. From Eqs. (2.56), (2.76) and (2.80) we obtain

$$\tilde{P}_{BB} = T_{BB}^{-1} P_{BB} (T_{BB}^{-1})^\dagger. \quad (2.82a)$$

Similarly

$$\tilde{P}_{AB} = T_{AA}^{-1} P_{AB} (T_{BB}^{-1})^\dagger. \quad (2.82b)$$

Combined with the trivial results

$$\tilde{P}_{AA} = T_{AA}^{-1} P_{AA} (T_{AA}^{-1})^\dagger, \quad (2.82c)$$

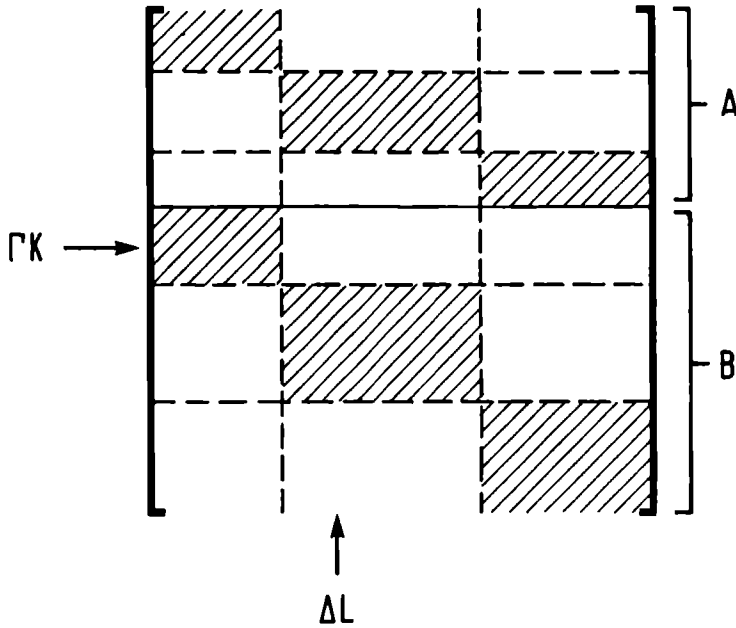
$$\tilde{P}_{BA} = T_{BB}^{-1} P_{BA} (T_{AA}^{-1})^\dagger, \quad (2.82d)$$

we finally obtain

$$\tilde{P}_{CC} = T_{CC}^{-1} P_{CC} (T_{CC}^{-1})^\dagger, \quad (2.82e)$$

as required.

Our next step is the symmetry adaptation of the basis χ . Let T be of the form (2.73) and such that the elements of $\tilde{\chi}$ transform as basis functions for irreducible representations of the symmetry group. We will denote a general element of T by $T_{\mu, \Gamma k}$, where μ labels a function of the original basis χ , Γ labels an irreducible representation, and k is a multiplicity label. The matrix \tilde{C} with eigenvectors of the embedded cluster problem will have the structure



where only shaded elements can be nonzero. Thus,

$$\tilde{C}_{\Gamma k, \Delta l}^{\Gamma} = \delta_{\Gamma \Delta} \tilde{C}_{kl}^{\Gamma} \quad (2.83)$$

Similarly,

$$\tilde{C}_{\Gamma k, \Delta l}^{\Gamma^f} = \delta_{\Gamma \Delta} \tilde{C}_{kl}^{\Gamma^f} \quad (2.84)$$

In the symmetry adapted basis $\tilde{\chi}$ the coupling matrix \tilde{M} is also symmetry blocked, as we will show now. Again it is simplest to consider the matrix D:

$$\tilde{D}_{\Gamma k, \Delta l} = \sum_{\Theta m} \tilde{S}_{\Gamma k, \Theta m} (\tilde{S}_{SS}^{-1})_{\Theta m, \Delta l} \quad (2.85)$$

The unit operator is totally symmetric, so

$$\tilde{S}_{\Gamma k, \Theta m} = \delta_{\Gamma \Theta} \tilde{S}_{\Gamma k, \Gamma m} \equiv \delta_{\Gamma \Theta} \tilde{S}_{km}^{\Gamma} \quad (2.86)$$

and

$$\begin{aligned}
 (\tilde{S}_{SS}^{-1})_{\Theta m, \Delta l} &= \delta_{\Theta \Delta} (\tilde{S}_{SS}^{-1})_{\Theta m, \Theta l} \\
 &\equiv \delta_{\Theta \Delta} (\tilde{S}_{SS}^{\Theta -1})_{ml}.
 \end{aligned} \tag{2.87}$$

Substituting Eqs. (2.86) and (2.87) into Eq. (2.85) we find

$$\begin{aligned}
 \tilde{D}_{\Gamma k, \Delta l} &= \delta_{\Gamma \Delta} \sum_m \tilde{S}_{km}^{\Gamma} (\tilde{S}_{SS}^{\Gamma -1})_{ml} \\
 &\equiv \delta_{\Gamma \Delta} D_{kl}^{\Gamma}.
 \end{aligned} \tag{2.88}$$

Therefore also

$$\tilde{M}_{\Gamma k, \Delta l}(e) = \delta_{\Gamma \Delta} \tilde{M}_{kl}^{\Gamma}(e). \tag{2.89}$$

Finally we look at the construction of the density matrix for $\Gamma k \in C$,

$\Delta l \in B$:

$$\begin{aligned}
 \tilde{P}_{\Gamma k, \Delta l} &= \sum_{\Theta m} \sum_{\Omega n} \tilde{C}_{\Gamma k, \Omega n} \tilde{C}_{\Theta m, \Omega n}^* \tilde{M}_{\Theta m, \Delta l}(\bar{e}_{\Omega n}) \\
 &= \delta_{\Gamma \Delta} \sum_m \sum_n \tilde{C}_{kn}^{\Gamma} \tilde{C}_{mn}^* \tilde{M}_{ml}^{\Gamma}(\bar{e}_{\Gamma n}) \\
 &\equiv \delta_{\Gamma \Delta} \tilde{P}_{kl}^{\Gamma},
 \end{aligned} \tag{2.90}$$

where we have used Eqs. (2.83) and (2.89).

We conclude that it is indeed possible to treat the embedding problem in a symmetry adapted manner. The density matrix in the original basis may be recovered from

$$P_{CC} = T_{CC} \tilde{P}_{CC} T_{CC}^\dagger, \quad (2.91)$$

so

$$\begin{aligned} P_{\mu\nu} &= \sum_{\Gamma k, \Delta l} T_{\mu, \Gamma k} \tilde{P}_{\Gamma k, \Delta l} T_{\nu, \Delta l}^* \\ &= \sum_{\Gamma} \sum_{k, l} T_{\mu, \Gamma k} \tilde{P}_{k l}^\Gamma T_{\nu, \Gamma l}^*, \end{aligned} \quad (2.92)$$

i.e., as a sum over irreducible representations of the symmetry group.

3. Implementation

The present embedding approach to the chemisorption problem leads to a computational scheme that essentially consists of three steps. Implicit in the procedure is the choice of a one-electron model to describe the chemisorption phenomenon. We reiterate that capitals A,B,... are used to indicate both localized regions in space and the basis sets centered in these regions. The three steps involved are:

- I. Choose a description S of the solid surface, to be used as substrate, and perform a self-consistent cluster calculation.
- II. Define a cluster $B \subset S$ to be used in the chemisorption cluster, at the same time defining the representation of the defective solid, $D = S \setminus B$. The electronic structure of S is reflected in the matrices D , X , C_B^f , E^f , which occur in the coupling matrix M , and the additional terms due to the defective solid in the Fock matrix for the chemisorption cluster.
- III. Perform a self-consistent embedded cluster calculation for the adsorbate A , chemisorbed on B . The iterative procedure to be followed is described in Sec. 2G.

As one-electron model we use the Hartree-Fock-Slater (HFS) model. We have implemented the embedding scheme in the pseudopotential HFS-LCAO program of Baerends et. al. [17-19]. The major characteristics of our chain of programs are (i) full use of symmetry, (ii) optional use of nonorthogonal or semi-orthogonal basis sets [cf. Sec. 2H], and (iii) analytic evaluation of the coupling matrices at the relevant energies. At present we have only implemented the spin-restricted formalism.

Steps I and III of the computational procedure involve the use of the extended HFS-LCAO program, step II involves the use of an auxiliary program, which we named PISANI. In the following we will discuss some features of both programs. In Appendix C we describe the structure of the embedding HFS-LCAO program.

A. Additional terms in the Fock matrix

For a system of interacting atoms a the Fock operator in the pseudo-potential HFS model reads

$$F(1) = T(1) + V_N(1) + V_C[\rho(1)] + V_x[\rho(1)] + V_{ps}(1), \quad (3.1)$$

where T is the kinetic energy operator, V_N the nuclear potential, V_C the electronic Coulomb potential, V_x the electronic exchange potential and V_{ps} the pseudopotential shift operator. In atomic units:

$$T(1) = -\frac{1}{2} \nabla(1)^2, \quad (3.2)$$

$$V_N(1) = -\sum_a Z_a R_{a1}^{-1}, \quad (3.3)$$

$$V_C[\rho(1)] = \int r_{12}^{-1} \rho(2) d\tau_2, \quad (3.4)$$

$$V_x[\rho(1)] = -3\alpha \left[\frac{3}{8\pi} \rho(1) \right]^{1/3}, \quad (3.5)$$

and

$$V_{ps}(1) = \sum_{a,i} (\bar{\epsilon} - \epsilon_{core,i}^a) |\psi_{core,i}^a(1)\rangle \langle \psi_{core,i}^a(1)|. \quad (3.6)$$

We note that V_{ps} shifts the core orbitals $\psi_{core,i}^a$ from their one-electron energies $\epsilon_{core,i}^a$ to the average valence energy $\bar{\epsilon}$. The one-electron density occurring in Eqs. (3.4) and (3.5) is written as

$$\rho(1) = \sum_a \left[\rho_{core}^a(1) + \Delta\rho^a(1) \right] + \rho_{ps}(1), \quad (3.7)$$

where the atomic difference density $\Delta\rho^a(1)$ is defined as

$$\Delta\rho^a(1) \equiv \rho_{\text{valence}}^a(1) - \rho_{\text{ps}}^a(1), \quad (3.8)$$

and $\rho_{\text{ps}}^a(1)$ is the pseudo density. See Refs. [20] and [21] for a more extensive discussion of the Fock operator and its inherent assumptions.

In the HFS-LCAO method of Baerends et. al. the matrix elements of the Fock operator are evaluated with a numerical integration scheme. Defining

$$\tilde{F} \equiv T + V_N + V_C + V_X, \quad (3.9)$$

one approximates

$$\begin{aligned} \tilde{F}_{\mu\nu} &= \langle \chi_\mu | \tilde{F} | \chi_\nu \rangle \\ &\equiv \sum_k W(\vec{r}_k) \chi_\mu^*(\vec{r}_k) F(\vec{r}_k) \chi_\nu(\vec{r}_k), \end{aligned} \quad (3.10)$$

with $W(\vec{r}_k)$ the weight of integration point \vec{r}_k . The matrix representation of the pseudopotential operator (3.6), which essentially involves overlap integrals only, is treated analytically. At each cycle of the iterative procedure it is constructed from the two matrices

$$P^C = \langle \chi | [\sum_{a,i} | \psi_{\text{core},i}^a \rangle \langle \psi_{\text{core},i}^a |] | \chi \rangle, \quad (3.11)$$

and

$$P^E = \langle \chi | [\sum_{a,i} \epsilon_{\text{core},i}^a | \psi_{\text{core},i}^a \rangle \langle \psi_{\text{core},i}^a |] | \chi \rangle. \quad (3.12)$$

The Fock matrix entering the embedded cluster calculation is the Fock matrix of the full chemisorption system (ABD), confined to the embedded cluster. In comparison with a nonembedded cluster calculation a number of additional terms

occur, all pertaining to the indented solid. The computational scheme of the HFS-LCAO method allows these terms to be included in a natural way.

Inclusion of the potential due to the indented solid requires the calculation at each integration point of

- the nuclear potential

$$- \sum_a^D Z_a R_{a1}^{-1}, \quad (3.13)$$

- the density

$$\sum_a^D [\rho_{\text{core}}^a(1) + \Delta\rho^a(1)] + [\rho^f(1) - \rho_{\text{BB}}^f(1)], \quad (3.14)$$

to be used in the evaluation of the exchange potential (3.5). ρ_{BB}^f denotes the density that corresponds to the density matrix P_{BB}^f .

- the Coulomb potential due to the density (3.14).

Since all these contributions remain constant during the iterative calculation on the embedded cluster, they can conveniently be added to the corresponding constant terms occurring in the nonembedded cluster calculation, viz., to

- the nuclear potential

$$- \sum_a^C Z_a R_{a1}^{-1}, \quad (3.15)$$

- the density

$$\sum_a^C [\rho_{\text{core}}^a(1) + \Delta\rho^a(1)], \quad (3.16)$$

- the Coulomb potential due to the density (3.16).

Inclusion of the indented solid in V_{ps} requires the calculation of the

matrices P^C and P^E pertaining to D, in the basis $\chi_A \cup \chi_B$, and adding them to the corresponding matrices calculated for the nonembedded cluster.

We note that, once the additional terms are evaluated, the construction of the Fock matrix in the embedded cluster calculation proceeds in the same way as in the nonembedded cluster calculation, i.e., there are no extra storage or computation time requirements. The evaluation of the additional terms can be quite time consuming, however. In fact, it is one of the major steps in the calculation.

B. Construction of the density matrix in embedded cluster calculations

In the embedded cluster calculations the density matrix is evaluated according to Eq. (2.56). The coupling matrices involved in this expression are evaluated analytically at the appropriate energy points. The calculation of the density matrix is essentially a n^3 operation (and not a n^4 operation, as stated by Pisani [7]). Furthermore, the symmetry blocking reduces the dimensions of the matrices involved. This analytic procedure is computationally quite cheap, so we do not need interpolation or fitting procedures in our calculations. The matrices D, X, C_B^f and E^f , needed in the calculation, are read from a file created by program PISANI.

In order to reduce storage requirements, the HFS-LCAO program uses only the lower triangle of the density matrix P. In our implementation we calculate the density matrix for each irreducible representation, symmetrize as $\frac{1}{2}(P + P^\dagger)$ and transform the resulting lower triangle to the basis $\chi_A \cup \chi_B$. Note that the symmetrization does not affect the one-electron density.

In calculations employing the semi-orthogonal basis the constant part R [cf. Eq. (2.72)] of the density matrix is read from the file containing D, X, C_B^f and E^f .

C. Miscellaneous features

In the limit of very large substrate clusters the number of electrons introduced into the system by the adsorbate is vanishingly small. Therefore we take the Fermi level fixed in our calculations. The embedding HFS-LCAO program requires the specification of the Fermi level for each irreducible representation and checks the formal conditions

$$\epsilon_{\text{homo}}^f \leq \epsilon_{\text{Fermi}} \leq \epsilon_{\text{lumo}}^f, \quad (3.17)$$

where ϵ_{homo}^f and ϵ_{lumo}^f are determined by the free solid calculation. The average orbital energies $\bar{\epsilon}$ (one for each irreducible representation) in the pseudo-potential operator (3.6) are treated in the same spirit, i.e., they are frozen at their free solid value.

In the HFS-LCAO program a standard damping procedure is employed in the iterative calculation of the density matrix. Let $P_{i-1}^!$ be the density matrix used in cycle (i-1) and P_i the density matrix constructed from the eigenvectors of cycle i. Instead of using P_i as input for cycle (i+1) one uses

$$P_i^! = \alpha P_i + (1-\alpha)P_{i-1}^! \quad (0 < \alpha \leq 1). \quad (3.18)$$

The risk of divergencies (or oscillatory behaviour) in embedded cluster calculations is enhanced by the fact that the charge in the embedded cluster is not conserved: the number of electrons in the cluster is determined by the position of the Fermi level. Indeed, in our test calculations the damping procedure (3.18) was generally not sufficient to obtain convergence. Therefore we have used the following charge renormalization in the initial stage of the iterative procedure.

Let the matrix P_i correspond to N_i electrons ($i \geq 1$), and let N_0 be the

number of electrons corresponding to P_{BB}^f plus the number of (valence) electrons of the adsorbate (N_A):

$$N_0 = \text{Tr}(P_{BB}^f S_{BB}) + N_A. \quad (3.19)$$

Instead of Eq. (3.18) we use

$$P_i' = C_i [\alpha P_i + (1-\alpha) P_{i-1}'], \quad (3.20)$$

where

$$C_i = 1 + \left[\frac{N_0 - N_i}{N_i} \right] f_i; \quad (3.21)$$

f_i is a switching function with limiting properties $f_1 \cong 1$ and $\lim_{i \rightarrow \infty} f_i = 0$.

We obtained satisfactory results with the Fermi function

$$f_i = \left[1 + e^{\beta(i-i_0)} \right]^{-1}, \quad (3.22)$$

with typical choices $\beta = 0.3$, $i_0 = 10$.

D. Program PISANI

Program PISANI performs step II of the computational procedure as outlined in the introduction of this section, i.e., it serves as a bridge between the free solid and the embedded cluster calculations. Its main functions are:

- definition of the cluster $B \subset S$ in terms of atoms, basis sets, density fit sets and core orbitals, including validity checks of the atoms selected with the symmetry group chosen.
- calculation of the matrices D and X, needed in the evaluation of the coupling

matrices M; in the case of a semi-orthogonal basis also the matrix R is calculated.

- fit of the density $(\rho^f - \rho_{BB}^f)$, which corresponds to the matrix

$$\begin{bmatrix} 0_{BB} & P_{BD}^f \\ P_{DB}^f & P_{DD}^f \end{bmatrix} \quad (3.23)$$

[cf. Eq. (3.14)]. This density fit is used in the pointwise calculation of the density and the Coulomb potential due to the indented solid.

Apart from these essential functions program PISANI has a number of useful additional functions. We mention the possibility to check the case where the adsorbate is absent, the calculation of the coupling matrices at energy points to be specified and a population analysis of the free solid density in terms of B and D.

We note that the computation times needed by the program are very modest. E.g., for the case $Li_{18} \subset Li_{79}$ in a double-zeta-plus-polarization-function basis the execution time is 20 seconds on the AS9040, which is to be compared with the execution time of approximately one hour for the embedded cluster calculation.

4. Results and discussion

Due to the small number of basis functions needed to describe lithium atoms, lithium is a convenient testing ground for methods dealing with metals. We performed test calculations with the MLEC method for the on-top adsorption of hydrogen on the lithium (100) surface. In all calculations we used the spin-restricted formalism.

A. The substrate: Li₇₉

As a representation of the substrate in our embedding calculations we used a Li₇₉(21,16,21,12,9) cluster, i.e., with 21 atoms in the first layer, 16 in the second, etc. The cluster is supposed to represent the unreconstructed (100) surface of the body-centered-cubic lattice (with bulk lattice constant 6.60 a.u. [22]). In table 1 we summarize the geometric data for the cluster. For future reference we note that atoms of type I, III, X, and XIV lie in the surface plane.

The double-zeta s, single-zeta p STO basis set [23] and the integration parameters used in the calculations are listed in table 2. It was shown by Post [24] that for the Li₅-CO interaction this basis set satisfactorily reproduces the details of the interaction energy vs. distance curve calculated with a triple zeta basis. We note that the basis set of table 2 was used for all atoms in the Li₇₉ cluster, i.e., the basis consisted of 395 STOs.

In the Li₇₉ calculation as well as in all other calculations we used the C_{4v} point group symmetry. To obtain the electronic configuration we did not optimize the cohesive energy, but simply followed the Aufbau principle. It appears, however, that for lithium clusters both schemes yield the same result [1,25]. Due to near-degeneracies in the orbital energies the Li₇₉ calculation

Table 1

Geometric data for the Li_{79} cluster ($a = 6.60$ a.u.)

atom type	coordinate	distance to $\text{Li(I)} \cdot a^{-1}$	multiplicity	cumulative cluster
I	(0, 0, 0)	0.000	1	Li_1 (1, 0, 0, 0,0)
II	($\frac{a}{2}$, $\frac{a}{2}$, $-\frac{a}{2}$)	0.866	4	Li_5 (1, 4, 0, 0,0)
III	(a, 0, 0)	1.000	4	Li_9 (5, 4, 0, 0,0)
IV	(0, 0, - a)	1.000	1	Li_{10} (5, 4, 1, 0,0)
V	(a, a, 0)	1.414	4	Li_{14} (9, 4, 1, 0,0)
VI	(a, 0, - a)	1.414	4	Li_{18} (9, 4, 5, 0,0)
VII	($\frac{3a}{2}$, $\frac{a}{2}$, $-\frac{a}{2}$)	1.658	8	Li_{26} (9,12, 5, 0,0)
VIII	($\frac{a}{2}$, $\frac{a}{2}$, $-\frac{3a}{2}$)	1.658	4	Li_{30} (9,12, 5, 4,0)
IX	(a, a, - a)	1.732	4	Li_{34} (9,12, 9, 4,0)
X	(2a, 0, 0)	2.000	4	Li_{38} (13,12, 9, 4,0)
XI	(0, 0, -2a)	2.000	1	Li_{39} (13,12, 9, 4,1)
XII	($\frac{3a}{2}$, $\frac{3a}{2}$, $-\frac{a}{2}$)	2.179	4	Li_{43} (13,16, 9, 4,1)
XIII	($\frac{3a}{2}$, $\frac{a}{2}$, $-\frac{3a}{2}$)	2.179	8	Li_{51} (13,16, 9,12,1)
XIV	(2a, a, 0)	2.236	8	Li_{59} (21,16, 9,12,1)
XV	(2a, 0, - a)	2.236	4	Li_{63} (21,16,13,12,1)
XVI	(a, 0, -2a)	2.236	4	Li_{67} (21,16,13,12,5)
XVII	(2a, a, - a)	2.449	8	Li_{75} (21,16,21,12,5)
XVIII	(a, a, -2a)	2.449	4	Li_{79} (21,16,21,12,9)

Table 2

Basis sets and integration parameters

	H	Li
basis ^{a)}		
1s	0.76	
	1.28	
2s		1.16
		0.60
2p	1.00	0.60
integration ^{b)}		
r_0	2.00	2.00
α_0	0.50	0.50

a) Ref.23

b) Parameters in Fermi-like distribution $[1 + \exp(\alpha_0(r-r_0))]^{-1}$

Table 3

Deviations from the exact value, caused by a perturbation in the Fock matrix, for net cluster populations of Li_{18} embedded in Li_{79}

λ	A_1 representation		E representation		total	
	nonorth	semi-orth	nonorth	semi-orth	nonorth	semi-orth
10^{-8}	.000 000	.000 000	.000 000	.000 000	.000 000	.000 000
10^{-7}	-.000 007	.000 000	-.000 001	-.000 001	-.000 012	-.000 002
10^{-6}	-.000 077	-.000 001	-.000 013	-.000 008	-.000 130	-.000 039
10^{-5}	-.000 773	-.000 012	-.000 125	-.000 076	-.001 311	-.000 400
10^{-4}	-.007 398	-.000 120	-.001 041	-.000 753	-.012 370	-.003 984
10^{-3}	-.047 501	-.000 501	+.004 908	-.006 613	-.065 747	-.036 316
10^{-2}	+2.616 654	+0.69 901	+2.492 540	+0.082 439	+4.455 967	+0.098 174

converged very slowly: it took 200 iterations to converge to a mean change of 2×10^{-6} in the diagonal of the density matrix.

B. The coupling matrices

Having performed the free solid calculation, we can define subclusters for use in embedded cluster calculations. In figures 2 and 3 we show the energy dependence for some elements of the coupling matrices M in clusters of increasing size. The elements pertain to symmetry adapted linear combinations of basis functions located in the central part of the Li_{79} cluster. Except for a discontinuity at the Fermi energy the energy dependence is quite smooth.

In figure 2 we show some representative elements in the nonorthogonal basis. We see that the behaviour is not at all close to the step function $\theta(\epsilon_F - e)$. The elements can assume values up to $10^2 - 10^3$; furthermore, the variation with energy is quite large. This behaviour causes severe numerical problems, as can be understood qualitatively from the following argument. The elements of the eigenvectors \bar{C} and the density matrix P are of the same order. Thus, in the calculation of the density matrix, cancellation of relatively large terms $\bar{C}_{\mu k} \bar{C}_{\alpha k}^* M_{\alpha \nu}(\bar{e}_k)$ [Eq. (2.56b)] has to occur to produce the correct $P_{\mu \nu}$. This cancellation leads to severe demands to be imposed on the numerical integration scheme in the HFS-LCAO embedded cluster calculation. In fact, the demands are so severe that the effort involved in the numerical integration becomes prohibitively large. This problem led us to introduce the semi-orthogonal basis in Sec. 2H.

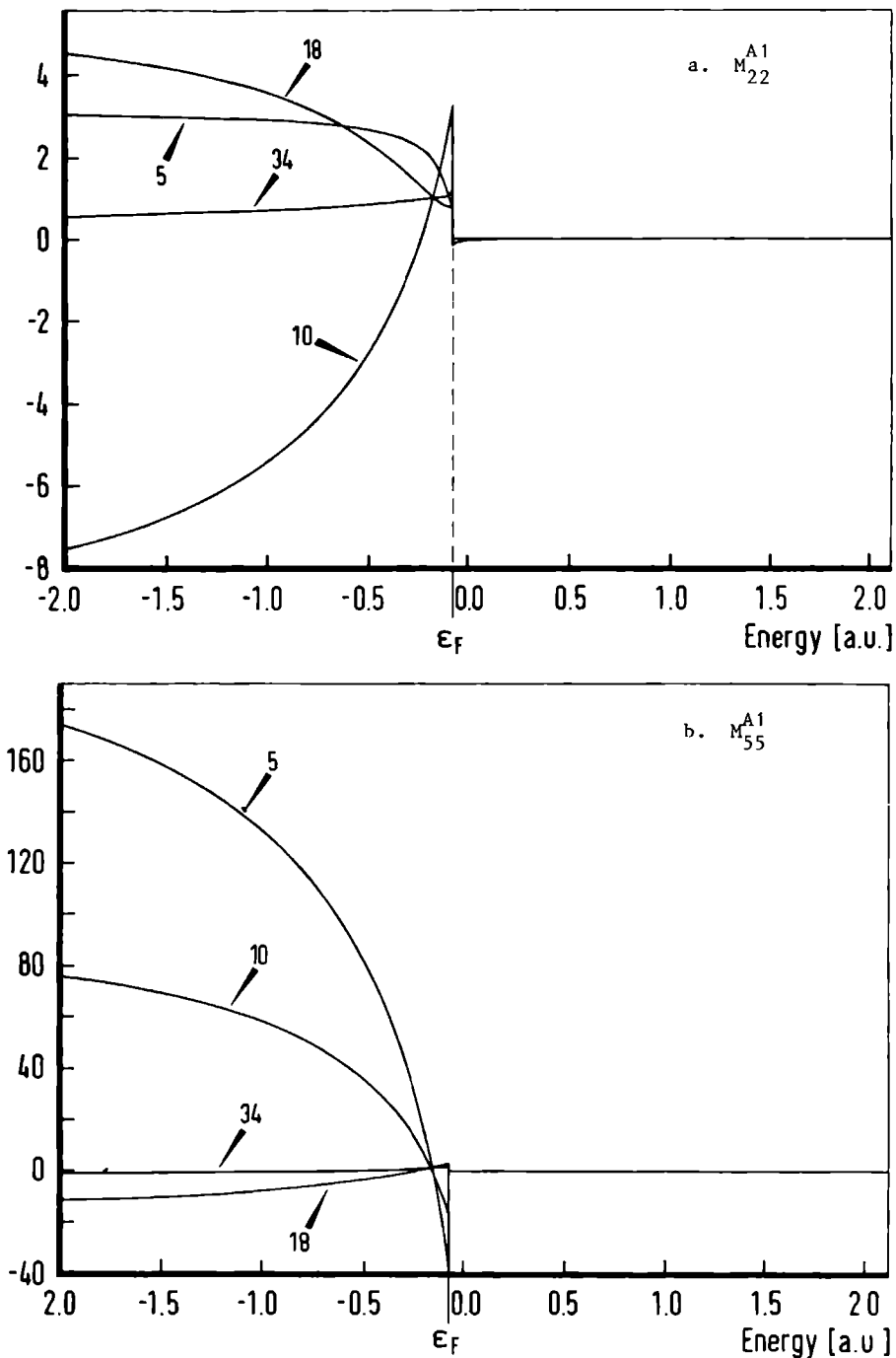


Figure 2. Coupling matrix elements in nonorthogonal basis for different clusters $B \subset Li_{79}$

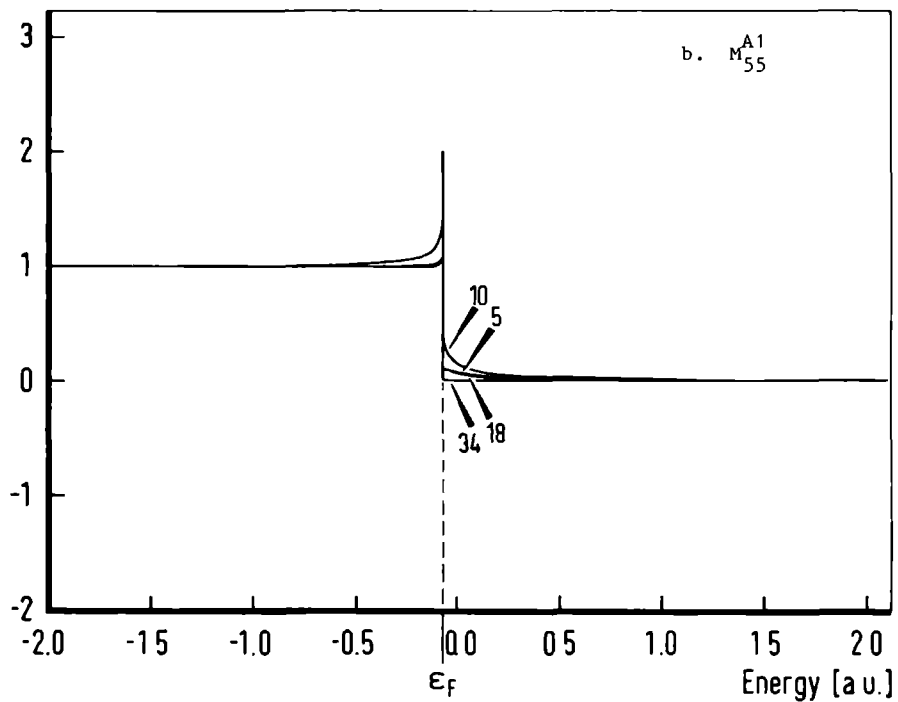
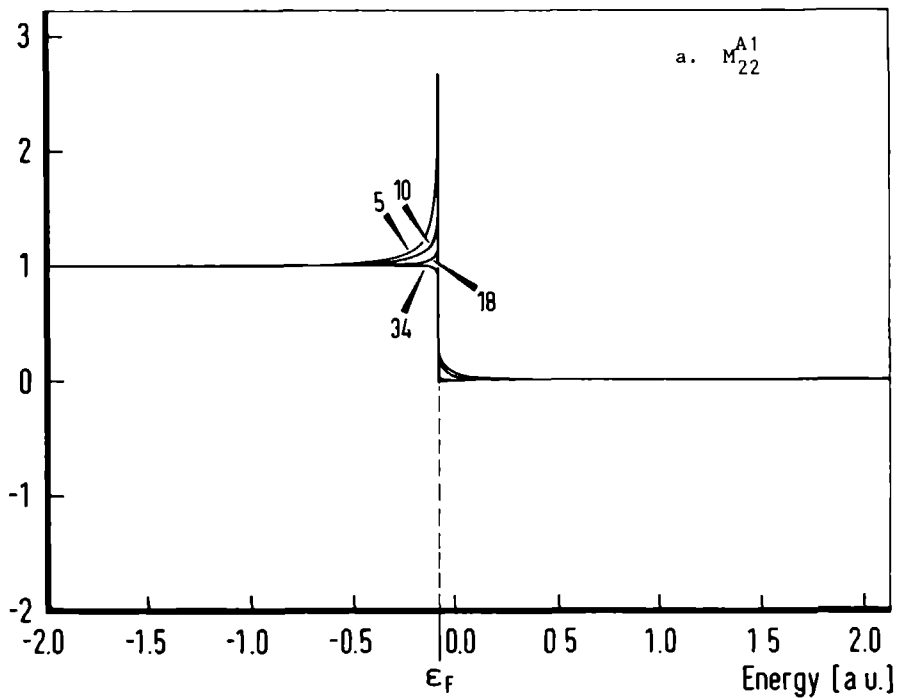


Figure 3. Coupling matrix elements in semi-orthogonal basis for different clusters $B \subset Li_{79}$

In figure 3 we display some elements of the coupling matrices for the semi-orthogonal basis. It is clear that the coupling matrices are much more well-behaved, now. With increasing cluster size the elements pertaining to the central region rapidly approach the step function $\Theta(\epsilon_p - e)$. The elements belonging to the border region, where the connection with the free solid is made, show a more complex behaviour. Off-diagonal elements are generally an order of magnitude smaller than diagonal ones. This behaviour is much the same as found by Pisani [7].

In order to illustrate the instability caused by an inaccurate integration scheme we consider the embedding of Li_{18} in Li_{79} , in the absence of an adsorbate. In that case, the results of Li_{79} should be reproduced exactly: after solving the generalized eigenvalue problem of F_{BB}^f and constructing the density matrix we should obtain P_{BB}^f , both for nonorthogonal and semi-orthogonal bases [Sec. 2F]. This serves as an important check of the programs used. We now simulate the effect of inaccuracies in the Fock matrix caused by the numerical integration with a small perturbation:

$$F = F_{BB}^f + \lambda\Delta, \quad (4.1)$$

where

$$\Delta_{ij} = (-1)^{i+j}. \quad (4.2)$$

In table 3 we list the effect of increasing λ from 10^{-8} , with factors of 10, on the number of electrons corresponding to the resulting density matrix, the net cluster population

$$n_{CC} = \text{Tr}(P_{CC}S_{CC}). \quad (4.3)$$

It can clearly be seen that the perturbation has a more pronounced effect in the nonorthogonal case. We note that integrated quantities, such as the net cluster population, are the more stable ones in our embedding HFS-LCAO scheme, as will become clear in the sequel.

C. The numerical integration

The numerical integration scheme employed in the HFS-LCAO program [cf. Sec. 3A] is the discrete variational method, introduced by Ellis and Painter [26,27]. The density of integration points is taken as a superposition of Fermi-like distributions, centered at the atoms in the system. We note that the HFS-LCAO program directly calculates matrix elements over symmetry adapted linear combinations of basis functions, thus obviating the need for storage of large numbers of integrals over primitive basis functions.

The influence of the integration scheme on the embedded cluster calculations was investigated for Li_{10} and Li_{10}H embedded in Li_{79} . In tables 4 and 5 we list some details of the electronic structure obtained with various schemes. The parameters entering the numerical integration are those of the Fermi-like distributions and the number of points in each atomic distribution. We have only varied the latter.

The first columns of tables 4 and 5 refer to calculations with 500 points per atom for all atoms in the embedded cluster C, which gives stable results in the usual nonembedded cluster calculations. The last columns give the results obtained when using the complete Li_{79} integration grid, with an extra 500 points on H in the Li_{10}H calculations. The interjacent columns refer to calculations with increasing numbers of points (N_C) in C and to calculations with (N_D) additional points in the indented solid.

From these and similar calculations which we have performed, a number of conclusions can be drawn with respect to the accuracy of the integration procedure:

Table 4

Influence of integration scheme in Li_{10} embedded cluster calculation using the semi-orthogonal basis

integration	I	II	III	IV	$v^a)$
N_C	5 000	10 000	5 000	5 000	2 500
N_D	0	0	800	3 850	17 250
net atomic populations					
Li(I)	0.19	0.18	0.23	0.29	0.26
Li(II)	0.36	0.54	0.59	0.37	0.34
Li(III)	0.12	0.26	0.24	0.33	0.27
Li(IV)	0.85	0.71	0.45	0.43	0.32
atomic overlap populations					
Li(I)-Li(II)	0.31	0.31	0.29	0.19	0.21
Li(I)-Li(III)	0.08	0.10	0.11	0.16	0.14
Li(I)-Li(IV)	-0.02	-0.02	0.03	0.14	0.12
gross atomic charges					
Li(I)	0.15	0.15	0.09	0.08	0.12
Li(II)	-0.18	-0.22	-0.21	-0.13	-0.14
Li(III)	0.22	0.23	0.20	0.16	0.18
Li(IV)	-0.02	0.07	0.17	0.02	-0.05
net populations in Li_{10}					
A_1	3.18	3.08	3.07	2.89	2.84
A_2'	0.01	0.00	0.00	-0.00	0.00
B_1	0.44	0.46	0.33	0.41	0.43
B_2	0.28	0.28	0.27	0.25	0.26
E	3.22	3.37	3.51	3.66	3.66
total	7.12	7.18	7.19	7.21	7.20

a) Integration scheme of free solid (Li_{79}) calculation

Table 5

Influence of integration scheme in Li_{10}H embedded cluster calculation using the semi-orthogonal basis

integration	I	II	III	IV	V	VI ^{a)}
N_C	5 500	22 000	5 500	5 500	5 500	3 000
N_D	0	0	800	1 600	3 850	17 250
net atomic populations						
H	0.72	0.86	0.93	0.91	0.83	0.80
Li(I)	0.81	0.67	0.64	0.65	0.73	0.77
Li(II)	0.27	0.23	0.45	0.33	0.32	0.32
Li(III)	0.17	0.11	0.15	0.16	0.21	0.22
Li(IV)	0.89	0.16	0.13	-0.13	0.06	0.04
atomic overlap populations						
H-Li(I)	0.62	0.64	0.62	0.63	0.66	0.67
H-Li(II)	0.05	0.05	0.04	0.05	0.04	0.05
H-Li(III)	-0.02	-0.02	-0.01	-0.02	-0.02	-0.02
H-Li(IV)	0.04	0.03	0.03	0.03	0.03	0.03
gross atomic charges						
H	-0.11	-0.25	-0.30	-0.30	-0.23	-0.21
Li(I)	-0.01	-0.01	+0.01	-0.00	-0.06	-0.11
Li(II)	-0.16	-0.18	-0.19	-0.19	-0.16	-0.13
Li(III)	0.28	0.31	0.32	0.33	0.29	0.28
Li(IV)	-0.09	-0.03	-0.00	+0.01	-0.06	-0.06
net populations in Li_{10}H						
A_1	4.42	4.42	4.45	4.37	4.42	4.42
A_2	0.01	0.01	-0.00	0.02	0.00	0.01
B_1	0.47	0.48	0.45	0.39	0.41	0.43
B_2	0.35	0.26	0.28	0.27	0.26	0.26
E	2.91	3.02	3.03	3.13	3.15	3.12
total	8.17	8.18	8.20	8.18	8.24	8.23

a) Integration scheme of free solid (Li_{79}) calculation supplemented with 500 points on hydrogen

- The electronic structure of the embedded cluster is more stable in its central region than in the region bordering the indented solid. In figure 4 we illustrate this point by showing the pseudo-density $\rho_{BB}(1)$ along the principle axis of the cluster in various integration schemes.
- Increasing the number of integration points in the embedded cluster alone is ineffective in improving the accuracy; it is better to include points in the region of the indented solid bordering the embedded cluster.
- Even with quite extensive integration schemes the populations are accurate to a few hundredths of an electron only. However, the inaccuracies are substantially smaller than the changes induced by the adsorbate.
- Integrated quantities are more stable than their constituent parts: gross atomic populations vs. net atomic populations and overlap populations; the net cluster population [Eq. (4.3)] vs. its contributions from various irreducible representations.
- In agreement with the conclusion of Sec. 4B, we find that the observed instabilities with the nonorthogonal basis are much more pronounced than with the semi-orthogonal basis.

The inefficiency of Fermi-like grid point distributions solely localized in the embedded cluster, in the integration for the embedded cluster calculation may be understood as follows. For isolated molecules the superposition of atomic grid point distributions more or less follows the electron density, i.e., regions of space with a low density obtain also a small weight. For embedded cluster calculations, however, the (total) density does not fall off outside the cluster, but stays approximately constant. Therefore, integration points outside the cluster are needed to obtain sufficiently accurate values for integrals over functions located in the border region of the cluster.

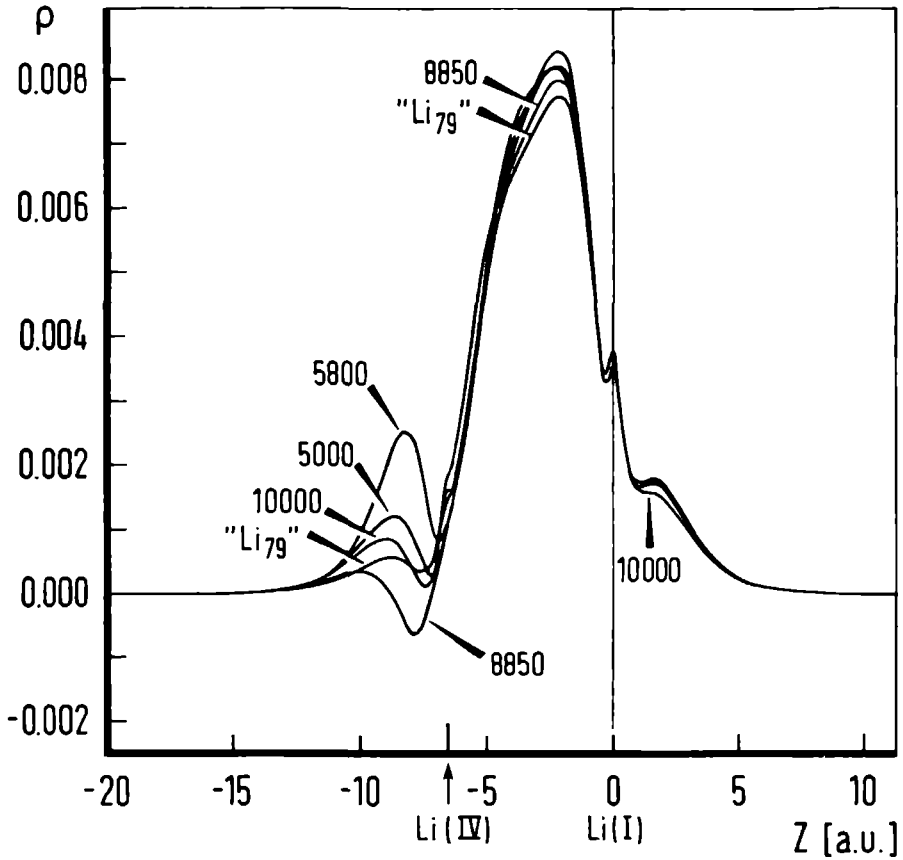


Figure 4. Pseudo density ρ_{BB} in various integration schemes. Numbers indicate number of integration points used. "Li₇₉" indicates Li₇₉ integration grid

D. Convergence with cluster size; effect of embedding

We studied the convergence of the electronic structure as a function of cluster size for the on-top adsorption of hydrogen. The hydrogen-lithium distance used was the free LiH distance (3.015 a.u.), which was found to be close to the minimum of the interaction energy curve in several cluster studies [28,29]. In the embedded cluster calculation we used the semi-orthogonal formalism. The integration schemes consisted of the Li_{79} grid supplemented with 500 points on hydrogen in the embedded cluster calculations, and 500 points per atom in the nonembedded cluster calculations.

In table 6 we present the converged values for the atomic populations and the net cluster population [Eq. (4.3)] in the embedded cluster calculations, in table 7 the adsorbate induced changes in these populations and in table 8 the corresponding numbers for the nonembedded cluster calculations. We note that, due to the averaging over symmetry equivalent atoms, the populations pertaining to Li(II) and Li(III) are more accurate than those of H, Li(I) and Li(IV). Further we recall that the surface atoms in the Li_{10} cluster are Li(I) and Li(III).

From the calculations a number of conclusions may be drawn:

- Once again it can be seen that integrated quantities show better convergence, now with respect to cluster size, than their constituent parts.
- The gross atomic charges convergence more rapidly in the embedded cluster calculations than in the non-embedded calculations. They are converged for the Li_{10} cluster. The more detailed populations need somewhat larger clusters; still they converge more rapidly in the embedded cluster calculations.
- The embedded clusters show a more adequate screening of the perturbation induced by the adsorbate. The changes in the gross atomic charges seem to be localized in the Li_5 cluster formed by the central lithium atom and its four surface neighbours.

Table 6

Atomic populations in Li_nH embedded cluster calculations using the semi-orthogonal basis

n	1	5 ^{a)}	10	18	26
net atomic populations					
H	0.96	0.79	0.80	0.84	0.84
Li(I)	0.45	0.42	0.77	0.54	0.45
Li(II)	-	-	0.32	0.34	0.32
Li(III)	-	0.18	0.22	0.26	0.26
Li(IV)	-	-	0.04	0.26	0.31
atomic overlap populations					
H-Li(I)	-0.05	0.57	0.67	0.69	0.70
H-Li(II)	-	-	0.05	0.03	0.02
H-Li(III)	-	-	-0.02	-0.01	-0.01
H-Li(IV)	-	-	0.02	-0.01	0.00
Li(I)-Li(II)	-	-	0.04	0.10	0.19
Li(I)-Li(III)	-	0.10	0.01	0.05	0.02
Li(I)-Li(IV)	-	-	0.04	0.08	0.04
gross atomic charges					
H	0.06	-0.08	-0.21	-0.20	-0.20
Li(I)	-0.05	-0.25	-0.11	-0.07	-0.08
Li(II)	-	-	-0.13	-0.13	-0.12
Li(III)	-	0.28	0.28	0.25	0.26
Li(IV)	-	-	-0.06	-0.06	-0.07

a) $\text{Li}_5(5,0)$ cluster

Table 7

Chemisorption induced changes in atomic populations in Li_nH embedded
cluster calculations using semi-orthogonal basis

n	1	5 ^{a)}	10	18	26
net atomic populations					
H	-0.04	-0.21	-0.20	-0.16	-0.16
Li(I)	+0.19	+0.16	+0.52	+0.28	+0.19
Li(II)	-	-	-0.01	+0.00	-0.02
Li(III)	-	-0.09	-0.05	-0.01	-0.01
Li(IV)	-	-	-0.28	-0.06	-0.00
atomic overlap populations					
H-Li(I)	-0.05	+0.57	+0.67	+0.69	+0.70
H-Li(II)	-	-	+0.05	+0.03	+0.02
H-Li(III)	-	-	-0.02	-0.01	-0.01
H-Li(IV)	-	-	+0.02	-0.01	+0.00
Li(I)-Li(II)	-	-	-0.17	-0.11	-0.02
Li(I)-Li(III)	-	-0.04	-0.12	-0.09	-0.12
Li(I)-Li(IV)	-	-	-0.09	-0.04	-0.09
gross atomic charges					
H	+0.06	-0.08	-0.21	-0.20	-0.20
Li(I)	-0.17	-0.37	-0.22	-0.19	-0.20
Li(II)	-	-	+0.00	+0.01	+0.01
Li(III)	-	+0.10	+0.10	+0.07	+0.07
Li(IV)	-	-	-0.01	-0.01	-0.01
net population in Li_nH					
	+0.108	+0.038	+0.028	+0.029	+0.019

a) $\text{Li}_5(5,0)$ cluster

Table 8

Chemisorption induced changes in atomic populations in Li_nH
nonembedded cluster calculations

n	1	5 ^{a)}	10	18	26
net atomic populations					
H	+0.06	-0.20	-0.31	-0.14	-0.15
Li(I)	-0.78	+0.30	+0.52	+0.12	+0.29
Li(II)	-	-	+0.05	+0.03	+0.01
Li(III)	-	-0.01	-0.07	-0.03	-0.02
Li(IV)	-	-	+0.02	+0.03	-0.01
atomic overlap populations					
H-Li(I)	+0.72	+0.91	+0.87	+0.76	+0.79
H-Li(II)	-	-	+0.00	+0.01	+0.01
H-Li(III)	-	-	-0.03	-0.01	-0.00
H-Li(IV)	-	-	+0.01	-0.00	-0.01
Li(I)-Li(II)	-	-	-0.13	-0.12	-0.15
Li(I)-Li(III)	-	-0.26	-0.26	-0.11	-0.11
Li(I)-Li(IV)	-	-	+0.11	+0.02	-0.02
gross atomic charges					
H	-0.42	-0.15	-0.07	-0.24	-0.23
Li(I)	+0.42	-0.24	-0.23	-0.09	-0.16
Li(II)	-	-	-0.03	-0.01	+0.03
Li(III)	-	+0.10	+0.10	+0.07	+0.06
Li(IV)	-	-	+0.04	-0.04	-0.01

a) $\text{Li}_5(5,0)$ cluster

- The adsorbate induced total charge of the embedded cluster is very small. This result agrees with the model calculations by Grimley [6]. Furthermore, it can be seen that the charge approaches zero as the cluster size increases. Although in the MLEC formalism with finite substrate clusters the latter condition holds exactly for $B \rightarrow S$, i.e., $D \rightarrow \emptyset$, we think that the clusters B are sufficiently small relative to D for this effect to be physical.

E. Computation times

In table 9 we give an indication of the computation times needed in various cluster calculations. Obviously the embedded cluster calculations are expensive compared to nonembedded cluster calculations. However, compared to the full (ABD) chemisorption calculations they are relatively cheap.

The causes for the increased computation times with respect to nonembedded cluster calculations are, in order of decreasing importance:

- i) The large number of iterations needed to reach convergence. Due to the increased instability of the calculations severe measures must be taken to ensure convergence. In our calculations we used heavy damping (admixing 5-10% of the new density matrix in each iteration only) and charge renormalization in the initial stage of the self-consistent procedure [Sec. 3C]. Thus we reached convergence in all cases investigated but one: $(Li_5 \leftarrow Li_{79})H$, with the Li_5 cluster consisting of the type I and II atoms.
- ii) The extended integration scheme, needed to incorporate the effect of the indented solid to sufficient accuracy. At present most time in the embedding HFS-LCAO program is spent in sections that depend linearly on the number of integration points.
- iii) The inclusion of the contribution of the indented solid in the constant terms for each integration point requires 10-25% of the time in embedded cluster calculations.

Table 9

Computation times of some representative cluster calculations on the AS9040

calculation	time	ratio
Li ₇₉ ; free solid	20 hours	1.00
Li ₁₈ H; nonembedded	12 minutes	0.01
Li ₁₈ H; embedded, standard integration	1 hour	0.05
Li ₁₈ H; embedded, extended integration	2 hours	0.10

iv) The calculation of the density matrix with the analytically evaluated coupling matrices. With standard integration schemes the overhead per iteration is somewhat less than 10%, which is quite acceptable.

In order to accelerate the embedded cluster calculations, further research is necessary. From the preceding analysis it becomes clear that the improvement of the integration scheme must play a central rôle. A possibility that could be investigated is the use of two independent point grids: the "standard" grid for the nonembedded cluster and an additional grid for the indented solid. The latter grid could be the one used for the free solid calculation. The information from the indented solid could then be stored, but it should be made more compact.

Convergence problems seem to be intrinsic; they will depend strongly on the system under investigation. Pisani [7] needed relatively few iterations in MLEC calculations for the chemisorption of hydrogen on graphite, for instance. In our test calculations for the on-top adsorption of fluorine on lithium (100) we obtained faster convergence than for the corresponding hydrogen adsorption calculations. Still, it would be surprising if convergence behaviour would not remain a difficult point in calculations for adsorption on metals.

Appendix AThe Green's matrix

Given a nonorthogonal, not necessarily complete basis $\chi = \{\chi_\mu\}$; the overlap matrix is denoted by S . Let \hat{H} be any one-electron Hamiltonian and H its matrix representation afforded by χ . The Green's matrix $G(\zeta)$ is defined by

$$(\zeta S - H) G(\zeta) = 1, \quad \zeta = \epsilon + i\eta. \quad (\text{A1})$$

The elements of $G(\zeta)$ may be expressed in terms of the solution of the generalized eigenvalue problem

$$HC = SCE, \quad E_{k\ell} = \delta_{k\ell} e_k, \quad (\text{A2})$$

$$C^\dagger SC = 1. \quad (\text{A3})$$

Starting from Eq. (A1) one obtains

$$\begin{aligned} (C^\dagger)^{-1} C^\dagger (\zeta S - H) C C^{-1} G(\zeta) &= 1, \\ (C^\dagger)^{-1} (\zeta C^\dagger SC - C^\dagger HC) C^{-1} G(\zeta) &= 1, \\ (\zeta I - E) G'(\zeta) &= 1, \end{aligned} \quad (\text{A4})$$

where

$$G'(\zeta) = C^{-1} G(\zeta) (C^\dagger)^{-1}. \quad (\text{A5})$$

From Eq. (A4) it follows that

$$G'_{kl}(\zeta) = \frac{\delta_{kl}}{\zeta - e_k}, \quad (\text{A6})$$

and hence

$$\begin{aligned} G_{\mu\nu}(\zeta) &= [CG'(\zeta)C^\dagger]_{\mu\nu} \\ &= \sum_k \frac{C_{\mu k} C_{\nu k}^*}{\zeta - e_k}. \end{aligned} \quad (\text{A7})$$

Further it follows that

$$\begin{aligned} \lim_{\eta \rightarrow 0^+} G_{\mu\nu}(\varepsilon + i\eta) &= \lim_{\eta \rightarrow 0^+} \sum_k \frac{C_{\mu k} C_{\nu k}^*}{(\varepsilon - e_k) + i\eta} \\ &= P \sum_k \frac{C_{\mu k} C_{\nu k}^*}{\varepsilon - e_k} - i\pi \sum_k C_{\mu k} C_{\nu k}^* \delta(\varepsilon - e_k), \end{aligned} \quad (\text{A8})$$

where P denotes the principal part and δ the Dirac delta function.

The connection between the Green's matrix and the density matrix is now easily established:

$$\begin{aligned} P_{\mu\nu} &= \sum_k^{\text{occ}} C_{\mu k} C_{\nu k}^* \\ &= \int_{-\infty}^{\varepsilon_F} d\varepsilon C_{\mu k} C_{\nu k}^* \delta(\varepsilon - e_k) \\ &= -\frac{1}{\pi} \lim_{\eta \rightarrow 0^+} \text{Im} \int_{-\infty}^{\varepsilon_F} d\varepsilon G_{\mu\nu}(\varepsilon + i\eta). \end{aligned} \quad (\text{A9})$$

Appendix BThe inverse of a partitioned matrix

Consider the nonsingular partitioned matrix

$$X = \begin{bmatrix} X_{AA} & X_{AB} \\ X_{BA} & X_{BB} \end{bmatrix} . \quad (B1)$$

Denote its inverse by Y, then

$$Y = \begin{bmatrix} Y_{AA} & -(X_{AA})^{-1} X_{AB} Y_{BB} \\ -(X_{BB})^{-1} X_{BA} Y_{AA} & Y_{BB} \end{bmatrix} \quad (B2)$$

$$= \begin{bmatrix} Y_{AA} & -Y_{AA} X_{AB} (X_{BB})^{-1} \\ -Y_{BB} X_{BA} (X_{AA})^{-1} & Y_{BB} \end{bmatrix} , \quad (B3)$$

where

$$Y_{AA} = [X_{AA} - X_{AB} (X_{BB})^{-1} X_{BA}]^{-1}, \quad (B4)$$

$$Y_{BB} = [X_{BB} - X_{BA} (X_{AA})^{-1} X_{AB}]^{-1}. \quad (B5)$$

Eq. (B2) is obtained by performing the matrix multiplication in

$$\begin{bmatrix} X_{AA} & X_{AB} \\ X_{BA} & X_{BB} \end{bmatrix} \begin{bmatrix} Y_{AA} & Y_{AB} \\ Y_{BA} & Y_{BB} \end{bmatrix} = \begin{bmatrix} 1_{AA} & 0_{AB} \\ 0_{BA} & 1_{BB} \end{bmatrix} , \quad (B6)$$

and by actually solving the submatrices Y_{PQ} ($P, Q = A, B$) from the four resulting

equations. Eq. (B3) may be found by similarly solving $YX = 1$ or by the following algebra:

$$\begin{aligned}
 X_{AB} - X_{AB}(X_{BB})^{-1}X_{BA}(X_{AA})^{-1}X_{AB} &= X_{AB} - X_{AB}(X_{BB})^{-1}X_{BA}(X_{AA})^{-1}X_{AB}, \\
 X_{AB}(X_{BB})^{-1}(Y_{BB})^{-1} &= (Y_{AA})^{-1}(X_{AA})^{-1}X_{AB}, \\
 Y_{AA}X_{AB}(X_{BB})^{-1} &= (X_{AA})^{-1}X_{AB}Y_{BB}, \tag{B7}
 \end{aligned}$$

and the analogous result obtained by interchanging A and B.

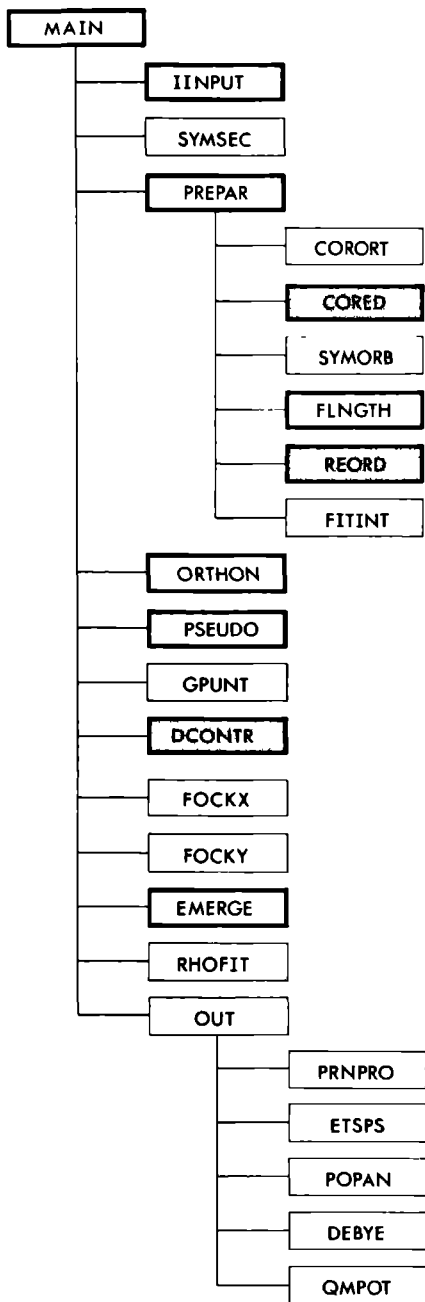
Appendix CStructure of the embedding HFS-LCAO program

In figure C1 we have schematically indicated the structure of the embedding HFS-LCAO program. We will discuss the various sections below.

Section MAIN contains the driver routine of the program and frequently used service routines. Most input data for the program is read in IINPUT, viz., run type (frozen-core, pseudopotential, embedding, etc.), coordinates, basis and density fit sets, core descriptions and integration parameters. In SYMSEC the point group symmetry specified is used to generate data for the symmetry adaptation of the basis functions; the fit functions are joined to totally symmetric linear combinations.

Section PREPAR is a driver routine for integral evaluation. In CORORT overlap integrals between the core orbitals and the basis functions are calculated. In CORED the overlap integrals between core orbitals of the indented solid and the basis functions (of the chemisorption cluster) are dealt with. In SYMORB the symmetry adapted linear combinations of basis functions (SALCs) are constructed; in frozen-core calculations they are orthogonalized to the core orbitals, using the overlaps from CORORT. At this point one can actually calculate the storage requirements of the program; in section FLNGTH these requirements are checked against the available storage. Section REORD performs validity checks for the substrate cluster B and reorders the SALCs in a computationally convenient way. In FITINT the integrals needed in the density fit procedure are evaluated.

In section ORTHON the SALCs are orthogonalized. In embedding calculations the transformation matrices from nonorthogonal to orthogonal SALCs are stored. In PSEUDO the matrices P^C and P^E [cf. Eqs. (3.11) and (3.12)] are calculated



= modified section
 = new section

Figure C1.

The HFS-LCAO program

in the symmetry adapted basis; in embedded cluster calculations the contribution of the indented solid is taken into account, using the overlaps calculated in CORED.

We now reach the sections in which the numerical integration is performed. In GPUNT the integration points are generated and the core density and Coulomb potential are evaluated at these points. In section DCONTR the constant density due to the indented solid is dealt with [cf. Sec. 3A]; the density and the Coulomb potential are added to the data calculated in GPUNT. In FOCKX integrals are evaluated for the calculation of the valence Coulomb potential; also the initial Fock matrix is calculated. Section FOCKY is used in subsequent iterations for the construction of the Fock matrix.

In EMERGE the Fock matrix is diagonalized and the density matrix constructed. In embedded cluster calculations this is done using the coupling matrices, evaluated at the appropriate energies. Also convergence of the HFS calculation is monitored here. In RHOFIT the density fit is performed.

The iterative steps of the calculation are FOCKY, EMERGE and RHOFIT. After termination of the iterative procedure the driver routine OUT is entered. In PRNPRO printing and/or punching of the density matrix and the eigenvectors is dealt with. In ETSPS pseudopotential energy terms are calculated. In section POPAN a population analysis is performed; here also the (converged) SCF data is stored. Optionally in DEBYE and QMPOT the dipole moment and the potential at the nuclei are evaluated.

References

1. D. Post, E.J. Baerends, Surf. Sci. 109 (1981) 167.
2. D. Post, E.J. Baerends, Surf. Sci. 116 (1982) 177.
3. D. Post, E.J. Baerends, J. Chem. Phys. 78 (1983) 5663.
4. P.S. Bagus, H.F. Schaefer III, C.W. Bauschlicher, Jr.,
J. Chem. Phys. 78 (1983) 1390.
5. T.B. Grimley, C. Pisani, J. Phys. C7 (1974) 2831.
6. T.B. Grimley, in: Electronic Structure and Reactivity of Metal Surfaces,
edited by E.G. Derouane and A.A. Lucas (Plenum, New York, 1976) p.113.
7. C. Pisani, Phys. Rev. B17 (1978) 3143.
8. C. Pisani, R. Dovesi, P. Carosso, Phys. Rev. B20 (1979) 5345.
9. O. Gunnarson, H. Hjelmberg, Phys. Scr. 11 (1975) 97.
10. R.A. van Santen, L.H. Toneman,
Intern. J. Quantum Chem., Suppl. 2 (1977) 83.
11. J. Bernholc, S.T. Pantelides, Phys. Rev. B18 (1978) 1780.
12. G.A. Baraff, M. Schlüter, G. Allan, Phys. Rev. B27 (1983) 1010.
13. A.R. Williams, P.J. Feibelman, N.D. Lang, Phys. Rev. B26 (1982) 5433.
14. J.L. Whitten, T.A. Pakkanen, Phys. Rev. B21 (1980) 4357.
15. G.F. Koster, J.C. Slater, Phys. Rev. 96 (1959) 1208.
16. J. Callaway, Phys. Rev. 154 (1967) 515.
17. E.J. Baerends, D.E. Ellis, P. Ros, Chem. Phys. 2 (1973) 41.
18. E.J. Baerends, P. Ros, Chem. Phys. 2 (1973) 52.
19. J.G. Snijders, E.J. Baerends, Mol. Phys. 33 (1977) 1651.
20. W. Ravenek, E.J. Baerends, J. Chem. Phys. 81 (1984) 865.
21. W. Ravenek, F.M.M. Geurts, Chem. Phys. 90 (1984) 73.
22. R.W.G. Wyckoff, Crystal Structures, 2nd ed.,
(Interscience, New York, 1963).

23. P. Vernooijs, J.G. Snijders, E.J. Baerends,
Slater Type Basis Functions for the Whole Periodic System,
Internal Report, (Vrije Universiteit, Amsterdam, 1981).
24. D. Post, Thesis, Vrije Universiteit, Amsterdam (1981).
25. K. Hermann, P.S. Bagus, Phys. Rev. B17 (1978) 4082.
26. D.E. Ellis, Intern. J. Quantum Chem. 2S (1968) 35.
27. D.E. Ellis, G.S. Painter, Phys. Rev. B2 (1970) 2887.
28. A.L. Companion, Chem. Phys. 14 (1976) 1.
29. H. Stoll, H. Preuss, Surf. Sci. 65 (1977) 229.

S U M M A R Y

This thesis, entitled "Cluster embedding and pseudopotentials in the Hartree-Fock-Slater-LCAO method", treats a number of quantum chemical computational methods based on the nonempirical Hartree-Fock-Slater(HFS)-LCAO method of Baerends and Ros. These methods, intended for the study of large molecular systems, are building blocks for an embedding formalism for chemisorption calculations.

In chapter II the Mössbauer parameters of a series antimony compounds are studied. The calculated isomer shifts correlate very well with experiment. The calculated quadrupole splittings are too small; for the systematic deviation in the results for the Sb(III) compounds some reasons are suggested. Furthermore, it is shown that the HFS-LCAO method is capable of yielding accurate core polarization corrections to the quadrupole splitting, albeit at the cost of an expensive numerical integration scheme.

In chapter III a new, self-consistent perturbational formalism for the calculation of binding energies with the pseudopotential HFS-LCAO method is developed. Test calculations show that the results agree well with those of the less approximate frozen-core HFS-LCAO method. Moreover, the calculated spectroscopic constants of a number of diatomic molecules agree well with experiment.

In chapter IV the pseudopotential HFS-LCAO method is investigated on its capability to yield accurate one-electron properties. It appears that results obtained with the frozen-core HFS-LCAO method can be reproduced very well if the pseudo-orbitals are core orthogonalized. The calculated electric dipole and quadrupole moments are also in good agreement with available experimental data.

In chapter V a simplified method is introduced for the calculation of the pseudo-orbitals in the pseudopotential HFS-LCAO formalism.

In chapter VI a computational scheme for chemisorption studies is developed in which the chemisorption cluster is embedded in the rest of the substrate. Problems that arise in the implementation in the pseudopotential HFS-LCAO method are discussed and solutions are given. Test calculations for hydrogen adsorbed on lithium show that the convergence of the electronic structure with cluster size is influenced favourably by the embedding. However, the numerical integration scheme used still needs improvement.

S A M E N V A T T I N G

Dit proefschrift, getiteld "Cluster inbedding en pseudopotentialen in de Hartree-Fock-Slater-LCAO methode", behandelt een aantal kwantumchemische rekenmethoden die gebaseerd zijn op de niet-empirische Hartree-Fock-Slater (HFS)-LCAO methode van Baerends en Ros. Deze methoden, bestemd voor de bestudering van grote moleculaire systemen, zijn bouwstenen voor een inbeddingsformalisme voor het uitvoeren van chemisorptie-berekeningen.

In hoofdstuk II worden de Mössbauer parameters van een aantal antimoonverbindingen bestudeerd. De berekende isomeer-verschuivingen correleren zeer goed met het experiment. De berekende kwadрупool-splitsingen zijn te klein; voor de systematische afwijking in de resultaten voor de Sb(III)-verbindingen worden enkele oorzaken gesuggereerd. Verder blijkt dat de HFS-LCAO methode nauwkeurige core-polarisatie-korrekties op de kwadрупool-splitsing kan leveren, zij het ten koste van een duur numeriek integratieschema.

In hoofdstuk III wordt een nieuw, zelf-konsistent storingsformalisme ontwikkeld voor de berekening van bindingsenergieën met behulp van de pseudopotentiaal HFS-LCAO methode. Testberekeningen wijzen uit dat de resultaten goed overeenstemmen met die van de minder benaderde frozen-core HFS-LCAO methode. Bovendien stemmen de berekende spektroskopische konstanten van een aantal twee-atomige molekulen goed overeen met het experiment.

In hoofdstuk IV wordt de pseudopotentiaal HFS-LCAO methode onderzocht op haar geschiktheid voor het nauwkeurig berekenen van één-elektron eigenschappen. Het blijkt dat resultaten verkregen met de frozen-core methode zeer goed gereproduceerd kunnen worden, indien de pseudo-orbitals op de cores worden georthogonaliseerd. De berekende elektrische dipool- en kwadрупoolmomenten stemmen bovendien goed overeen met voorhanden zijnde experimentele gegevens.

In hoofdstuk V wordt een vereenvoudigde methode geïntroduceerd voor de berekening van pseudo-orbitals in het pseudopotentiaal HFS-LCAO formalisme.

In hoofdstuk VI wordt een formalisme voor chemisorptie-berekeningen ontwikkeld, waarin het chemisorptie-cluster ingebed wordt in de rest van het substraat. Problemen die zich voordoen bij de implementatie in de pseudopotentiaal HFS-LCAO methode worden besproken en oplossingen hiervoor uitgewerkt. Testberekeningen voor waterstof geadsorbeerd op lithium tonen aan dat de convergentie van de elektronische structuur met de cluster grootte gunstig beïnvloed wordt door het inbedden. Het numerieke integratieschema dat gebruikt wordt behoeft echter nog verbetering.

CURRICULUM VITAE

van

Walter Ravenek

geboren 13 november 1953 te Pijnacker

juni	1972	Eindexamen Atheneum-B, Christelijk Lyceum voor Delft en Rijswijk
augustus	1976	Kandidaatsexamen Scheikundige Technologie, Technische Hogeschool Delft
oktober	1976	Studieprijs van de Afdeling der Scheikundige Technologie, Technische Hogeschool Delft
september	1978	Deelnemer "Charles Coulson Summer School in Theoretical Chemistry", Oxford, Engeland
november	1979	Doktoraalexamen Scheikunde (cum laude), Universiteit van Amsterdam. hoofdvak: theoretische chemie bijvak : chemische fysica
december	1979	Wetenschappelijk medewerker,
- november	1983	Instituut voor Theoretische Chemie, Katholieke Universiteit Nijmegen (in dienstverband met ZWO/SON)
juni/juli	1980	Deelnemer CECAM workshop "Computational methods for small molecules adsorbed on solid surfaces", Orsay, Frankrijk
oktober	1984	Wetenschappelijk medewerker,
- heden		FOM-instituut voor Atoom- en Molecuulfysica, Amsterdam

STELLINGEN

1. De methode van Northrup et al. voor de berekening van de vibratiefrequentie van het silicium dimeer is zo onnauwkeurig, dat vergelijking van het resultaat met de experimentele waarde zinloos is.

J.E. Northrup, M.T. Yin, M.L. Cohen, Phys. Rev. A28 (1983) 1945.

2. De aard van de bindingen in het neon trimeer is zodanig dat een adiabatische scheiding van hoekafhankelijke en radiële vibraties niet gerechtvaardigd is. Dit blijkt ook uit de door Frey met deze benadering verkregen resultaten.

J.G. Frey, Chem. Phys. Lett. 102 (1983) 421.

3. Het gebruik van de voor zelf-interactie gekorrigeerde exchange potentiaal van Gázquez en Ortiz voor de berekening van de exchange bijdrage aan de intermoleculaire potentiaal leidt tot fysisch onjuiste resultaten.

J.L. Gázquez, E. Ortiz, Chem. Phys. Lett. 77 (1981) 186.

4. Het is fysisch onjuist om bij de berekening van relaxatie-effecten op core-elektron bindingsenergieën in vaste stoffen een gat te creëren in elk van de atomen van het systeem.

J.R. Smith, F.J. Arlinghaus, J.G. Gray, Phys. Rev. B26 (1982) 1071.

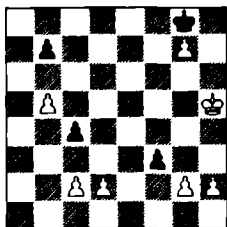
5. In lokale dichtheidsfunktionaalmethoden wordt het exchange-korrelatiegat zeer slecht gepresenteerd. Het introduceren van dichtheidsgradiënt correcties ten opzichte van het referentiepunt kan hierin geen fundamentele verbetering brengen.

6. Het model van Matsushita en Terasaka voor de beschrijving van vibrati-
nele chaos in lineaire molekulen mist enkele fundamentele fysische aspecten.

T. Matsushita, T. Terasaka, Chem. Phys. Lett. 105 (1984) 511.

7. Bij veel beschouwingen over de prestaties van parallelle computers wordt
de I/O overhead überhaupt over het hoofd gezien.

8.



Deze stelling is niet met succes te verdedigen.

9. Het besluit van de Nederlandse regering inzake de kruisraketten valt niet
bepaald als kernachtig te karakteriseren.

10. Lange-afstandstourfietsers ontmoeten bij fietshandelaren veel onbegrip.

22 november 1984

W. Ravenek

